Dissertations, Theses, and Masters Projects   Theses, Dissertations, & Master Projects

2004

Application of effective field theory to the study of hypernuclei

Jeffrey William McIntire
College of William & Mary - Arts & Sciences

Follow this and additional works at: https://scholarworks.wm.edu/etd

APPLICATION OF EFFECTIVE FIELD THEORY TO THE STUDY OF HYPERNUCLEI

A Dissertation

Presented to

The Faculty of the Department of Physics

The College of William and Mary in Virginia

In Partial Fulfillment

Of the Requirements for the Degree of

Doctor of Philosophy

by

Jeffrey William McIntire

2004

APPROVAL SHEET

This dissertation is submitted in partial fulfillment of

the requirements for the degree of

Doctor of Philosophy

Jeffrey William McIntire

Approved, February 2004

John D. Walecka

David S. Armstrong

Carl E. Carlson

Marc Sher

John LeRose
TJNAF

ii

DEDICATION

This work is dedicated to my family.

CONTENTS

vi

ACKNOWLEDGMENTS

LIST OF TABLES

viii

ix

LIST OF FIGURES

xii

xiii

ABSTRACT

Furnstahl, Serot, and Tang have developed a methodology for constructing an effective lagrangian for the nuclear many-body system which contains the underlying symmetries of QCD. Density Functional Theory is used as a theoretical justification for the relativistic Hartree (Kohn-Sham) equations derived from this effective lagrangian. In the present work, this approach is extended to the region of nonzero strangeness in two applications. First, this procedure is applied to strange, neutral, superheavy systems and the surface properties of these nuclei are extracted. Second, single-particle states in Λ-hypernuclei are investigated, the effective lagrangian is determined to various levels of truncation, and where appropriate, ground-state particle-hole splittings are calculated.

APPLICATION OF EFFECTIVE FIELD THEORY TO THE STUDY OF

HYPERNUCLEI

CHAPTER 1

Introduction

Quantum Chromodymamics (QCD) is the underlying theory of the strong interaction. Unfortunately, QCD is not directly solvable at low-energy. One solution to this quandary is to use an effective field theory to represent QCD. In this energy regime, confinement traps the quarks in hadrons. Thus hadrons, and not quarks, are the desired degrees of freedom. As a result, effective theories using hadrons as degrees of freedom, so-called hadronic field theories, have been developed to solve the nuclear many-body problem. In the present work, we consider one of these theories, proposed by Furnstahl, Serot, and Tang (FST) [1, 2]. The framework they devised directly incorporates all of the following: special relativity, quantum mechanics, the nonlinear realization of spontaneously broken chiral symmetry, and the underlying symmetry structure of QCD. Furthermore, density functional theory (DFT) provides a theoretical justification for this approach [2, 3]. Therefore, it is of interest to extend this methodology, with all its intrinsic strengths, to the strangeness sector.

The focus of this work is the expansion of the effective field theory approach of FST to hypernuclei. Two specific applications are considered here. First, we use this framework to model the surface structure and calculate the surface energy of

2

large, neutral, self-bound, multi-strange systems. Second, we construct a general lagrangian, consistent with the methodology of FST, for the addition of a single Λ to the theory. This lagrangian is then used to calculate the ground-state (GS) energies (i.e. chemical potentials), densities, and single-particle spectra of single Λ-hypernuclei. Another property of this class of nuclei that is considered here, and of particular interest, is the GS Λ-particle—nucleon-hole doublet splitting.

This introduction is a self-contained overview that includes some relevant background and a brief discussion of the specific topics considered in this thesis. As part of this overview, the main results of this work are also presented. Subsequent chapters will discuss in more detail the problems of interest here, the methodology used to tackle these problems, and the results of this research.

1.1   Background

In modern physics phenomenology, the fundamental forces of nature are modeled by particle exchange. The four known forces are the strong nuclear force, the weak nuclear force, the electromagnetic force, and gravity. The particles whose exchange simulate these forces, referred to here as gauge bosons, are the gluon, the $W^{\pm}$ and Z^0, the photon, and the graviton respectively.[1] The gluons are exchanged by strongly interacting particles referred to as quarks, which are classified as fermions.[2] There are six known varieties, or flavors, of quarks: u (up), d (down), s (strange), c (charm), b (bottom), and t (top). They are listed in Table 1.1 with some of their properties, which we now discuss. Notice that all of the quarks have baryon number $B = 1/3$; as we will see later objects called baryons are composed of three quarks

---

[1] A boson is a particle that obeys Bose-Einstein statistics, or there is no restriction on the number of particles that can occupy a given state. It has an intrinsic angular momentum, or spin, in integer units of $\hbar$.

[2] A fermion is a particle that obeys Fermi-Dirac statistics, or there is the restriction that only one particle can occupy a given state. It has spin in half integer units of $\hbar$.

	B	Q	S	T	M
u	1/3	+2/3	0	1/2	0.0015-0.0045
d	1/3	-1/3	0	1/2	0.005-0.0085
s	1/3	-1/3	-1	0	0.08-0.155
c	1/3	+2/3	0	0	1.0-1.4
b	1/3	-1/3	0	0	4.0-4.5
t	1/3	+2/3	0	0	174 ± 5

TABLE 1.1: The quarks are listed here with their respective baryon number (B), charge (Q) in units of e, strangeness (S), total isospin (T), and mass (M) in GeV [4].

and therefore have $B = 1$. Quarks are also characterized by their charge (Q), a property upon which the electromagnetic force acts. Strangeness (S) is a property intrinsic to only the s quark; it is defined such that $S = -1$ for an s quark and $S = +1$ for an $\bar{s}$ antiquark. The total isospin (T) denotes a quantity which accounts for the relative similarity in the masses of the u and d quarks. These properties (B, Q, S, T) are all conserved quantities in the strong interaction; that is to say they do not change during a reaction. In addition, the quarks carry an intrinsic strong interaction "charge," known as color, of which there are three types.

Lets us now return to the discussion of the four forces. Gravity is too weak and long range to have any significant effect in nuclear physics. The weak nuclear force and the electromagnetic force do have some impact on nuclear physics; however, by far the most important force governing the structure and dynamics of nuclei is the strong force.[3] As a result, a brief discussion of the strong interaction is warranted. This force has the following properties [5]:

- it is attractive, as can be seen from the fact that the nuclei are bound;

- it is short range, effective out to only a few fm ($1\text{fm} = 10^{-13}\text{cm}$);

---

[3]The electromagnetic force will be incorporated later into the theory. The weak force is largely neglected in this work as it will have little effect on the phenomena of interest.

- it is repulsive at short distances (< 0.5 fm);

- it is spin-dependent;

- and it is charge-independent.

The underlying theory that describes this force is QCD. QCD models the interaction of particles with color charge, quarks and gluons, and is constructed to be symmetric under color exchange. This theory is characterized by a single coupling parameter, α_S. The behavior of this parameter is shown in Fig. 1.1. Notice that α_S is small at high-energy, or equivalently, short distances; this allows the QCD lagrangian to be solved by a perturbative expansion in α_S. However, at low-energy, or long distances, the strong coupling parameter becomes large. Thus, a perturbative expansion in α_S will not converge at nuclear physics energy scales. Recall that the gluons carry color, and as a result, can couple to each other. It is this fact that leads to asymptotic freedom at high-energy. Conversely, at sufficiently low-energy, a process referred to as confinement occurs in which color is completely screened by the strong interaction. Here the quarks and gluons become "confined" in objects known as hadrons. There are two main configurations in which hadrons occur: three quark states (qqq), known as baryons, and quark-antiquark pairs (q$\bar{q}$), called mesons.[4,5] These hadrons always occur in color singlets, i.e. the color charges of the constituent quarks cancel resulting in a net neutral color charge. As a result of confinement, the realm of low-energy nuclear physics is dominated not by quarks and gluons, but by hadrons and the interactions between them.

---

[4]There are other possible configurations, such as the recently discovered pentaquark (qqqq$\bar{q}$), but they are beyond the scope of this work.

[5]Here we are considering only the valence quark structure of the hadrons. The valence quarks are the objects which contribute all of the quantum numbers to the hadrons in the quark model. However, these valence quarks are continuously exchanging gluons, which can couple to other gluons or become quark-antiquark pairs. Quarks formed in this manner are referred to as sea quarks. Although the sea quarks and gluons make up a large portion of the mass of a hadron, the contributions of these particles are not considered here.
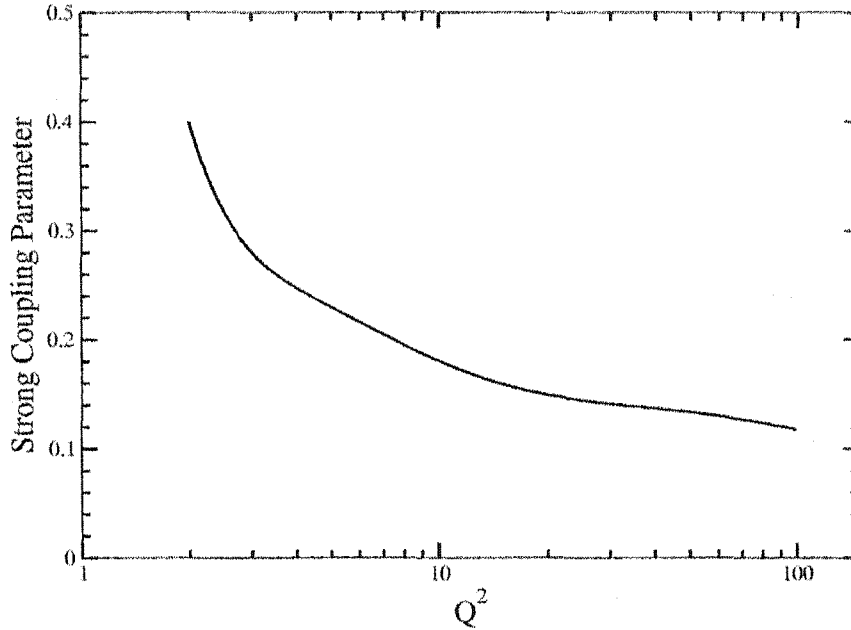
FIG. 1.1: Qualitative behavior of the strong coupling parameter, α_S, vs. Q^2. Here Q^2 (in GeV^2) is a measure of the energy scale [6].

Baryons can be classified based on their constituent valence quark content. Two groups of importance to the current work are nucleons and hyperons. Nucleons occur in two varieties: protons (uud) and neutrons (udd). It is these objects which make up the composition of ordinary nuclei. Notice that they are composed solely of u and d quarks. Other systems composed only of u and d quarks exist, such as the Δ^{++} (uuu); however, these systems decay rapidly via the strong interaction (strong interaction timescales are $\sim 10^{-23}$s). The other group of baryons that is of interest here is the hyperons. If a baryon contains one or more s quarks, it is referred to as a hyperon. Examples of this type of baryon are the following: Λ (uds), Ξ^0 (uss), and Ω^- (sss). As previously mentioned, the s quark has an intrinsic property called strangeness, as can be seen in Table 1.1. As this is a conserved quantity in the strong interaction, only a weak interaction will convert the s quark to another

	B	Q	S	T	M	qqq
p	1	+1	0	1/2	938.27	uud
n	1	0	0	1/2	939.57	udd
Λ	1	0	-1	0	1115.68	uds
Σ^+	1	+1	-1	1	1189.37	uus
Σ^0	1	0	-1	1	1192.64	uds
Σ^-	1	-1	-1	1	1197.45	dds
Ξ^0	1	0	-2	1/2	1314.83	uss
Ξ^-	1	-1	-2	1/2	1321.31	dss
Ω^-	1	-1	-3	0	1672.45	sss

TABLE 1.2: The nucleons and hyperons are listed here with their respective baryon number (B), charge (Q) in units of e, strangeness (S), total isospin (T), mass (M) in MeV, and constituent valence quark content (qqq) [4].

flavor.[6] Therefore, the Λ will decay on weak interaction timescales ($\sim 10^{-8}$s).[7] In Table 1.2, the nucleons and hyperons are listed with some of their properties. As a result, if one operates on the strong interaction timescale, then nuclei containing nucleons and hyperons, or hypernuclei, exist and are stable.

Hypernuclei present an interesting test case in nuclear physics. The effectiveness of models that were developed to reproduce the properties of ordinary nuclei can be probed by their extension to hypernuclei. As it turns out, hypernuclear physics is in many ways both novel and puzzling. For instance, hypernuclei introduce an additional degree of freedom (strangeness) to nuclear physics. In the case of S = −1 physics, the entire range of possible states for the hyperon may be occupied as restrictions from the Pauli exclusion principle no longer apply. In addition, some other interesting features of S = −1 physics that differ form ordinary S = 0 physics include: "anomalous binding energies, a vanishing spin-orbit force, significant three-body force effects, ground-state spin inversion, and puzzling nonmesonic

---

[6] This is due to the fact that strangeness is also a conserved quantity in both the electromagnetic force and gravity.

[7] As will be discussed later, other hyperons may also decay on weak interaction timescales.

weak decays [7]." The study of hypernuclei also allows one to investigate all aspects of the interaction between a hyperon and a nucleon, an important extension of our knowledge of the interaction between two nucleons. Furthermore, large, multistrange systems may potentially exist, due to the fact that negatively charged hyperons can be included to offset the Coulomb repulsion of the protons while the system remains stable against strong decay. Experimentally, the accessibility of hypernuclear states is becoming easier and the resolution possible on these states is improving. The old method of (π^+, K^+) and (K^-, π^-) reactions [8, 9, 10] is now being supplemented by electroproduction $(e, e'K^+)$ [11, 12] and gamma-ray spectroscopy [13]. As a result, hypernuclei are an excellent proving ground for testing models designed for the $S = 0$ sector. The present thesis examines the successful extension of one particular theory, developed by FST [1, 2], to the strangeness sector.

In order to model nuclear systems, we use a mathematical framework known as quantum field theory (QFT). QFT is a reformulation of quantum mechanics in terms of fields that retains all of the general principles of quantum mechanics: microscopic causality, Lorentz invariance, and electromagnetic gauge invariance [6, 14]. The mathematical object referred to as a field defines the value of a physical quantity at all points in a given space. For the purposes of this work, the hadrons will be described in terms of fields and our approach will incorporate the general structure of QFT into an effective field theory.

Now we digress shortly to discuss two important symmetries of the strong interaction: isospin and chiral symmetry. We begin by stating Noether's theorem:

"For every continuous transformation of the field functions and coordinates which leaves the action unchanged, there is a definite combination of the field functions and their derivatives which is conserved (i.e. a constant in time) [6]."

In other words, for any continuous symmetry of a system, there exists a corresponding conserved current in that system, or vice versa. A current is conserved if it satisfies the relation

$$\frac{\partial}{\partial x_\mu} J_\mu = 0 \tag{1.1}$$

Here we use the conventions of [5].[8] If we consider the nucleons in Table 1.2, we notice that their masses are very similar.[9] This is taken as evidence that the proton and neutron are two manifestations of the same particle, the nucleon [14]. Now we define the nucleon field as a two component column vector

$$N = \begin{pmatrix} p \\ n \end{pmatrix} \tag{1.2}$$

where p and n represent the proton and neutron fields respectively. If one assumes that the masses of the proton and neutron are exactly equal, or $m_p = m_n$, then a transformation of N according to the elements of a special unitary group in two dimensions, or SU(2), leaves the action (i.e. the four dimensional integral over the lagrangian density) unchanged [6]. This transformation is given by

$$N \rightarrow N' = exp(-\frac{i}{2}\vec{\tau} \cdot \vec{\theta})N \tag{1.3}$$

where $\vec{\tau}$ are the Pauli matrices and $\vec{\theta}$ is an arbitrary constant vector. This symmetry is known as isospin. Noether's theorem tells us that as isospin is a good symmetry of the strong interaction, there is a corresponding conserved isospin current

$$J_\mu^k = i\bar{N}\gamma_\mu \frac{1}{2}\tau_k N + \cdots \tag{1.4}$$

---

[8]In this work, we define the conventions $x_\mu = (\vec{x}, it)$, $\gamma_\mu = (i\vec{\alpha}\beta, \beta)$, and $\hbar = c = 1$. The gamma matrices are hermitian, $\gamma_\mu^\dagger = \gamma_\mu$, and satisfy the relation $\gamma_\mu\gamma_\nu + \gamma_\nu\gamma_\mu = 2\delta_{\mu\nu}$. Also, we define the quantity $\gamma_5 \equiv \gamma_1\gamma_2\gamma_3\gamma_4$. Note that repeated Greek indices are summed from 1 to 4.

[9]Also notice in Table 1.2 that the Σ's or Ξ's each have nearly identical masses, i.e. $m_{\Sigma^0} \cong m_{\Xi^-}$.

which in this case is a Lorentz vector. At the QCD lagrangian level, SU(2) isospin symmetry dictates that $m_u = m_d$. The success of this symmetry is due largely to the fact that $m_u \cong m_d$. This flavor symmetry can be extended to SU(3) and beyond. However, SU(3) flavor symmetry would suggest that $m_u = m_d = m_s$, which is not as good an assumption as SU(2) [14]. This can be seen from the mass difference between the u and s quarks, shown in Table 1.1.

As it turns out, there is also a partially conserved axial vector current

$$J^k_{\mu 5} = i\bar{N}\gamma_\mu\gamma_5\frac{1}{2}\tau_k N + \cdots \tag{1.5}$$

If we assume for now that $J^k_{\mu 5}$ is exactly conserved and invoke Noether's theorem again, the corresponding continuous symmetry of the strong interaction is known as chiral symmetry. The transformation that characterizes this symmetry is

$$N \to N' = exp(-\frac{i}{2}\gamma_5\vec{\tau}\cdot\vec{\theta})N \tag{1.6}$$

Assuming that chiral symmetry is exact, the full symmetry group is now written as $SU(2)_L \otimes SU(2)_R$. The corresponding transformation is

$$exp(-\frac{i}{2}P_+\vec{\tau}\cdot\vec{\theta}_1)exp(-\frac{i}{2}P_-\vec{\tau}\cdot\vec{\theta}_2) \tag{1.7}$$

where $\vec{\theta}_1$ and $\vec{\theta}_2$ are independent and

$$P_\pm = \frac{1}{2}(1 \pm \gamma_5) \tag{1.8}$$

The $P_\pm$ are projection operators; they project out right or left handed helicity states respectively. Helicity defines the alignment of spin and momentum of a particle.

However, chiral symmetry is exact only in the limit of vanishing pion mass, or

$$\lim_{m_\pi \to 0} \frac{\partial}{\partial x_\mu} J^k_{\mu 5} \to 0 \qquad (1.9)$$

It turns out that although chiral symmetry is only an approximate symmetry, it is a very good one [6], as the pion mass, $m_\pi \approx 140$ MeV, is small on the particle physics mass scale. On the QCD lagrangian level, chiral symmetry forces all the quarks to be massless, i.e. $m_u = m_d = \ldots = 0$. Again, this is not such a bad assumption if we consider the u and d quarks only. However, it becomes increasingly unrealistic as the heavier quarks are included.

The imposition of both isospin and chiral symmetry on the theory dictates that the baryon and pion masses must be zero. In order to produce both a nonzero baryon and pion mass, a process known as symmetry breaking is employed. There are two types of symmetry breaking: spontaneous and explicit. Spontaneous symmetry breaking occurs when the underlying lagrangian is invariant under the symmetry transformation, yet develops a nonzero vacuum expectation value, or

$$\langle \mathcal{L} \rangle_{\mathrm{vac}} \neq 0 \qquad (1.10)$$

It should also be mentioned that when a symmetry is spontaneously broken, massless bosons are left behind.[10] Explicit symmetry breaking is when the lagrangian contains a small term which is not invariant under the symmetry transformation. In the case of chiral symmetry, both forms of breaking are required; the baryon and pion masses are generated through spontaneous and explicit symmetry breaking respectively [5, 6]. It is worth noting that, as a result of explicit symmetry breaking,

---

[10]These are known as Goldstone bosons. The number of Goldstone bosons created is always $n^2 - 1$ for a symmetry $SU(n)$.

the axial vector current is no longer conserved, or [5]

$$\frac{\partial}{\partial x_\mu} J_{\mu 5}^k \propto m_\pi^2 \tag{1.11}$$

In QCD, the finite quark masses explicitly break the chiral symmetry.

Now let us return to the discussion of the strong nuclear force. It was established that for low-energy nuclear physics, hadrons are the particles observed in nature and as a result, the appropriate degrees of freedom. Therefore, in this energy regime we model the strong force as meson exchange between baryons; this is a direct analogy to the situation in QCD where gluons are exchanged between quarks. The generic form of the potential (known as a Yukawa potential) for an exchanged meson of mass m is

$$V(r) = -\frac{g^2}{4\pi} \frac{e^{-mr}}{r} \tag{1.12}$$

where g is the strength of the interaction [6]. The exponential dominates as r increases; this gives the potential a short range. The main characteristics of the strong force, the medium-range attraction and the short-range repulsion, can be qualitatively reproduced by the sum of Yukawa scalar and vector meson exchange, or

$$V(r) = -\frac{g_S^2}{4\pi} \frac{e^{-m_S r}}{r} + \frac{g_V^2}{4\pi} \frac{e^{-m_V r}}{r} \tag{1.13}$$

where m_S and m_V are the respective masses of the mesons whose coupling strengths are g_S and g_V respectively [5]. One pion exchange gives rise to an additional potential similar in form to a Yukawa [15]. Pion and multi-pion exchange are ultimately responsible for the long-range, attractive part of the strong interaction.

Thus, in this picture the continuous exchange of mesons is what binds the baryons in nuclei. Given that the characteristic energy scale in nuclear physics is about 1 GeV, or the mass of the nucleon, the relevant degrees of freedom are the

low-lying hadrons. In the case of ordinary nuclei this corresponds to the nucleon, the pion, and other light mesons. The addition of hyperons allows one to extend this model to hypernuclei.

1.2 Effective Field Theory Approach

Now we turn to the topic of effective field theories. As we have seen, QCD is not directly solvable at low-energy. One solution to this problem is to use an effective field theory to simulate the effects of QCD in this energy regime. An effective field theory is a framework in which an underlying theory is represented by an expansion in a small parameter(s) relevant to the energy scale under consideration. Effective field theories take advantage of two important facts [2]:

1. QFT is an efficient way to parameterize the observables of a system consistent with analyticity, unitarity, causality, cluster decomposition, and symmetries;

2. most problems in modern physics have a characteristic length, or energy, scale. Only those degrees of freedom that can be excited at this energy scale, or can resolve this characteristic length, are relevant [16].

In the regime of low-energy nuclear physics, the appropriate degrees of freedom are the low-lying hadrons. The hadrons are then introduced into the theory as quantum fields, from which the effective lagrangian is constructed. Heavier degrees of freedom are included in the form of coupling constants attached to the interaction terms of lighter fields. These constants can be fit to experimental data, from which relationships between different observables in the dynamical regime of interest can be derived [2]. We now consider a specific effective field theory developed by FST.

FST approach the nuclear many-body problem by developing a self-consistent framework for constructing an effective lagrangian. Their methodology incorporates

the principles of both quantum mechanics and special relativity as well as the underlying symmetries of QCD [1]. As this is a low-energy theory, the appropriate low lying hadrons are used as degrees of freedom. Spontaneously broken chiral symmetry is realized nonlinearly through a system of the following three fields [1]:

- Goldstone pion fields, $\pi(x_\mu) = \frac{1}{2}\vec{\tau} \cdot \vec{\pi}$, which enter through the combinations

$$U(x_\mu) \equiv \xi(x_\mu)\mathbf{1}\xi(x_\mu) = e^{i\pi(x_\mu)/f_\pi}\mathbf{1}e^{i\pi(x_\mu)/f_\pi} \tag{1.14}$$

$$v_\mu = -\frac{i}{2}\left(\xi^\dagger\frac{\partial\xi}{\partial x_\mu} + \xi\frac{\partial\xi^\dagger}{\partial x_\mu}\right) = v_\mu^\dagger \tag{1.15}$$

and

$$a_\mu = \frac{i}{2}\left(\xi^\dagger\frac{\partial\xi}{\partial x_\mu} - \xi\frac{\partial\xi^\dagger}{\partial x_\mu}\right) = a_\mu^\dagger \tag{1.16}$$

where f_π is the pion decay constant;

- an isodoublet nucleon field, N;

- and an isovector-vector rho meson field, $\rho_\mu(x_\nu) = \frac{1}{2}\vec{\tau} \cdot \vec{\rho}$.

Next, the following pair of isoscalar chiral singlets simulate the nucleon-nucleon interaction:

- a scalar field, ϕ, which reproduces the medium-range attraction of the strong interaction;

- and a vector field, V_μ, which simulates the short-range nuclear repulsion.

Finally, a photon field, A_μ, describes the electromagnetic structure of nuclei.

As all possible combinations of these fields consistent with this framework are included, in principle, this lagrangian contains an infinite number of terms. In order to make any meaningful calculation, the lagrangian must be truncated in some way.

To accomplish this, FST group the terms according to a system involving both naive dimensional analysis (NDA) and relativistic mean field theory (RMFT).[11] NDA is a framework that allows one to identify all the dimensional factors associated with specific components in any given term. Furthermore, NDA tells us that once all the dimensional factors are absorbed in a given term, only a dimensionless constant of $O(1)$ remains [17, 18]. This assumption is known as "naturalness." RMFT states that in the limit of appropriately large baryon density, expectation values can replace the sources and classical fields can replace the meson fields [2, 5]. These mean meson fields, while large, are small with respect to the chiral symmetry breaking scale M, or

$$\frac{\Phi}{M}, \quad \frac{W}{M} \sim \frac{1}{3}; \qquad \frac{k_F}{M} \sim \frac{1}{4} \qquad (1.17)$$

where the scaled mean fields are $\Phi = g_S \phi_0$ and $W = g_V V_0$. Here k_F is the Fermi wave number and represents the last, filled momentum state of a collection of non-interacting identical fermions in nuclear matter.[12] As a result, NDA and RMFT provide a formalism in which higher order terms are, in general, successively smaller; this allows for a systematic expansion in the effective lagrangian. One added benefit is that the lagrangian can now be truncated in a meaningful fashion. FST investigate various levels of sophistication in their lagrangian. The fermion sector of their full

---

[11]See appendix B for a more detailed discussion of NDA and RMFT.

[12]The spatial variations of the meson fields and baryon densities are observed to occur on the scale of the nuclear surface [3]. k_F provides a characteristic inverse length scale for the nuclear surface. As a result, we can now employ the relation $\nabla \propto k_F$.

lagrangian density is shown here [1]

$$\mathcal{L}_N(x_\mu) = -\bar{N}\left\{\gamma_\mu\left[\frac{\partial}{\partial x_\mu} + iv_\mu - ig_A\gamma_5 a_\mu - ig_V V_\mu - ig_\rho\rho_\mu\right.\right.$$
$$\left.\left. -\frac{i}{2}eA_\mu(1+\tau_3)\right] + (M - g_S\phi)\right\}N + \frac{f_\rho g_\rho}{4M}\bar{N}\sigma_{\mu\nu}\rho_{\mu\nu}N$$
$$+\frac{f_V g_V}{4M}\bar{N}\sigma_{\mu\nu}V_{\mu\nu}N + \frac{\kappa_\pi}{M}\bar{N}\sigma_{\mu\nu}v_{\mu\nu}N + \frac{e}{4M}\bar{N}\lambda\sigma_{\mu\nu}F_{\mu\nu}N$$
$$+\frac{ie}{2M^2}\bar{N}\gamma_\mu(\beta_S + \beta_V\tau_3)N\frac{\partial}{\partial x_\nu}F_{\mu\nu} \tag{1.18}$$

where we have defined

$$V_{\mu\nu} \equiv \frac{\partial V_\nu}{\partial x_\mu} - \frac{\partial V_\mu}{\partial x_\nu} \tag{1.19}$$

$v_{\mu\nu}$, $\rho_{\mu\nu}$, and $F_{\mu\nu}$ are similarly defined for v_μ, ρ_μ, and A_μ respectively. The meson sector of the full FST lagrangian is [1]

$$\mathcal{L}_M(x_\mu) = -\frac{1}{2}\left(1 + \alpha_1\frac{g_S\phi}{M}\right)\left(\frac{\partial\phi}{\partial x_\mu}\right)^2 - \frac{f_\pi^2}{4}\text{tr}\left(\frac{\partial U}{\partial x_\mu}\frac{\partial U^\dagger}{\partial x_\mu}\right) - \frac{1}{2}\text{tr}\left(\rho_{\mu\nu}\rho_{\mu\nu}\right)$$
$$-\frac{1}{4}\left(1 + \alpha_2\frac{g_S\phi}{M}\right)V_{\mu\nu}V_{\mu\nu} - g_{\rho\pi\pi}\frac{2f_\pi^2}{m_\rho^2}\text{tr}\left(\rho_{\mu\nu}v_{\mu\nu}\right) + \frac{m_\pi^2 f_\pi^2}{4}\text{tr}\left(U + U^\dagger - 2\right)$$
$$-\frac{1}{2}\left(1 + \eta_1\frac{g_S\phi}{M} + \frac{\eta_2}{2}\frac{g_S^2\phi^2}{M^2}\right)m_V^2 V_\mu V_\mu + \frac{1}{4!}\zeta_0 g_V^2(V_\mu V_\mu)^2 - \frac{1}{4}F_{\mu\nu}F_{\mu\nu}$$
$$-\left(1 + \eta_\rho\frac{g_S\phi}{M}\right)m_\rho^2\text{tr}\left(\rho_\mu\rho_\mu\right) - m_S^2\phi^2\left(\frac{1}{2} + \frac{\kappa_3}{3!}\frac{g_S\phi}{M} + \frac{\kappa_4}{4!}\frac{g_S^2\phi^2}{M^2}\right) \tag{1.20}$$

M, m_V, and m_ρ are taken to be the physical masses of the nucleon, ω-meson, and ρ-meson respectively. The remaining parameters are free and are listed in Table 1.3.

FST now utilize relativistic Hartree theory to reduce the many-body field equations derived from these lagrangians to single-particle equations for Dirac nucleons moving in the condensed classical meson fields.[13] Hartree theory assumes that each particle moves in a single-particle potential. This potential is representative of the average interaction of the particle with all of the other particles [19]. Then, the

---

[13]The Dirac field and sources are then obtained from a superposition of these solutions.

	ν	L2	NLC	Q1	G2
m_S/M	2	0.55378	0.53333	0.53735	0.55410
$g_S/4\pi$	2	0.83321	0.77607	0.81024	0.83522
$g_V/4\pi$	2	1.09814	0.97114	1.02125	1.01560
$g_\rho/4\pi$	2	0.64271	0.68912	0.70261	0.75467
η_1	3				0.64992
η_2	4				0.10975
κ_3	3		1.9195	1.6582	3.2467
κ_4	4		-7.3928	-6.6045	0.63152
ζ_0	4				2.6416
η_ρ	3				0.3901
α_1	5				1.7234
α_2	5				-1.5798
$f_V/4$	3				0.1734
$f_\rho/4$	3			1.0332	0.9619
β_S	4			-0.10689	-0.09328
β_V	4			-0.26545	-0.45964

TABLE 1.3: Parameter sets relevant to this work [1, 2]. Notice that the sets correspond to different levels of truncation in the FST lagrangian and that the naturalness assumption essentially holds.

Euler-Lagrange equation is used to determine the equation of motion for the baryon field (the Dirac equation). Due to the fact that this equation is linear in the baryon field (and because the meson fields are classical), one may seek normal mode solutions of the form $\psi(x_\mu) = \psi(\vec{x})exp\{iEt\}$ [20].[14]

To illustrate the Hartree formalism, consider a simple single-particle hamiltonian

$$h(\vec{x}) = -i\vec{\alpha} \cdot \vec{\nabla} + g_V V_0(r) + \beta\left[M - g_S\phi_0(r)\right] \tag{1.21}$$

which satisfies the Dirac equation

$$h(\vec{x})\psi_n(\vec{x}) = E_n\psi_n(\vec{x}) \tag{1.22}$$

where E_n is the energy eigenvalue. The solution to Eq. (1.22) is

$$\psi_n(\vec{x}) = \frac{1}{r}\begin{pmatrix} iG_n(r)\Phi_{\kappa m} \\ -F_n(r)\Phi_{-\kappa m} \end{pmatrix}\zeta_t \tag{1.23}$$

Here ζ_t is a two component spinor and t is 1/2 (-1/2) for protons (neutrons). The $\Phi_{\kappa m}$ are the spin spherical harmonics. Substituting this wave function into the Dirac equation, we acquire the following Hartree equations

$$\left[\frac{\partial}{\partial r} + \frac{\kappa}{r}\right]G_n(r) - \left[E_n - g_V V_0(r) + M - g_S\phi_0(r)\right]F_n(r) = 0 \tag{1.24}$$

$$\left[\frac{\partial}{\partial r} - \frac{\kappa}{r}\right]F_n(r) + \left[E_n - g_V V_0(r) - M + g_S\phi_0(r)\right]G_n(r) = 0 \tag{1.25}$$

This system of equations can readily be extended to incorporate the higher order effects included in the full FST lagrangian.

---

[14]The framework of Hartree theory is discussed in appendix C.

In order to solve these Hartree equations, the free parameters in the lagrangian must be fixed. These constants are determined by least-squares fits to experimental data from ordinary nuclei along the valley of stability. These fits are conducted at various levels of truncation in the underlying lagrangian [1]. The results of these parameter fits are shown in Table 1.3. Note that the addition of still higher order terms to the full FST lagrangian has little or no positive effect on the calculations [1]. Once the values of these parameters are known, this lagrangian can be used to predict other properties of ordinary nuclei. One example which demonstrates the predictive power of this method is its application to the study of nuclei far from stability [16, 21]. This is illustrated in part by Figs. 1.2 and 1.3.

To justify this approach, we directly employ density functional theory (DFT). DFT is a theoretical framework which allows one to calculate the GS properties of many-body systems without carrying around all the baggage contained in the many-particle wave functions [22]. Two points are of interest here:

- first, the GS expectation value of any observable is a unique functional of the exact GS density; moreover, if the expectation value of the hamiltonian is considered as a functional of the density, the exact GS density can be determined by minimizing the energy functional;

- second, the exact GS scalar and vector densities, energy, and chemical potential for the fully interacting many-fermion system can be reproduced by a collection of (quasi) fermions moving in appropriately defined local, classical fields [3].

This result follows from the Kohn-Sham analysis [22]. Therefore, instead of having to solve the many-body equations with quantum fields, one only needs to solve a series of self-consistent, single-particle equations with classical fields. In other words, Kohn-Sham theory is formally equivalent to relativistic Hartree theory. Once the exact energy functional is determined, in principle all many-body effects are
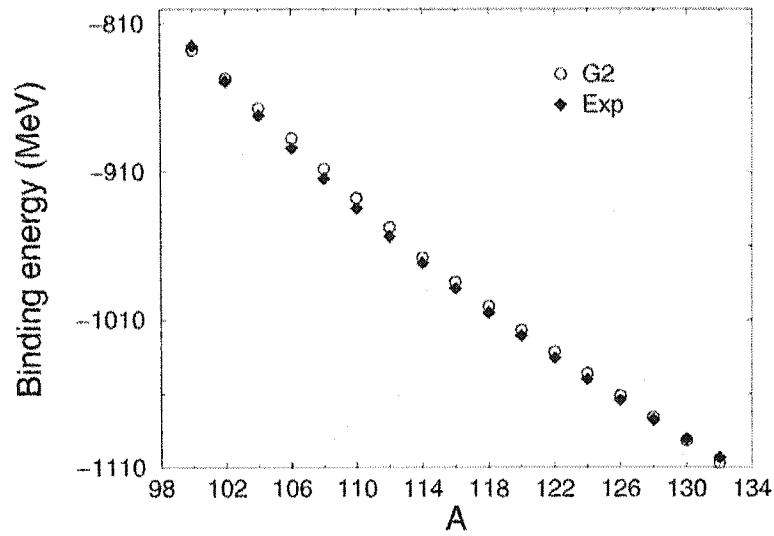
FIG. 1.2: Comparison between experimental and calculated total binding energies for Sn-isotopes using the G2 parameter set. Courtesy of Huertas [21].
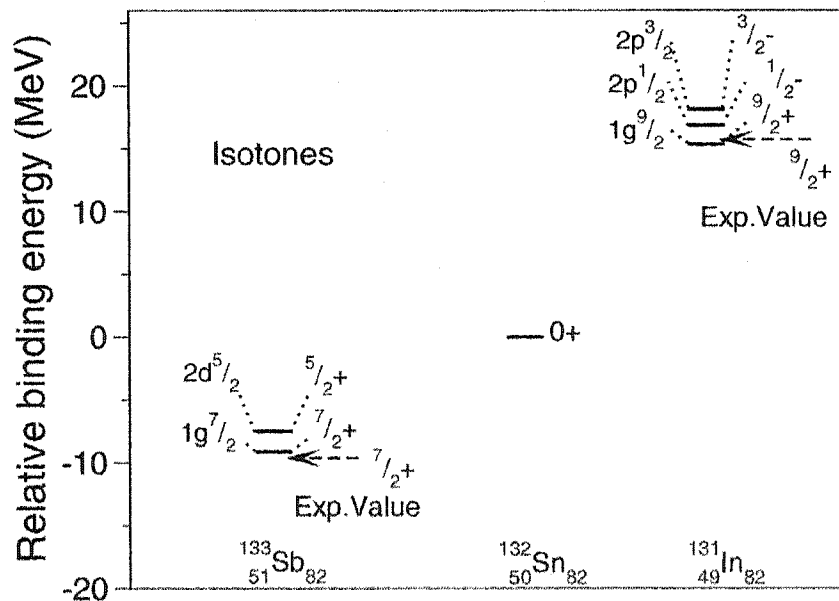
FIG. 1.3: Level spectrum of isotones of $^{132}_{50}Sn_{82}$ differing by one proton. Courtesy of Huertas [21].

included. Consequently, the problem is now reduced to determining the correct form of the energy functional, which follows from the appropriate lagrangian. The full interacting lagrangian of FST gives a suitable energy functional from which the relativistic Hartree (Kohn-Sham) equations follow essentially as field equations. As a result, DFT provides an underlying theoretical justification for this approach.[15]

We now turn our attention to applying the above framework to the specific problems considered in this thesis.

1.3 Strange Superheavy Nuclei

The semi-empirical mass formula (SEMF) is a useful expression for the average energy of a nucleus in the GS. It uses the liquid drop model to simulate the nucleus [5]. The SEMF is given by

$$\frac{E}{B} = a_1 + a_2 \frac{1}{B^{1/3}} + a_3 \frac{Z(Z-1)}{B^{4/3}} + a_4 \frac{(B-2Z)^2}{B^2} + a_5 \frac{\lambda}{B^{7/4}} \qquad (1.26)$$

where E is the total energy, Z is the number of protons, and $\lambda = +1$ for odd-odd, 0 for odd-even, and -1 for even-even nuclei.[16] The first term in Eq. (1.26) is the bulk term, which is essentially the binding energy of infinite nuclear matter. The second term is the surface term; the nucleons at the surface only feel an attraction from nucleons in the interior, which gives rise to a surface energy. The energy of the Coulomb interaction of the Z protons is represented by the third term in Eq. (1.26). The fourth term, the symmetry energy, results from the fact that nuclei prefer to have N = Z. The final term is the pairing energy; nuclei like to have even numbers

---

[15]The scalar and vector meson fields here play the role of relativistic Kohn-Sham potentials [3, 22].

[16]Odd-odd refers to a nucleus with an odd number of both protons and neutrons. Odd-even and even-even are similarly defined.

of the same particles. The constants $a_1, \ldots a_5$ are determined by fitting the SEMF to experimental data; they are given in [5].

An inspection of this SEMF reveals that the single largest limiting factor in the creation of very large nuclei is the Coulomb repulsion. One way to overcome this barrier is to include hyperons in nuclei [23, 24, 25]. Consider the hyperons Λ^0, $\Sigma^{(\pm,0)}$, and $\Xi^{(-,0)}$. The lightest hyperon, the Λ, has a negative binding energy in nuclear matter [26] and decays weakly into non-strange matter. The Σ's appear to have a repulsive nuclear potential [27, 28, 29]. Next in mass are the Ξ's; experimental evidence suggests that the binding energy of a single Ξ in nuclear matter is negative [30, 31, 32]. In addition, the reaction

$$2\Lambda \to N + \Xi \tag{1.27}$$

becomes energetically favorable for some critical number of Λ's in the nuclear medium [23]. As a result, we expect that for large systems the addition of Λ's and Ξ's is desirable, but the inclusion of Σ's would have little or no positive effect. Therefore we consider matter composed solely of N's, Λ's, and Ξ's. The inclusion of the Ξ^-'s offsets the Coulomb repulsion of the protons; this potentially allows for the creation of arbitrarily large nuclei by diminishing the importance of the Coulomb term in the SEMF. To minimize the effect of the Coulomb term we investigate this class of nuclei such that $Q = 0$. These nuclei are stable against strong decay. Consequently, they decay on weak interaction timescales, which enhances the potential for their detection. The purpose of this section of the thesis is to model the surface structure, and acquire the surface energy from the calculated SEMF, for this class of nuclei.

To accomplish this, we must solve the nuclear many-body problem. Using the framework of FST, we construct a rudimentary effective lagrangian density invariant under $SU(2)_L \otimes SU(2)_R$ symmetry using hadrons as degrees of freedom [1, 5]. For

the purposes of this calculation, we consider simple scalar and neutral vector meson exchange exclusively. Keeping only the lowest order terms and a pair of nonlinear scalar field self-couplings, the resulting lagrangian density is

$$\mathcal{L}(x_\mu) = -\bar{N}\left[\gamma_\mu\left(\frac{\partial}{\partial x_\mu} - ig_V V_\mu\right) + M - g_S\phi\right]N - \frac{1}{2}\left[\left(\frac{\partial\phi}{\partial x_\mu}\right)^2 + m_S^2\phi^2\right]$$
$$-\frac{1}{4}V_{\mu\nu}V_{\mu\nu} - \frac{1}{2}m_V^2 V_\mu V_\mu - \frac{\kappa_3 g_S m_S^2}{3!M}\phi^3 - \frac{\kappa_4 g_S^2 m_S^2}{4!M^2}\phi^4 \tag{1.28}$$

This lagrangian density is then converted into a hamiltonian density, which in this problem is equivalent to the energy density. The effective nucleon mass,

$$M^* \equiv M - g_S\phi_0 \tag{1.29}$$

is determined by solving the scalar field equation self-consistently at each point [5, 20]. The coupling constants are fit to reproduce experimental values of various ordinary nuclei; specifically the parameter sets NLC and Q1, which include the nonlinear scalar self-couplings, are used [1, 2].[17]

In order to calibrate our approach, we calculate the GS densities of ordinary finite nuclei with N = Z. To model finite nuclei we must retain the spherically symmetric spatial variations of the meson fields in the lagrangian density, shown by

$$\delta\mathcal{L} = -\frac{1}{2}\left(\nabla\phi_0\right)^2 + \frac{1}{2}\left(\nabla V_0\right)^2 \tag{1.30}$$

The source terms are evaluated using a local density approximation; at every point within the nucleus the baryons are assumed to be a local Fermi gas with states filled up to $k_F(r)$. We acquire the scalar mean field equation by minimizing the energy functional with respect to the scalar field; a similar approach yields the vector mean

---

[17]These parameter sets is listed in Table 1.3.

field equation [20]. The resulting meson equations are given by the following:

$$\left(\nabla^2 - m_S^2\right)\phi_0 - \frac{\kappa_3 g_S m_S^2}{2M}\phi_0^2 - \frac{\kappa_4 g_S^2 m_S^2}{6M^2}\phi_0^3 = -g_S \rho_S \tag{1.31}$$

$$\left(\nabla^2 - m_V^2\right)V_0 = -g_V \rho_B \tag{1.32}$$

where the baryon and scalar densities are

$$\rho_B(r) = \frac{4}{(2\pi)^3}\int_0^{k_F} d^3k \tag{1.33}$$

$$\rho_S(r) = \frac{4}{(2\pi)^3}\int_0^{k_F} d^3k \frac{M^*}{(k^2 + M^{*2})^{1/2}} \tag{1.34}$$

respectively (with the degeneracy $\gamma = 4$ for nuclear matter).

The nonlinear scalar field equation is solved as a finite difference equation utilizing a shooting method. The boundary conditions are determined by noting that the baryon density vanishes at the surface in this approach, and then solving the linear scalar field equation outside [20]. However, these boundary conditions are exact only in the linear case; a correction term must be added to compensate for the effects of nonlinear terms in the scalar field equation. Also, it was initially assumed (as in [20]) that because the derivative term in the vector field equation is small compared to the vector meson mass, it can be neglected. However, due to the fact that the vector field energy is so large, iteration on the vector field has a significant effect on the calculations. The total energy is minimized with respect to the local Fermi wave number, while keeping fixed the baryon number, B. The constraint of fixed B is incorporated with a Lagrange multiplier, which is the chemical potential. The resulting constraint equation is

$$\mu = g_V V_0(r) + [k_F^2(r) + M^{*2}(r)]^{1/2} \tag{1.35}$$

	a_1	a_2
L2	-15.76	26.51
NLC	-15.77	18.01
Q1	-16.10	19.11
Expt.	-15.75	17.8

TABLE 1.4: Calculated values of the bulk and surface energy (in MeV) for nucleon matter (N = Z) using the parameter sets in Table 1.3. The experimental values are also included [5].

and states that the chemical potential must be constant throughout the nucleus [20]. This equation is solved for $k_F(r)$ with given $[\phi_0(r), V_0(r)]$ at each point in space at each step in the calculation.

This approach is more sophisticated than a simple Thomas-Fermi method because we self-consistently solve for the source terms at each point. With the calculated binding energy and baryon number for finite nuclei as well as the binding energy of infinite nuclear matter, we fit the second term in the SEMF, the surface energy, for nuclear matter. As can be seen in Table 1.4, the calculated a_2 is in good agreement with the known experimental value [5], particularly for the more sophisticated FST parameter sets NLC and Q1, thereby validating our approach.

Now we add in hyperons; however, existing experimental data requires that the following assumptions be made:

1. we couple universally to the conserved baryon and isovector currents;

2. a different scalar coupling is used for each baryon. The scalar coupling for the Λ's is fit such that the binding energy of a single Λ in nuclear matter is -28 MeV [26]. However the binding energy of a single Ξ is relatively uncertain, values appearing in the literature range from -40 to -14 MeV. Recent experiments with light nuclei suggest that the value lies on the less bound side of this range [31, 32]; however, it may be more deeply bound for heavy nuclei

	$g_{s\Xi}/g_s$	a_2
NLC	1.0	72.69
	0.95	55.64

TABLE 1.5: Values of the surface energy (in MeV) for matter composed of N's and Ξ's using the NLC parameter set from Table 1.3 for two values of $g_{s\Xi}/g_s$.

[33]. As a result, a number of values for the Ξ scalar coupling are investigated;

3. we continue to utilize the parameter sets for ordinary nuclear matter, NLC and Q1, to generate the nucleon and non-linear scalar couplings.

The addition of new baryons in the theory only requires the inclusion of new source terms in the effective lagrangian density. We investigate a specific sector of the theory by imposing the restrictions

$$Q = 0 \tag{1.36}$$

and

$$|S|/B = 1 \tag{1.37}$$

where S is the total strangeness.[18] Note that the minimum binding energy always occurs such that there are equal numbers of n and p (and consequently equal numbers of Ξ^0 and Ξ^-); therefore the symmetry term in the SEMF is rendered irrelevant. Since there is only one chemical potential, the reactions

$$2\Lambda \rightleftharpoons N + \Xi \tag{1.38}$$

and

$$n + \Xi^0 \rightleftharpoons p + \Xi^- \tag{1.39}$$

---

[18]We also assume an average cascade mass.

are both in equilibrium. Again, using DFT to model finite nuclei, we now investigate the role of the first two terms in the calculated SEMF, shown by

$$\frac{E}{B} = a_1 + a_2 \frac{1}{B^{1/3}} \tag{1.40}$$

Also, by determining the baryon density, we acquire the structure of the surface. An example of the surface structure for a finite nucleus composed of equal numbers of (n, p, Ξ^0, Ξ^-) is shown in Fig. 1.4. Once a number of finite nuclei of this type have been calculated, their binding energy is plotted vs. $B^{-1/3}$; the resulting graph is given in Fig. 1.5. The surface energy, a_2, is then extracted using a fit of the form in Eq. (1.40) and is given in Table 1.5. It was found that the addition of Λ's had little effect on the results.

In addition, an investigation of the possible hyperon-hyperon interaction is conducted by coupling a Φ meson to the conserved strangeness current; we allow the Φ coupling to increase until the many-body system is no longer bound in order to find the maximum allowable value of this coupling.

The work described in this section has been published [34].

1.4   Single Λ-hypernuclei

In chapter 5 of this thesis, the approach developed by FST is expanded to the particular region of the strangeness sector that corresponds to Λ-hypernuclei with $S = -1$ and $T = 0$. To this end, we include a single, isoscalar Λ field in the theory.[19] Now, a Λ-lagrangian is constructed as an additional contribution to the full interact-

---

[19]The Σ is not explicitly included in the present calculation. An idea of the possible impact of $\Lambda - \Sigma$ mixing can be taken from [35]; here the small deviation of hypernuclear magnetic moments from the Schmidt values is discussed as possible evidence for this type of mixing. It should be mentioned that if one views the scalar meson as a two-pion resonance, then the Σ enters implicitly as an intermediate state in our formalism.
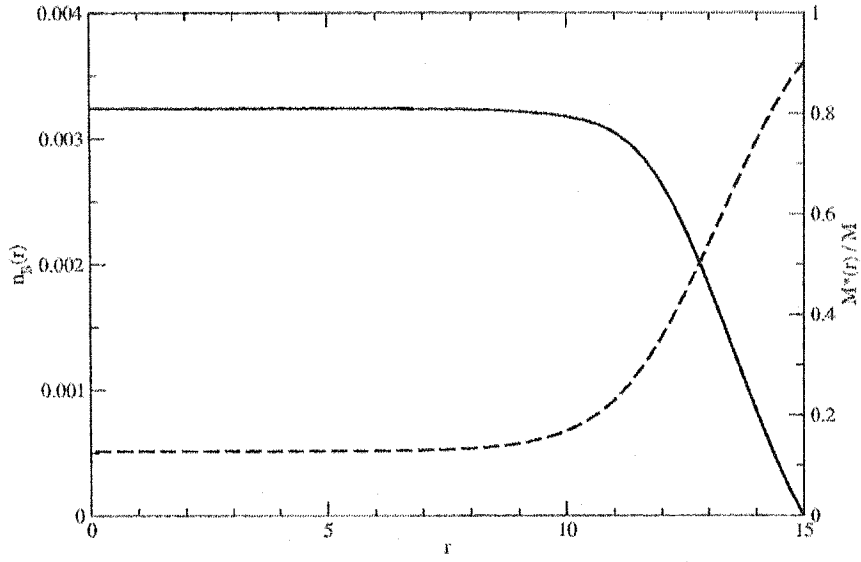
FIG. 1.4: Plot of the baryon density $n_B(r) = \rho_B(r)/M^3$ (solid line) and the effective mass $M^*(r)/M$ (dashed line) vs. r (in units of m_S^{-1}) for a nucleus composed of nucleons and cascades with $r_0 = 15/m_S$, B = 164.918, and $g_{S\Xi}/g_S = 1$ subject to the constraints Q = 0 and $|S|/B = 1$. These results were obtained using the NLC parameter set.
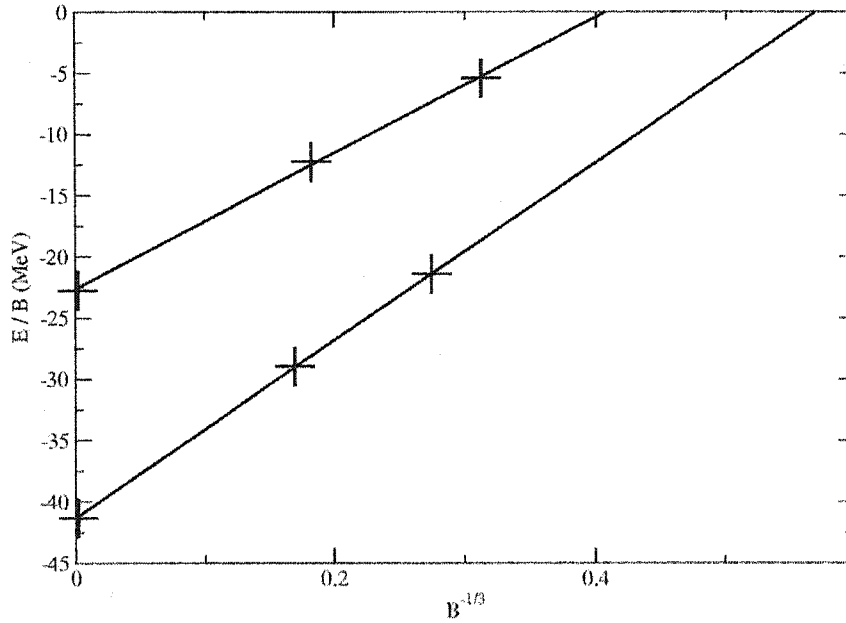
FIG. 1.5: Binding energy vs. $B^{-1/3}$ for matter composed of equal numbers of cascades and nucleons for the NLC coupling set. The upper and lower curves correspond to $g_{S\Xi}/g_S = 0.95$ and 1 respectively. The surface energy is just the slope of these lines.

ing effective lagrangian of FST, consistent with their methodology. Since the Λ is an isoscalar, it does not couple to either a single Yukawa pion or the rho meson. Furthermore, we confine our theory to the mesons already included[20]; thus, the meson lagrangian is unaltered. Note that in this approach, the majority of the complexity is contained within the meson sector of the lagrangian. In the literature, it has been proposed that a tensor coupling to the vector field be included to reproduce the correct experimental spin-orbit splitting of the p-states in Λ-hypernuclei [36, 37]. As it turns out, such a term is in fact a natural extension of our lagrangian in this framework. Additional higher order terms are also included to better approximate the exact energy functional. The full interacting Λ-lagrangian used in this work is

$$
\begin{aligned}
\mathcal{L}_\Lambda(x_\mu) =& -\bar{\Lambda}\left[\gamma_\mu\left(\frac{\partial}{\partial x_\mu} - ig_{V\Lambda}V_\mu\right) + (M_\Lambda - g_{S\Lambda}\phi)\right]\Lambda + \frac{g_{T\Lambda}g_V}{4M}\bar{\Lambda}\sigma_{\mu\nu}V_{\mu\nu}\Lambda \\
&+ \frac{e}{4M}\bar{\Lambda}\lambda_\Lambda\sigma_{\mu\nu}F_{\mu\nu}\Lambda + \mu_1\frac{g_S^2}{2M}\bar{\Lambda}\Lambda\phi^2 + \mu_2\frac{g_V^2}{2M}\bar{\Lambda}\Lambda V_\mu V_\mu \\
&+ i\mu_3\frac{g_S g_V}{M}\bar{\Lambda}\gamma_\mu\Lambda\phi V_\mu
\end{aligned}
\tag{1.41}
$$

This system is treated in the same manner as the Hartree theory discussed previously.

Following the methodology of FST, our Λ-lagrangian contains a number of free parameters. The constants in both the nucleon and meson sectors are taken from the FST parameter set G2, shown in Table 1.3 and corresponding to their full lagrangian. As before, the remaining unconstrained parameters must be determined; they are fixed here via least-squares fits to a series of experimental data: Λ single-particle levels, spin-orbit splittings, and s-p shell excitations of the Λ [8, 9, 10, 38, 39, 40]. The fits are conducted at four different levels of truncation in the Λ-lagrangian. First, a rudimentary 2-parameter fit (essentially based on the assumptions of the

---

[20]The kaon is not included as a degree of freedom in this work. The reason is that, as with the pion, the kaon has no mean field and does not effect the RMFT calculations.

preceding section) reproduces the GS binding energies well, but fails to simulate either the small spin-orbit splitting or s-p shell excitation energies. The 3-parameter fit, with its tensor coupling to the vector field, corrects for the inadequacy in the spin-orbit splitting while maintaining excellent agreement with the GS binding energies. Unfortunately, the 3-parameter fit falls short in describing the full s-p shell excitations for the lightest Λ-hypernuclei, although by $^{40}_{\Lambda}$Ca the correct excitation energy is obtained. The excellent overall quality of this fit is illustrated by Figs. 1.6 and 1.7. Lastly, the new parameters included in the 5-parameter and 6-parameter fits do not make a significant improvement. Once these parameters are fixed, this lagrangian can be used to predict other properties of single Λ-hypernuclei.

1.5 $s_{1/2}$-splittings

One other property that is of interest to calculate here is what we refer to as $s_{1/2}$-splittings. These are GS particle-hole splittings of select single Λ-hypernuclei, such as $^{16}_{\Lambda}$O, which have a Λ in the GS and a hole in the last filled nucleon (proton or neutron) shell. The angular momenta of the Λ and the nucleon hole couple to form a multiplet. For the GS, the Λ is in the $1s_{1/2}$ state; thus, these multiplets have only two states. The size of these splittings is determined by the difference of two particle-hole matrix elements [19]. These particle-hole matrix elements are sums of Dirac two-body matrix elements. The effective interaction utilized here follows directly from the effective theory of the preceding discussion. This interaction, to lowest order, is just that of simple scalar and neutral vector meson exchange [41],
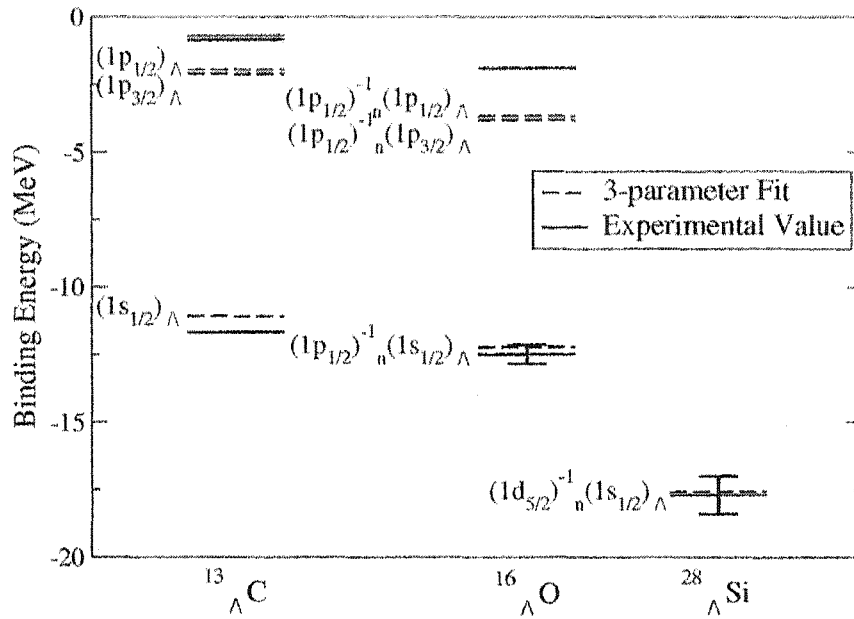
FIG. 1.6: Results of the unweighted 3-parameter fit, along with Fig. 1.7, to a series of experimental data. The G2 parameter set of FST is used for both the nucleon and meson sectors [1]. Note that the experimental splitting between the excited states in $^{16}_{\Lambda}$O is effectively zero.
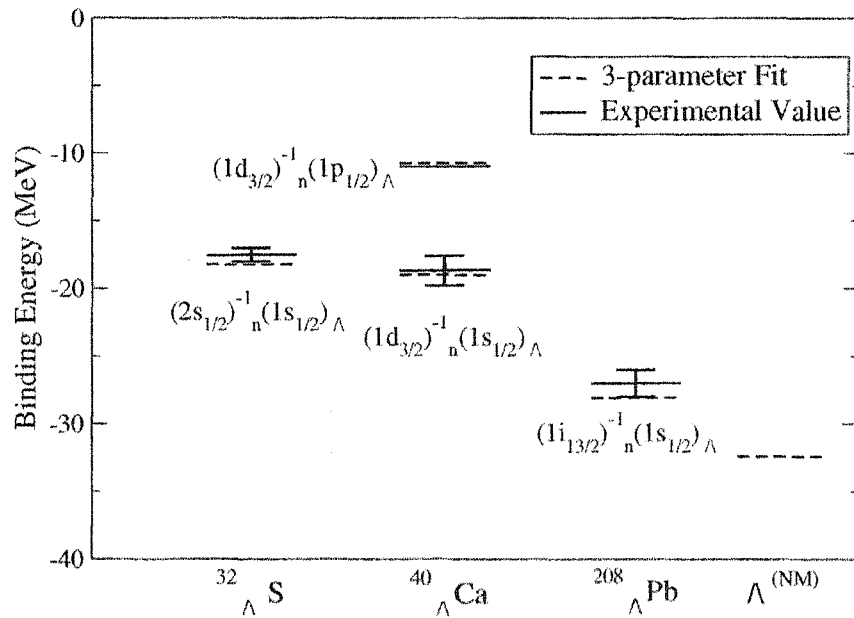
FIG. 1.7: Results of the unweighted 3-parameter fit, along with Fig. 1.6, to a series of experimental data. The G2 parameter set of FST is used for both the nucleon and meson sectors [1]. The calculated binding energy of a single Λ in infinite nuclear matter is also shown.

or[21]

$$V(r_{12}) = \gamma_4^{(1)}\gamma_4^{(2)} \left[\frac{-g_S g_{S\Lambda}}{4\pi} \frac{e^{-m_S r_{12}}}{r_{12}} + \gamma_\mu^{(1)}\gamma_\mu^{(2)} \frac{g_V g_{V\Lambda}}{4\pi} \frac{e^{-m_V r_{12}}}{r_{12}} \right] \qquad (1.42)$$

This simple Yukawa spatial dependence is obtained when retardation is neglected in the meson propagators. With this exception, the full Lorentz structure is maintained [41]. Note that as this effective interaction follows directly from our Λ-lagrangian, there is no isovector contribution in the Λ-N case. In addition, the Λ and nucleon are here distinguishable particles and therefore, no exchange contribution is required in two-body matrix elements. Through angular momentum relations [45] and some algebra, the Dirac matrix elements are reduced to radial Slater integrals. Using the Hartree wave functions from the Λ single-particle calculations to evaluate the integrals, these matrix elements, and consequently the $s_{1/2}$-splitting, can now be fully determined. Once the parameters in the Λ-lagrangian are known, the effective particle-hole interaction is completely specified in this approach. It turns out that in the case of $s_{1/2}$-splittings in Λ-hypernuclei, the only term that contributes to the splitting is the spatial part of the vector exchange. It is of interest to note that this component vanishes in the static limit ($M \rightarrow \infty$) and hence has no direct interpretation in terms of static two-body potentials. This is an interaction between two baryon currents.[22] The results of our calculations are shown in Table 1.6. We note that the calculated doublet splittings shown in Figs. 1.6 and 1.7 all lie within the experimental error bars on the GS binding energies. Predictions are made for $s_{1/2}$-splittings to be measured in an upcoming high-resolution $(e, e'K^+)$ experiment at

---

[21]The retention of higher diagrams in the effective interaction, particularly those including the tensor coupling to the Λ, is left for future work. Also, it is worth noting that while the kaon makes no contribution at the mean field level, kaon exchange may play a role in the effective interaction. Some idea of the relative contribution of kaon exchange can be obtained from the Nijmegen potentials [42, 43, 44]. An investigation of the effect of kaon exchange on the $s_{1/2}$-splittings in effective field theory is also left to future work.

[22]An analog of this current-current interaction in the electromagnetic case is Møller scattering; the spatial components of the currents vanish in the non-relativistic limit [14].
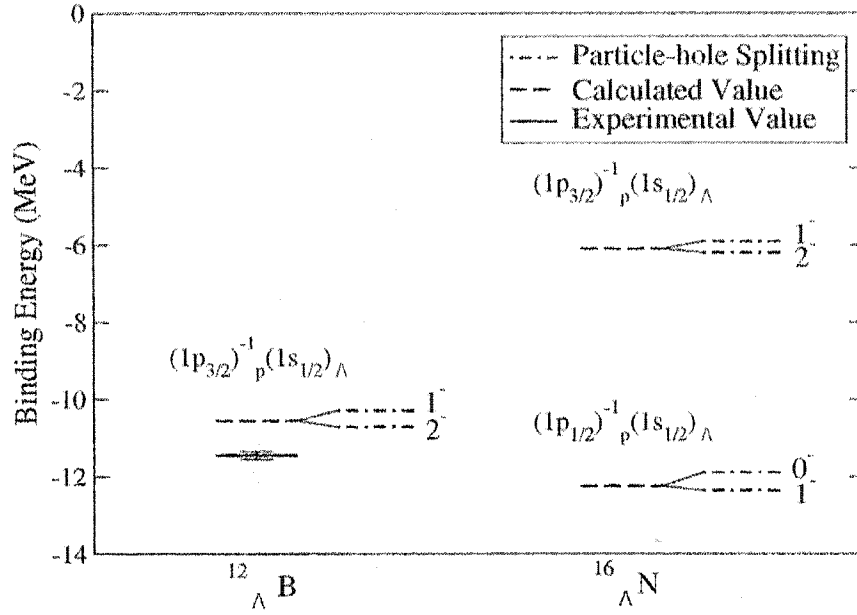
FIG. 1.8: Graph of particle-hole splittings for $^{12}_\Lambda B$ and $^{16}_\Lambda N$ and their respective level orderings. In addition to the GSs, the first calculated excited state in $^{16}_\Lambda N$ is also included. The single-particle calculations were conducted using the 3-parameter fit.

Jefferson National Laboratory; these doublets are shown in Fig. 1.8. Non-relativistic calculations of similar particle-hole splittings have been carried out [46]. The present approach, when applied to ordinary nuclei, is far more complicated as isovector interactions and exchange contributions are both required [41]. As an example of a comparable system in an ordinary nucleus, and to at least partially calibrate the present approach, the calculation of the $s_{1/2}$-splitting in $^{32}_{15}P_{17}$ is included here. The result of this calculation is shown in Fig. 1.9. Comparable systems for ordinary nuclei have also been examined [47].

The work described in the last two sections is currently under review for publication [48].

Nucleus	State	Levels	$|\delta\epsilon|$
$^{12}_{\Lambda}\text{B}$	$(1\text{p}_{3/2})^{-1}_{\text{p}}(1\text{s}_{1/2})_{\Lambda}$	$2^-_{\text{GS}},\ 1^-$	430
$^{16}_{\Lambda}\text{N}$	$(1\text{p}_{1/2})_{\text{p}}(1\text{s}_{1/2})_{\Lambda}$	$1^-_{\text{GS}},\ 0^-$	481
	$(1\text{p}_{3/2})^{-1}_{\text{p}}(1\text{s}_{1/2})_{\Lambda}$	$2^-_{\text{LL}},\ 1^-$	318
$^{16}_{\Lambda}\text{O}$	$(1\text{p}_{1/2})_{\text{n}}(1\text{s}_{1/2})_{\Lambda}$	$1^-_{\text{GS}},\ 0^-$	489
	$(1\text{p}_{1/2})_{\text{n}}(1\text{p}_{3/2})_{\Lambda}$	$2^+_{\text{LL}},\ 1^+$	128
	$(1\text{p}_{1/2})_{\text{n}}(1\text{p}_{1/2})_{\Lambda}$	$1^+_{\text{LL}},\ 0^+$	668
$^{28}_{\Lambda}\text{Si}$	$(1\text{d}_{5/2})^{-1}_{\text{n}}(1\text{s}_{1/2})_{\Lambda}$	$3^+_{\text{GS}},\ 2^+$	293
$^{32}_{\Lambda}\text{S}$	$(2\text{s}_{1/2})_{\text{n}}(1\text{s}_{1/2})_{\Lambda}$	$1^+_{\text{GS}},\ 0^+$	220
$^{40}_{\Lambda}\text{Ca}$	$(1\text{d}_{3/2})^{-1}_{\text{n}}(1\text{s}_{1/2})_{\Lambda}$	$2^+_{\text{GS}},\ 1^+$	310
	$(1\text{d}_{3/2})^{-1}_{\text{n}}(1\text{p}_{1/2})_{\Lambda}$	$2^-_{\text{LL}},\ 1^-$	394
$^{208}_{\Lambda}\text{Pb}$	$(1\text{i}_{13/2})^{-1}_{\text{n}}(1\text{s}_{1/2})_{\Lambda}$	$7^+_{\text{GS}},\ 6^+$	24

TABLE 1.6: $\text{s}_{1/2}$-splittings, and some excited states, are shown with their respective configurations, level orderings, and doublet magnitudes. Here LL denotes lower level and $|\delta\epsilon|$ is in keV.

FIG. 1.9: Particle-hole splitting for the GS of $^{32}_{15}\text{P}_{17}$. The level orderings and splittings are shown for both theory and experiment. Here the FST parameter set G2 was used [1].

1.6 Previous Work

A significant body of work on the subject of hypernuclei exists in the literature; the following is a short summary of previous research relevant to the present study. To begin with, we review the previous work on the topic of large, multi-strange hypernuclei. Then, the literature relevant to the two main approaches that have been developed for studying hypernuclei, effective field theories and Y-N potential models, is discussed.[23]

At $T = 0$ and normal nuclear densities, the mass difference between strange and non-strange quarks is less then the Fermi energy of massless non-strange quarks. This opened the possibility that strange quark matter composed of u, d, and s quarks might be stable against strong decay and perhaps even absolutely stable [49, 50]. These systems are characterized by a small charge fraction $Q/B \sim 0$ and a large strangeness fraction $|S|/B \sim 1$. A number of experimental searches for strange matter have been conducted, examples of which are [51, 52, 53, 54]; all have yielded negative results. The plausibility of bound strange matter has also been explored in the hadronic sector. Theoretical investigations of multiple Λ-hypernuclei indicate that they are bound and stable against strong decay. These studies produced systems with binding energies as low as -9 MeV corresponding to $|S|/B \sim 0.2$ [55, 56, 57, 58, 59].

Gal *et al.* suggested that discussions of matter composed of n's, p's, and Λ's must also include Ξ^0's and Ξ^-'s due to the fact that the reaction

$$2\Lambda \rightarrow N + \Xi \tag{1.43}$$

is energetically favorable for some critical number of Λ's in the nuclear medium

---

[23]Here Y denotes a hyperon.

[23]. They investigated possible configurations of bulk matter in the relativistic mean field approach, suggesting binding energies per baryon as low as -25 MeV with a large strangeness fraction; finite nuclear calculations were also performed [24, 27, 60, 61]. In addition, Gal *et al.* fit to a generalized SEMF using a Fermi gas model [62, 63]. Extrapolating from the ordinary SEMF they estimate the bulk and symmetry terms, while leaving the Coulomb term unchanged. In this work the surface energy is simply scaled as inversely proportional to the average baryon mass, yielding a value of 15 MeV. Stoks and Lee challenged these findings using a many-body theory with baryon-baryon potential models. These potentials were developed using an SU(3) extension of the Nijmegen soft-core potentials [42, 43, 64, 65]. In contrast, the latter found that this type of matter is only slightly bound, $E/B \sim -3$ MeV or less [25, 66]. A quark-meson coupling model produced a minimum binding energy of -24.4 MeV with $|S|/B \sim 1.38$ [67]. The effect of adding hyperons has also been explored in application to neutron stars [68, 69, 70, 71].

Now we shift our focus to the literature relevant to the subject of single Λ-hypernuclei. Hadronic effective lagrangians using MFT have been developed to describe hypernuclei. Early models containing only the lowest order terms required much weaker meson couplings to the Λ than to the nucleons to achieve success [72, 73], particularly in the weak spin-orbit interaction. Later, it was suggested that large meson couplings to the Λ consistent with SU(3) were possible if the lagrangian was extended to include tensor couplings [36, 37, 74, 75, 76, 77, 78]. It turns out that the spin-orbit splitting is very sensitive to the size of the tensor coupling to the vector field. Some of these models were formulated to include additional hyperons. The quark mean field model [79], and a predecessor the quark-meson coupling model [80], couple the mesons self-consistently to the quarks within the baryons; these formalisms reproduce both the weak spin-orbit interaction and Λ single-particle levels. A density dependent relativistic hadronic field theory that was

extended to the strangeness sector by including octet hyperons was also applied to the case of single Λ-hypernuclei [81]. More recently, effective theories consistent with $SU(3)_L \otimes SU(3)_R$ have been constructed. The linear realization of chiral symmetry in this case was inadequate to fully describe the system [82]; as a result, this approach was reformulated into a nonlinear chiral framework [83, 84]. However, these systems require 8 Goldstone bosons. Another study of interest uses strangeness changing response functions calculated from a random phase approximation to an effective mean-field lagrangian [85]. Using this approach, the spectra of $^{16}_\Lambda O$ and $^{40}_\Lambda Ca$ are analyzed and the resulting GS particle-hole splittings are small.

The following studies have attempted to fit potentials to the hyperon-nucleon interaction. Experimental data from (π^+, K^+) and (K^-, π^-) reaction studies has been analyzed to obtain a nonlocal and density-dependent Λ-nucleus potential [26, 86]. Global optical potentials for Λ scattering off nuclei were developed from nucleon-nucleus Dirac optical potentials and the constituent quark-model values of the meson-baryon coupling constants [87]. The hypernuclear mass dependence of the binding energies is reproduced by a Λ moving in a Woods-Saxon potential [88]. The Nijmegen group has developed Y-N potentials based on the assumption of SU(3) symmetry [42, 65, 64]; this fixes the baryon-meson coupling constants from N-N scattering fits. Similarly, potentials were constructed by the Julich group assuming SU(6) symmetry [89]. G-matrix calculations using both the Nijmegen and Julich models for the free Y-N potential have been applied to hypernuclei [90, 91, 92]. Comparable G-matrix calculations with a SU(6) quark-model baryon-baryon interaction [93] and Skyrme-like hyperon-nucleon potentials [94] have also been investigated. However, the G-matrix is both energy-dependent and nonhermitian; the unitary-model-operator approach is an attempt to reformulate the problem to eliminate these drawbacks and is constructed on the basis of an effective interaction [95]. Self-consistent Brueckner-Hartree-Fock calculations with a Nijmegen soft-core

hyperon-nucleon potential are used to determine properties of single and multi-lambda hypernuclei in [96, 97]. Other recent approaches include microscopically using the Fermi hypernetted chain method to obtain the Λ-N and Λ-N-N potentials [98, 99] and using a quark model with one boson exchange potentials [100].

1.7 New Contributions in this Thesis

The effective field theory approach of FST, described in the preceding discussion, was developed to model the nuclear many-body system. This theory has the intrinsic strength of incorporating directly into its framework all of the following: microscopic causality, Lorentz invariance, electromagnetic gauge invariance, special relativity, spontaneously broken chiral symmetry, and the underlying symmetry structure of QCD. In addition, DFT acts as a theoretical justification for this approach. This methodology represents part of a ongoing effort to understand the dynamics and structure of the nucleus. Their formalism was designed specifically to describe nuclei in the valley of stability. Recently, research has been conducted to extend this approach outside of this region [16, 21, 34]. The present work focuses on the expansion of this theory to the strangeness sector. The main contributions of this thesis are divided into three sections below.

1. In chapter 4, we consider the application of the FST approach to strange superheavy nuclei. The new contributions to this subject are:

   - the coupled, nonlinear field equations following from Eqs. (1.28) and (1.31) - (1.35) are solved numerically with appropriate boundary conditions for ordinary finite nuclei;

   - the resulting baryon density and scalar field provide a picture of the size and shape of the surface of ordinary nuclei;

- the surface energy of ordinary nuclei is extracted by fitting to the SEMF and is in agreement with experiment. This successfully calibrates the approach;

- cascade-nucleon (ΞN) matter subject to the constraints $Q = 0$ and $|S|/B = 1$ is then similarly studied for a range of Ξ scalar couplings;

- the determined densities again give a picture of the size and shape of the surface of ΞN nuclei;

- the surface energy of ΞN nuclei is also acquired by fitting to the SEMF;

- with the Λ scalar coupling fit to experiment, the inclusion of Λ's has little effect on the results.

2. In chapter 5, we consider single Λ-hypernuclei using the methodology of FST. The following are a list of the main new contributions of the present work:

- a minimalist extension is made to the strangeness $S = -1$ sector in which an isoscalar Λ is included in the full FST effective lagrangian;

- Huertas' program to solve the relativistic Hartree equations of FST [16] is appropriately modified and extended;

- parameter fits to experimental data are conducted at various levels of truncation in the new Λ-lagrangian;

- it is found that the 3-parameter fit obtains excellent overall agreement with the experimental data;

- it is also determined that the inclusion of more parameters does not significantly improve the fit;

- the resulting effective lagrangian is used to predict the GS binding energies, densities, and single-particle spectra of other single Λ-hypernuclei.

3. Chapter 6 is dedicated to a specific phenomena of single Λ-hypernuclei, $s_{1/2}$-splittings. The new contributions of the present work are:

- the effective particle-hole interaction is derived from the previously determined effective lagrangian;

- it is discovered that the only term that contributes to the $s_{1/2}$-splittings is the spatial part of the neutral vector exchange;

- it is also found that the GS doublet splittings of all the Λ-hypernuclei used in the fitting procedure lie within current experimental error on the GS binding energies;

- predictions are made for the $s_{1/2}$-splittings in $^{12}_{\Lambda}$B and $^{16}_{\Lambda}$N which will be measured in an upcoming experiment at the Thomas Jefferson National Accelerator Facility [11, 12];[21]

- the $s_{1/2}$-splitting in a comparable ordinary nucleus $^{32}_{15}$P$_{17}$ successfully calibrates the approach; however, this calculation is more complicated as isovector interactions and exchange contributions are now required.

CHAPTER 2

Effective Field Theory

In this chapter we review the methodology of FST. They approach the nuclear many-body problem by constructing an effective field theory that retains the underlying symmetries of QCD as well as the principles of both special relativity and quantum mechanics [1]. At low-energy, the quarks are confined in hadrons. Therefore, hadrons are the desired degrees of freedom here and the ones which FST use to construct an effective lagrangian. The nonlinear realization of spontaneously broken chiral symmetry is illustrated through a system of pions, nucleons, and rho mesons. They incorporate Goldstone pions through the field

$$U(x_\mu) \equiv \xi(x_\mu) \mathbf{1} \xi(x_\mu) = e^{i\pi(x_\mu)/f_\pi} \mathbf{1} e^{i\pi(x_\mu)/f_\pi} \qquad (2.1)$$

where the pion field, $\pi(x_\mu) = \frac{1}{2}\vec{\tau} \cdot \vec{\pi}$, appears to all orders, τ is a Pauli matrix, and f_π is the pion-decay constant. Here the pion field enters as the phase in a chiral rotation of the identity matrix in isospin space [1]. An isodoublet nucleon field is included, represented by

$$N(x_\mu) = \begin{pmatrix} p(x_\mu) \\ n(x_\mu) \end{pmatrix} \qquad (2.2)$$

41

The upper (lower) component corresponds to the proton (neutron). To account for the symmetry energy in nuclear matter, an isovector-vector rho meson, $\rho_\mu(x_\nu) = \frac{1}{2}\vec{\tau}\cdot\vec{\rho}$, is also included.

The nonlinear realization of chiral symmetry is defined by global transformations, L and R of the subgroups $SU(2)_L$ and $SU(2)_R$ respectively, such that

$$L \otimes R: \quad (\xi, \rho_\mu, N) \to (\xi', \rho'_\mu, N') \tag{2.3}$$

where

$$\xi'(x_\mu) = L\xi(x_\mu)h^\dagger(x_\mu) = h(x_\mu)\xi(x_\mu)R^\dagger \tag{2.4}$$

$$\rho'_\mu(x_\mu) = h(x_\mu)\rho_\mu h^\dagger(x_\mu) \tag{2.5}$$

$$N'(x_\mu) = h(x_\mu)N(x_\mu) \tag{2.6}$$

Eq. (2.4) defines $h(x_\mu)$ as an implicit function of $\pi(x_\mu)$, L, and R. The transformations shown in Eqs. (2.4) - (2.6) are a realization of the chiral group [1].

The following boson fields are also incorporated into this framework, the first two of which are *isoscalar chiral singlets*. A scalar field, ϕ, is included to simulate the medium-range nuclear attraction; physically, the ϕ is an effective field that represents all of the two-pion (and multi-pion) resonances in the isoscalar-scalar channel. Next, they incorporate a neutral vector meson, V_μ, to reproduce the short-range nuclear repulsion; this is another effective field corresponding to all the multi-pion and ω meson exchanges in the isoscalar-vector channel. Lastly, a photon field, A_μ, is added to take into consideration the electromagnetic structure of nuclei.

FST now have the basic building blocks necessary to construct a lagrangian. However, as all possible combinations of the fields (and their derivatives), consistent with this framework, are included, this lagrangian contains an infinite number of

terms. To conduct any meaningful calculation, this lagrangian needs to be truncated at some level. This requires that the terms be organized is some logical manner; FST utilize both NDA and RMFT to accomplish this.[1] NDA is a framework which identifies all the dimensional factors of a given term. Once these dimensional factors, and some appropriate counting factors, are extracted from a term, the remaining dimensionless constant is of $O(1)$ [17, 18]. This assumption is known as "naturalness." RMFT states that when the baryon density becomes appropriately large, the sources and meson fields can be replaced by their expectation values; here, the expectation values of the meson fields are just their classical fields [5]. Then we notice that while the meson mean fields are large, the ratios of these fields to the chiral symmetry breaking scale, M, are small. Furthermore, the size of derivatives is related to k_F, which is also small compared to M. These effects are shown by [5]

$$\frac{\Phi}{M}, \frac{W}{M} \sim \frac{1}{3}; \qquad \frac{k_F}{M} \sim \frac{1}{4} \qquad (2.7)$$

where the scaled meson mean fields are defined as

$$\Phi(\vec{x}) \equiv g_S\phi_0; \quad W(\vec{x}) \equiv g_V V_0; \quad R(\vec{x}) \equiv g_\rho b_0; \quad A(\vec{x}) \equiv eA_0 \qquad (2.8)$$

The ordering principle developed by FST is

$$\nu = \frac{n}{2} + b + d \qquad (2.9)$$

where for a given term ν is the order, n is the number of fermion fields, b is the number of non-Goldstone bosons, and d is the number of derivatives.[2] Now a controlled

---

[1] A more detailed discussion of both NDA and RMFT is contained in appendix B.

[2] It should be mentioned that the number of derivatives in Eq. (2.9) does not include derivatives of the fermion fields as they are generally associated with the nucleon mass and not a small momentum [1].

expansion is performed in which higher order terms are, in general, progressively smaller.

Using this ordering principle, they construct an effective lagrangian in two components [1]

$$\mathcal{L}_{\mathrm{FST}} = \mathcal{L}_{\mathrm{N}} + \mathcal{L}_{\mathrm{M}} \tag{2.10}$$

The fermion part to order $\nu = 4$ is given by

$$
\begin{aligned}
\mathcal{L}_{\mathrm{N}}(\mathrm{x}_\mu) = & -\bar{\mathrm{N}} \left\{ \gamma_\mu \left[\frac{\partial}{\partial \mathrm{x}_\mu} + i v_\mu - i g_{\mathrm{A}} \gamma_5 a_\mu - i g_{\mathrm{V}} \mathrm{V}_\mu - i g_\rho \rho_\mu \right. \right. \\
& \left. \left. -\frac{i}{2} e \mathrm{A}_\mu \left(1 + \tau_3\right) \right] + (\mathrm{M} - \mathrm{g}_{\mathrm{S}} \phi) \right\} \mathrm{N} + \frac{f_\rho \mathrm{g}_\rho}{4\mathrm{M}} \bar{\mathrm{N}} \sigma_{\mu\nu} \rho_{\mu\nu} \mathrm{N} \\
& + \frac{f_{\mathrm{V}} \mathrm{g}_{\mathrm{V}}}{4\mathrm{M}} \bar{\mathrm{N}} \sigma_{\mu\nu} \mathrm{V}_{\mu\nu} \mathrm{N} + \frac{\kappa_\pi}{\mathrm{M}} \bar{\mathrm{N}} \sigma_{\mu\nu} v_{\mu\nu} \mathrm{N} + \frac{e}{4\mathrm{M}} \bar{\mathrm{N}} \lambda \sigma_{\mu\nu} \mathrm{F}_{\mu\nu} \mathrm{N} \\
& + \frac{ie}{2\mathrm{M}^2} \bar{\mathrm{N}} \gamma_\mu \left(\beta_{\mathrm{S}} + \beta_{\mathrm{V}} \tau_3\right) \mathrm{N} \frac{\partial}{\partial \mathrm{x}_\nu} \mathrm{F}_{\mu\nu} \tag{2.11}
\end{aligned}
$$

where $\lambda = \frac{1}{2} \lambda_{\mathrm{p}} (1 + \tau_3) + \frac{1}{2} \lambda_{\mathrm{n}} (1 - \tau_3)$ and $\lambda_{\mathrm{p}} = 1.793$ ($\lambda_{\mathrm{n}} = -1.913$) is the anomalous magnetic moment of the proton (neutron). Note that for the purposes of this work, the conventions of [5] are used. Here we have defined

$$\mathrm{V}_{\mu\nu} = \frac{\partial \mathrm{V}_\nu}{\partial \mathrm{x}_\mu} - \frac{\partial \mathrm{V}_\mu}{\partial \mathrm{x}_\nu} \tag{2.12}$$

$v_{\mu\nu}$, $\rho_{\mu\nu}$, and $\mathrm{F}_{\mu\nu}$ are similarly defined for v_μ, ρ_μ, and A_μ respectively. Notice that the pions only couple to the fermions through the combinations

$$v_\mu = -\frac{i}{2} \left(\xi^\dagger \frac{\partial \xi}{\partial \mathrm{x}_\mu} + \xi \frac{\partial \xi^\dagger}{\partial \mathrm{x}_\mu} \right) = v_\mu^\dagger \tag{2.13}$$

$$a_\mu = \frac{i}{2} \left(\xi^\dagger \frac{\partial \xi}{\partial \mathrm{x}_\mu} - \xi \frac{\partial \xi^\dagger}{\partial \mathrm{x}_\mu} \right) = a_\mu^\dagger \tag{2.14}$$

To lowest order, both v_μ and a_μ contain derivatives of the pion field; thus soft pions

decouple. The meson lagrangian to order $\nu = 4$ is

$$
\begin{aligned}
\mathcal{L}_{\mathrm{M}}(\mathrm{x}_\mu) =\ & -\frac{1}{2}\left(1 + \alpha_1 \frac{\mathrm{g_S}\phi}{\mathrm{M}}\right)\left(\frac{\partial \phi}{\partial \mathrm{x}_\mu}\right)^2 - \frac{f_\pi^2}{4}\mathrm{tr}\left(\frac{\partial \mathrm{U}}{\partial \mathrm{x}_\mu}\frac{\partial \mathrm{U}^\dagger}{\partial \mathrm{x}_\mu}\right) - \frac{1}{2}\mathrm{tr}\left(\rho_{\mu\nu}\rho_{\mu\nu}\right) \\
& -\frac{1}{4}\left(1 + \alpha_2 \frac{\mathrm{g_S}\phi}{\mathrm{M}}\right)\mathrm{V}_{\mu\nu}\mathrm{V}_{\mu\nu} - \mathrm{g}_{\rho\pi\pi}\frac{2f_\pi^2}{\mathrm{m}_\rho^2}\mathrm{tr}\left(\rho_{\mu\nu}v_{\mu\nu}\right) + \frac{\mathrm{m}_\pi^2 f_\pi^2}{4}\mathrm{tr}\left(\mathrm{U} + \mathrm{U}^\dagger - 2\right) \\
& -\frac{1}{2}\left(1 + \eta_1 \frac{\mathrm{g_S}\phi}{\mathrm{M}} + \frac{\eta_2}{2}\frac{\mathrm{g_S}^2\phi^2}{\mathrm{M}^2}\right)\mathrm{m}_\mathrm{V}^2\mathrm{V}_\mu\mathrm{V}_\mu + \frac{1}{4!}\zeta_0\mathrm{g_V}^2\left(\mathrm{V}_\mu\mathrm{V}_\mu\right)^2 - \frac{1}{4}\mathrm{F}_{\mu\nu}\mathrm{F}_{\mu\nu} \\
& -\left(1 + \eta_\rho\frac{\mathrm{g_S}\phi}{\mathrm{M}}\right)\mathrm{m}_\rho^2\mathrm{tr}\left(\rho_\mu\rho_\mu\right) - \mathrm{m}_\mathrm{S}^2\phi^2\left(\frac{1}{2} + \frac{\kappa_3}{3!}\frac{\mathrm{g_S}\phi}{\mathrm{M}} + \frac{\kappa_4}{4!}\frac{\mathrm{g_S}^2\phi^2}{\mathrm{M}^2}\right) \qquad (2.15)
\end{aligned}
$$

Terms such as $\bar{\mathrm{N}}\mathrm{N}\phi^2$ are redundant in this formulation. This stems from the fact that FST employ meson field redefinitions; since the parameters are free, they are also just redefined. A detailed description of how this lagrangian was constructed is presented in [1].

This still constitutes a system of many-body equations with quantum fields. FST now employ RMFT and Hartree theory to reduce the many-body system to a series of single-particle equations with classical fields.[3] First, the classical, local, time independent meson fields are obtained in terms of the baryon densities through the meson field equations. Next, the Euler-Lagrange equation is used to determine the Dirac equation (the baryon field equation) where the meson fields now provide the local potentials in which the baryons move. Then, it is assumed that each particle is moving in a single-particle potential, which is representative of the average interaction of the particle with all other particles [19]. Due to the fact that the Dirac equation is linear in the baryon field (and because the meson fields are classical), one may seek normal mode solutions of the form $\psi(\mathrm{x}_\mu) = \psi(\vec{\mathrm{x}})exp\{iEt\}$ [20]. The sources are now evaluated by summing over the contributions of the single-particle solutions. The resulting coupled, local, nonlinear, differential equations are referred to as the relativistic Hartree equations. This formalism is now equivalent to Kohn-

---

[3]A more detailed description of the Hartree formalism can be found in appendix C.

Sham theory in DFT; *therefore, DFT provides the theoretical justification for this methodology.*

The single-particle hamiltonian takes the form [1]

$$
\begin{aligned}
h(\vec{x}) = & -i\vec{\alpha}\cdot\vec{\nabla} + W + \frac{1}{2}\tau_3 R + \frac{1}{2}\left(1 + \tau_3\right)A + \beta\left(M - g_s\Phi\right) \\
& -\frac{i}{2M}\beta\vec{\alpha}\cdot\left(f_V\vec{\nabla}W + f_\rho\frac{1}{2}\tau_3\vec{\nabla}R\right) - \frac{i}{2M}\lambda\beta\vec{\alpha}\cdot\vec{\nabla}A \\
& +\frac{1}{2M^2}\left(\beta_S + \beta_V\tau_3\right)\nabla^2 A
\end{aligned}
\tag{2.16}
$$

Since the pion has no mean field in a spherically symmetric system, all of the pion couplings drop out. The Hartree wave functions are of the form

$$
\psi_\alpha(\vec{x}) = \frac{1}{r}\left(\begin{array}{c} iG_a(r)\Phi_{\kappa m} \\ -F_a(r)\Phi_{-\kappa m} \end{array}\right)\zeta_t
\tag{2.17}
$$

Here $\alpha = \{a, m\} = \{nlsj, m\}$, ζ_t is a two component spinor, and t_a is $1/2$ ($-1/2$) for protons (neutrons). The $\Phi_{\kappa m}$ are the spin spherical harmonics. Substituting this wave function into the Dirac equation,

$$
h(\vec{x})\psi_\alpha(\vec{x}) = E_a\psi_\alpha(\vec{x})
\tag{2.18}
$$

one arrives at the following radial Hartree equations

$$
\left[\frac{\partial}{\partial r} + \frac{\kappa}{r}\right]G_a(r) - \left[E_a - U_1 + U_2\right]F_a(r) - U_3G_a(r) = 0
\tag{2.19}
$$

$$
\left[\frac{\partial}{\partial r} - \frac{\kappa}{r}\right]F_a(r) + \left[E_a - U_1 - U_2\right]G_a(r) + U_3F_a(r) = 0
\tag{2.20}
$$

where the single-particle potentials are

$$U_1(r) = W(r) + t_a R(r) + \left(t_a + \frac{1}{2}\right) A(r) + \frac{1}{2M^2}\left(\beta_S + 2t_a\beta_V\right)\nabla^2 A(r) \quad (2.21)$$

$$U_2(r) = M - \Phi(r) \quad (2.22)$$

$$U_3(r) = \frac{f_V}{2M}\frac{\partial W(r)}{\partial r} + t_a\frac{f_\rho}{2M}\frac{\partial R(r)}{\partial r}$$
$$+ \frac{1}{2M}\frac{\partial A(r)}{\partial r}\left[\frac{1}{2}(\lambda_p + \lambda_n) + t_a(\lambda_p - \lambda_n)\right] \quad (2.23)$$

The scalar meson equation is determined by minimizing the variational derivative of the effective lagrangian with respect to the scalar meson field. The other meson equations are constructed in a similar fashion. These meson equations are [1]

$$-\nabla^2\Phi + m_S^2\Phi = g_S^2\rho_S(\vec{x}) - \frac{m_S^2}{M}\Phi^2\left(\frac{\kappa_3}{2} + \frac{\kappa_4}{3!}\frac{\Phi}{M}\right)$$
$$+ \frac{g_S^2}{2M}\left(\eta_1 + \eta_2\frac{\Phi}{M}\right)\frac{m_V^2}{g_V^2}W^2 + \frac{\alpha_1}{2M}\left[\left(\vec{\nabla}\Phi\right)^2 + 2\Phi\nabla^2\Phi\right]$$
$$+ \frac{\alpha_2 g_S^2}{2Mg_V^2}\left(\vec{\nabla}W\right)^2 + \frac{g_S^2\eta_\rho}{2M}\frac{m_\rho^2}{g_\rho^2}R^2 \quad (2.24)$$

$$-\nabla^2 W + m_V^2 W = g_V^2\left[\rho_B(\vec{x}) + \frac{f_V}{2M}\vec{\nabla}\cdot\left(\rho_B^T(\vec{x})\hat{r}\right)\right] - \left(\eta_1 + \frac{\eta_2}{2}\frac{\Phi}{M}\right)\frac{\Phi}{M}m_V^2 W$$
$$- \frac{1}{3!}\zeta_0 W^3 + \frac{\alpha_2}{M}\left(\vec{\nabla}\Phi\cdot\vec{\nabla}W + \Phi\nabla^2 W\right) - \frac{e^2 g_V}{3g_\gamma}\rho_{chg}(\vec{x}) \quad (2.25)$$

$$-\nabla^2 R + m_\rho^2 R = \frac{1}{2}g_\rho^2\left[\rho_3(\vec{x}) + \frac{f_\rho}{2M}\vec{\nabla}\cdot\left(\rho_3^T(\vec{x})\hat{r}\right)\right] - \eta_\rho\frac{\Phi}{M}m_\rho^2 R$$
$$- \frac{e^2 g_\rho}{g_\gamma}\rho_{chg}(\vec{x}) \quad (2.26)$$

$$-\nabla^2 A = e^2\rho_{chg}(\vec{x}) \quad (2.27)$$

The baryon sources become the densities in the meson equations and are given here

by [1]

$$\rho_S(\vec{x}) \ = \ \sum_a \frac{2j_a + 1}{4\pi r^2} \left(G_a^2(r) - F_a^2(r) \right) \tag{2.28}$$

$$\rho_B(\vec{x}) \ = \ \sum_a \frac{2j_a + 1}{4\pi r^2} \left(G_a^2(r) + F_a^2(r) \right) \tag{2.29}$$

$$\rho_B^T(\vec{x}) \ = \ \sum_a \frac{2j_a + 1}{4\pi r^2} 2G_a(r)F_a(r) \tag{2.30}$$

$$\rho_3(\vec{x}) \ = \ \sum_a \frac{2j_a + 1}{4\pi r^2} (2t_a) \left(G_a^2(r) + F_a^2(r) \right) \tag{2.31}$$

$$\rho_3^T(\vec{x}) \ = \ \sum_a \frac{2j_a + 1}{4\pi r^2} (2t_a) 2G_a(r)F_a(r) \tag{2.32}$$

The charge density is made up of two components

$$\rho_{chg}(\vec{x}) = \rho_d(\vec{x}) + \rho_m(\vec{x}) \tag{2.33}$$

where the first, the direct nucleon charge density, is

$$\rho_d(\vec{x}) = \rho_p(\vec{x}) + \frac{1}{2M} \vec{\nabla} \cdot \left(\rho_a^T(\vec{x})\hat{r} \right) + \frac{1}{2M^2} \left[\beta_S \nabla^2 \rho_B + \beta_V \nabla^2 \rho_3 \right] \tag{2.34}$$

and the second, the vector meson contribution, is

$$\rho_m(\vec{x}) = \frac{1}{g_\gamma g_\rho} \nabla^2 R + \frac{1}{3g_\gamma g_V} \nabla^2 W \tag{2.35}$$

The point proton and nucleon tensor densities in Eq. (2.34) are

$$\rho_p(\vec{x}) \ = \ \frac{1}{2} \sum_a \frac{2j_a + 1}{4\pi r^2} (1 + 2t_a)(G_a^2(r) + F_a^2(r))$$

$$= \ \frac{1}{2} (\rho_B + \rho_3) \tag{2.36}$$

$$\rho_a^T(\vec{x}) \ = \ \sum_a \frac{2j_a + 1}{4\pi r^2} 2\lambda G_a(r)F_a(r) \tag{2.37}$$

respectively. Finally, the energy functional is given by [1]

$$E = \sum_a E_a - \int d^3x U_m \tag{2.38}$$

where

$$
\begin{aligned}
U_m \equiv & -\frac{1}{2}\Phi\rho_S + \frac{1}{2}W\left(\rho_B + \frac{f_V}{2M}\vec{\nabla}\cdot\rho_B^T\hat{r}\right) + \frac{1}{4}R\left(\rho_3 + \frac{f_\rho}{2M}\vec{\nabla}\cdot\rho_3^T\hat{r}\right) + \frac{1}{2}A\rho_d \\
& + \frac{m_S^2}{g_S^2}\frac{\Phi^3}{M}\left(\frac{\kappa_3}{12} + \frac{\kappa_4}{24}\frac{\Phi}{M}\right) - \frac{\eta_\rho}{4}\frac{\Phi}{M}\frac{m_\rho^2}{g_\rho^2}R^2 - \frac{\Phi}{4M}\left(\eta_1 + \eta_2\frac{\Phi}{M}\right)\frac{m_V^2}{g_V^2}W^2 \\
& - \frac{1}{4!g_V^2}\zeta_0 W^4 + \frac{\alpha_1}{4g_S^2}\frac{\Phi}{M}(\nabla\Phi)^2 - \frac{\alpha_2}{4g_V^2}\frac{\Phi}{M}(\nabla W)^2
\end{aligned}
\tag{2.39}
$$

The radial Hartree equations and the meson equations form a system which is solved self-consistently until a global convergence is achieved. FST wrote a program to numerically solve the coupled, local, nonlinear, differential equations. Huertas has written an independent program which reproduces the results of FST [16, 21]. The free parameters in this system are g_S, g_V, g_ρ, η_1, η_2, η_ρ, κ_3, κ_4, ζ_0, m_S, f_V, α_1, α_2, f_ρ, β_S, and β_V. Here we take $m_V = 782$ MeV and $m_\rho = 770$ MeV; these numbers correspond to the physical masses of the ω and ρ mesons respectively. The constants are fit by FST to a series of experimental data along the valley of stability at various levels of truncation in the underlying effective lagrangian [1]. The last three parameters are fit to the electromagnetic properties of the nucleon. The remaining constants are determined by minimizing a least-squares χ^2 fit of the form

$$\chi^2 = \sum_i \sum_X \left[\frac{X_{exp}^{(i)} - X_{th}^{(i)}}{W_X^{(i)}X_{exp}^{(i)}}\right]^2 \tag{2.40}$$

where 29 pieces of experimental data were used, listed here with their respective weights, $W_X^{(i)}$:

- the binding energy per nucleon, E/B, with W = 0.15% for ^{16}O, ^{40}Ca, ^{48}Ca, ^{88}Sr,

and ^{208}Pb;

- the rms charge radii, $< r^2 >_{chg}^{1/2}$, with W $= 0.2\%$ for ^{16}O, ^{40}Ca, ^{48}Ca, ^{88}Sr, and ^{208}Pb;

- the diffraction-minimum-sharp (d.m.s.) radii, R_{dms}, with W $= 0.15\%$ for ^{16}O, ^{40}Ca, ^{48}Ca, ^{88}Sr, and ^{208}Pb;

- the spin-orbit splittings, ΔE_{SO}, of the least-bound proton and neutron with W $= 5\%$ for^{16}O, 15% for ^{208}Pb, 25% for both ^{40}Ca and ^{48}Ca, and 50% for ^{88}Sr;

- the proton energy, $E_p(1h_{9/2})$, and the proton level splitting, $E_p(2d_{3/2}) - E_p(1h_{11/2})$, in ^{208}Pb with W $= 5\%$ and 25% respectively;

- and the surface energy and symmetry energy coefficients, a_2 and a_4 respectively, with W $= 0.08\%$.

The results of these parameter fits are shown in Table 2.1. Note that these parameters do indeed satisfy the naturalness assumption made earlier and as a result, higher order terms are successively smaller. Also, note that increasing the level of truncation beyond that of the G1 and G2 parameter sets does not significantly improve the fit. Once the free parameters are determined, *this lagrangian can be used to predict other properties of ordinary nuclei* [1, 16, 21].

	ν	L2	NLC	Q1	Q2	G1	G2
m_S/M	2	0.55378	0.53333	0.53735	0.54268	0.53963	0.55410
$g_S/4\pi$	2	0.83321	0.77607	0.81024	0.78661	0.78532	0.83522
$g_V/4\pi$	2	1.09814	0.97114	1.02125	0.97202	0.96512	1.01560
$g_\rho/4\pi$	2	0.64271	0.68912	0.70261	0.68096	0.69844	0.75467
η_1	3					0.07060	0.64992
η_2	4					-0.96161	0.10975
κ_3	3		1.9195	1.6582	1.7424	2.2067	3.2467
κ_4	4		-7.3928	-6.6045	-8.4836	-10.090	0.63152
ζ_0	4				-1.7750	3.5249	2.6416
η_ρ	3					-0.2722	0.3901
α_1	5					1.8549	1.7234
α_2	5					1.7880	-1.5798
$f_V/4$	3					0.1079	0.1734
$f_\rho/4$	3			1.0332	1.0660	1.0393	0.9619
β_S	4			-0.10689	0.01181	0.02844	-0.09328
β_V	4			-0.26545	-0.18470	-0.24992	-0.45964

TABLE 2.1: Parameter sets developed by FST [1, 2]. Notice that the sets correspond to different levels of truncation in their lagrangian.

CHAPTER 3

Density Functional Theory

DFT is a theoretical framework which allows one to calculate GS properties of many-body systems without carrying around all the baggage contained in the many-particle wave functions. Two theorems are of interest here:

1. the Kohn-Hohenberg theorem — "The GS expectation value of any observable is a unique functional of the exact GS density; moreover, if the expectation value of the hamiltonian is considered as a functional of the density, the exact GS density can be determined by minimizing the energy functional [3]."

2. the Kohn-Sham approach — "The exact GS scalar and vector densities, energy, and chemical potential for the fully interacting many-fermion system can be reproduced by a collection of (quasi) fermions moving in appropriately defined local, classical fields [3]."

These theorems are proven in [22, 101, 102]. The following is a qualitative discussion of the above theorems designed to provide the reader with a basic theoretical justification for the present approach.

First, let us consider the Kohn-Hohenberg theorem. The GS energy of a system can be determined by the Rayliegh-Ritz minimal principle

$$E = \min_{\Psi} \langle \Psi | H | \Psi \rangle \tag{3.1}$$

where Ψ is some normalized trial wave function. Hohenberg and Kohn were the first to reformulate the minimal principle in terms of a trial density, $n(r)$ [101]. This $n(r)$ is determined by integrating $\Psi^*\Psi$ over all variables except one and multiplying by the number of particles. To conduct the minimization of Eq. (3.1), we fix $n(r)$ and denote the trial wave functions with this density as Ψ_n^α [22]. The constrained energy minimum with fixed $n(r)$ is defined as

$$
\begin{aligned}
E_v[n(r)] &\equiv \min_\alpha \langle \Psi_n^\alpha | H | \Psi_n^\alpha \rangle \\
&= \int v_{ext}(r)n(r)dr + F[n(r)]
\end{aligned}
\tag{3.2}
$$

where $v_{ext}(r)$ is some external potential. This potential is uniquely determined by $n(r)$; that is to say there is only one potential, up to an additive constant, that gives rise to the density $n(r)$, and vice versa. Also, the quantity $F[n(r)]$, which is a functional of the density, is defined as

$$F[n(r)] \equiv \min_\alpha \langle \Psi_n^\alpha | (T + U) | \Psi_n^\alpha \rangle \tag{3.3}$$

Here T and U are the kinetic and interaction energy operators. Next, Eq. (3.2) is minimized over all $n(r)$, or

$$
\begin{aligned}
E &= \min_{n(r)} E_v[n(r)] \\
&= \min_{n(r)} \left[\int v_{ext}(r)n(r)dr + F[n(r)] \right]
\end{aligned}
\tag{3.4}
$$

This is the minimum when $n(\mathrm{r})$ is the exact GS density [22].[1] Simply put, regardless of how complicated Eq. (3.1) is, by minimizing the energy functional, we acquire the exact GS density.

Next, we consider the Kohn-Sham approach. We write the Hohenberg-Kohn free energy for a collection of interacting particles as

$$F[n(\mathrm{r})] = F_{NI}[n(\mathrm{r})] + F_{INT}[n(\mathrm{r})] \qquad (3.5)$$

where F_{NI} is the non-interacting kinetic energy and F_{INT} is the interaction energy. F_{INT} is the sum of the Hartree energy, exchange correlation energy, etc., or

$$F_{INT}[n(\mathrm{r})] = E_H[n(\mathrm{r})] + E_{XC}[n(\mathrm{r})] + \cdots \qquad (3.6)$$

Here the Hartree energy is defined as

$$E_H[n(\mathrm{r})] = \frac{1}{2} \int \frac{n(\mathrm{r})n(\mathrm{r}')}{|\vec{r} - \vec{r}'|} d\mathrm{r}d\mathrm{r}' \qquad (3.7)$$

Substituting Eq. (3.5) into Eq. (3.2), we arrive at the relation

$$
\begin{aligned}
E_v[n(\mathrm{r})] &= \int v_{ext}(\mathrm{r})n(\mathrm{r})d\mathrm{r} + F_{NI}[n(\mathrm{r})] + \frac{1}{2} \int \frac{n(\mathrm{r})n(\mathrm{r}')}{|\vec{r} - \vec{r}'|} d\mathrm{r}d\mathrm{r}' + E_{XC}[n(\mathrm{r})] + \cdots \\
&\geq E
\end{aligned} \qquad (3.8)
$$

The corresponding Euler-Lagrange equation, for a given total number of particles, is [22]

$$\delta E_v[n(\mathrm{r})] = \int \delta n(\mathrm{r}) \left[v_{eff}(\mathrm{r}) + \frac{\delta}{\delta n(\mathrm{r})} F_{NI}[n(\mathrm{r})] - \epsilon \right] d\mathrm{r} = 0 \qquad (3.9)$$

___

[1] This statement holds for both nondegenerate and degenerate systems. In the case of degenerate systems, $n(\mathrm{r})$ is any one of the GS densities.

where we have defined

$$v_{eff}(\mathbf{r}) = v_{ext}(\mathbf{r}) + \int \frac{n(\mathbf{r}')}{|\mathbf{r} - \mathbf{r}'|} d\mathbf{r}' + \frac{\delta}{\delta n(\mathbf{r})} E_{XC}[n(\mathbf{r})] + \cdots \qquad (3.10)$$

and ϵ is a Lagrange multiplier introduced to assure particle conservation [22]. Equation (3.9) is identical to the Euler-Lagrange equation for a system of non-interacting particles moving in $v_{eff}(\mathbf{r})$ instead of $v_{ext}(\mathbf{r})$ [22].

Therefore, instead of having to solve the many-body equations with quantum fields, one only needs to solve a series of self-consistent, single-particle equations with classical fields. Thus, Kohn-Sham theory is formally equivalent to relativistic Hartree theory. Once the exact $v_{eff}(\mathbf{r})$ is determined, in principle all many-body effects are included. The problem is now reduced to determining the correct form of the energy functional. An appropriate energy functional is provided by the effective lagrangian density of FST, given in Eqs. (2.11) and (2.15). Here the meson fields play the role of Kohn-Sham potentials.

CHAPTER 4

Strange Superheavy Nuclei

4.1 Introduction

The possibility that very large nuclei exist is an interesting problem in nuclear physics. One can immediately see that the Coulomb repulsion limits the maximum size of nuclei composed solely of protons and neutrons. As ordinary nuclei become larger, more and more neutrons are required to keep the repulsive force exerted by the protons from destabilizing the nucleus. If, however, negatively charged baryons are introduced, this Coulomb barrier could be overcome. The addition of negatively charged baryons composed solely of u and d valence quarks, such as the Δ^- (ddd), is one solution. Unfortunately, these particles will decay rapidly via the strong interaction. The strong interaction timescale is $\sim 10^{-23}$ s, which is too short to be of any particular interest.[1] A second possibility, and the one we investigate in this chapter, is the inclusion of hyperons in nuclei. Hyperons are a class of baryons with non-zero strangeness. Strangeness, as we have seen, is a conserved quantity in the strong interaction. As we will see in the subsequent discussion some of the hyperons

---

[1] The strong interaction timescale is the time it takes light to travel the Compton wavelength of a pion, $\tau_{SI} = \lambda_\pi/c = \hbar/(m_\pi c^2)$.

56

	Q	S	T	M	qqq
p	+1	0	1/2	938.27	uud
n	0	0	1/2	939.57	udd
Λ	0	-1	0	1115.68	uds
Σ^+	+1	-1	1	1189.37	uus
Σ^0	0	-1	1	1192.64	uds
Σ^-	-1	-1	1	1197.45	dds
Ξ^0	0	-2	1/2	1314.83	uss
Ξ^-	-1	-2	1/2	1321.31	dss
Ω^-	-1	-3	0	1672.45	sss

TABLE 4.1: The nucleons and hyperons are listed here with their respective charge (Q) in units of e, strangeness (S), total isospin (T), mass (M) in MeV, and constituent valence quark content (qqq) [4].

will be stable against strong decay. The hyperons are listed in Table 4.1; notice that a number of these baryons have a negative charge.

Let us now consider the hyperons in order of increasing mass. The lightest of the hyperons is the Λ, which has a binding energy in nuclear matter of ~ -28 MeV [26]. The Λ cannot strongly decay into a nucleon because to do so would violate strangeness conservation. It turns out that the only mechanism capable of this type of reaction is the weak force (the weak interaction timescale is $\sim 10^{-8}$ s).[2] After the Λ, the least massive hyperons are the Σ's. The Σ has a repulsive nuclear potential [27, 28, 29]. There does exist the possibility of $\Lambda - \Sigma$ mixing, but this is assumed to have little effect[3]. The next hyperons are the Ξ's. In contrast to the Σ, the Ξ has a attractive nuclear potential [30, 31, 32]. Also, it has been shown that for some

---

[2]The weak interaction timescale is the typical lifetime of a particle decaying via the weak interaction.

[3]An idea of the possible impact of $\Lambda - \Sigma$ mixing can be taken from [35]; here the small deviation of hypernuclear magnetic moments from the Schmidt values is discussed as possible evidence for this type of mixing. It should be mentioned that if one views the scalar meson as a two-pion resonance, then the Σ enters implicitly as an intermediate state in our formalism.

critical number of Λ's in the nuclear medium, the reaction

$$2\Lambda \rightarrow N + \Xi \tag{4.1}$$

becomes favorable [23]. Finally, the most massive hyperon, the Ω^-, will rapidly decay via the strong interaction. Therefore, if one operates on strong interaction timescales, then it appears that the inclusion of Λ's and Ξ's in ordinary nuclei is favorable while the addition of Σ's and Ω's is not. This is significant because the Ξ^- provides a negative charge to offset the Coulomb repulsion between the protons. To minimize the overall effect of the Coulomb force, we will impose the condition $Q = 0$. The consequence of this condition is that the Coulomb term drops out of the SEMF. Furthermore, we will impose the condition $|S|/B = 1$; this will eliminate the symmetry term in the SEMF. After taking into consideration the above arguments, we believe that matter composed of N's, Λ's, and Ξ's exists and is stable with respect to the strong interaction.[4] The purpose of this chapter is to construct a method to model these systems and to determine their surface structure and energy.

4.2 Theory of Strange Superheavy Nuclei

Following the effective field theory approach of FST [1, 2], we construct an effective lagrangian density using hadronic degrees of freedom that remains invariant under $SU(2)_L \otimes SU(2)_R$ symmetry. We will use this lagrangian density to model both infinite and finite systems; to start with only systems of nucleons with N = Z, which we refer to as *nucleon* matter, are considered. In this chapter, we limit the theory to simple scalar and neutral vector meson exchange. The lagrangian density

---

[4]They will decay via the usual weak hyperon decays as well as weak non-mesonic two-body decays such as $\Lambda + N \rightarrow N + N$ and $\Xi + N \rightarrow \Lambda + N$ [103].

used here is given by

$$\mathcal{L}(\mathbf{x}_\mu) = -\bar{\mathrm{N}} \left[\gamma_\mu \left(\frac{\partial}{\partial \mathbf{x}_\mu} - i\mathrm{g}_\mathrm{V} \mathrm{V}_\mu \right) + \mathrm{M} - \mathrm{g}_\mathrm{S}\phi \right] \mathrm{N} - \frac{1}{2} \left[\left(\frac{\partial \phi}{\partial \mathbf{x}_\mu} \right)^2 + \mathrm{m}_\mathrm{S}^2 \phi^2 \right]$$
$$- \frac{1}{4} \mathrm{V}_{\mu\nu} \mathrm{V}_{\mu\nu} - \frac{1}{2} \mathrm{m}_\mathrm{V}^2 \mathrm{V}_\mu^2 - \frac{\kappa_3 \mathrm{g}_\mathrm{S} \mathrm{m}_\mathrm{S}^2}{3!\mathrm{M}} \phi^3 - \frac{\kappa_4 \mathrm{g}_\mathrm{S}^2 \mathrm{m}_\mathrm{S}^2}{4!\mathrm{M}^2} \phi^4 \tag{4.2}$$

We have retained only the lowest order terms and a pair of nonlinear scalar self-couplings. Notice that the Lorentz scalar meson field, ϕ, is coupled to the scalar density $\bar{\mathrm{N}}\mathrm{N}$ and V_μ, the Lorentz vector meson field, is coupled to the conserved baryon current $i\bar{\mathrm{N}}\gamma_\mu\mathrm{N}$. The ρ-meson and electromagnetic terms have been suppressed in Eq. (4.2). The source term contributed by the ρ-meson depends on the quantity $\mathrm{N} - \mathrm{Z}$, which vanishes for the systems under consideration.

We now employ RMFT, which is discussed in appendix B. The source terms are replaced by their expectation values and the meson fields are replaced by classical fields. Incorporating both Eq. (2.12) and RMFT, our lagrangian density becomes

$$\mathcal{L}(\mathbf{x}_\mu) = -\bar{\mathrm{N}} \left(\gamma_\mu \frac{\partial}{\partial \mathbf{x}_\mu} + \mathrm{M}^* \right) \mathrm{N} - \mathrm{g}_\mathrm{V} \mathrm{V}_0 \mathrm{N}^\dagger \mathrm{N} + \frac{1}{2} \left[(\nabla \mathrm{V}_0)^2 + \mathrm{m}_\mathrm{V}^2 \mathrm{V}_0^2 \right]$$
$$- \frac{1}{2} \left[(\nabla \phi_0)^2 + \mathrm{m}_\mathrm{S}^2 \phi_0^2 \right] - \frac{\kappa_3 \mathrm{g}_\mathrm{S} \mathrm{m}_\mathrm{S}^2}{3!\mathrm{M}} \phi_0^3 - \frac{\kappa_4 \mathrm{g}_\mathrm{S}^2 \mathrm{m}_\mathrm{S}^2}{4!\mathrm{M}^2} \phi_0^4 \tag{4.3}$$

where the effective mass is defined as

$$\mathrm{M}^* \equiv \mathrm{M} - \mathrm{g}_\mathrm{S}\phi_0 \tag{4.4}$$

Now the hamiltonian density is given by

$$
\begin{aligned}
\mathcal{H}(x_\mu) &= \Pi \frac{\partial N}{\partial t} - \mathcal{L} \\
&= i N^\dagger \frac{\partial N}{\partial t} + \bar{N} \left(\gamma_\mu \frac{\partial}{\partial x_\mu} + M^* \right) N + g_V \rho_B V_0 - \frac{1}{2} \left[(\nabla V_0)^2 + m_V^2 V_0^2 \right] \\
&\quad + \frac{1}{2} \left[(\nabla \phi_0)^2 + m_S^2 \phi_0^2 \right] + \frac{\kappa_3 g_S m_S^2}{3!M} \phi_0^3 + \frac{\kappa_4 g_S^2 m_S^2}{4!M^2} \phi_0^4
\end{aligned}
\tag{4.5}
$$

where $\rho_B = N^\dagger N$ is the baryon density and the canonical momentum density is

$$
\Pi = \frac{\partial \mathcal{L}}{\partial(\partial N / \partial t)} = i N^\dagger
\tag{4.6}
$$

As we are interested in very large systems, a more statistical approach is used here. To this end, it is assumed that a nucleus is a local Fermi gas filled up to some $k_F(r)$ at every point. Now, the source terms take the form

$$
\rho_B(r) = \langle N^\dagger N \rangle = \frac{\gamma}{(2\pi)^3} \int_0^{k_F(r)} d^3 k
\tag{4.7}
$$

$$
\langle N^\dagger (\vec{\alpha} \cdot \vec{p} + \beta M^*) N \rangle = \frac{\gamma}{(2\pi)^3} \int_0^{k_F(r)} d^3 k (k^2 + M^{*2})^{1/2}
\tag{4.8}
$$

where $\vec{p} = -i\nabla$ and γ is a degeneracy factor. The hamiltonian density is explicitly time-independent and, in this problem, it is equivalent to the energy density (with $\gamma = 4$ for nucleon matter)

$$
\begin{aligned}
\mathcal{E}(r) &= \frac{1}{2} \left[(\nabla \phi_0)^2 + m_S^2 \phi_0^2 \right] - \frac{1}{2} \left[(\nabla V_0)^2 + m_V^2 V_0^2 \right] + g_V \rho_B V_0 \\
&\quad + \frac{\kappa_3 g_S m_S^2}{3!M} \phi_0^3 + \frac{\kappa_4 g_S^2 m_S^2}{4!M^2} \phi_0^4 + \frac{4}{(2\pi)^3} \int_0^{k_F} d^3 k (k^2 + M^{*2})^{1/2}
\end{aligned}
\tag{4.9}
$$

The total energy and baryon number are

$$E = \int \mathcal{E}(r)d^3r \tag{4.10}$$

$$B = \int \rho_B(r)d^3r \tag{4.11}$$

respectively. The energy density above provides a lowest order density functional. As shown in chapter 3, DFT tells us that minimizing the exact energy functional yields the exact GS density.

To conduct *infinite nucleon matter* calculations, we neglect the spatial variations in the meson fields; the resulting energy density is

$$\mathcal{E} = \frac{1}{2}m_S^2\phi_0^2 + \frac{\kappa_3 g_S m_S^2}{3!M}\phi_0^3 + \frac{\kappa_4 g_S^2 m_S^2}{4!M^2}\phi_0^4 + g_V\rho_B V_0 - \frac{1}{2}m_V^2 V_0^2$$
$$+ \frac{4}{(2\pi)^3}\int_0^{k_F} d^3k(k^2 + M^{*2})^{1/2} \tag{4.12}$$

By minimizing the energy functional with respect to the scalar field, the scalar mean field equation is determined. The vector mean field equation is similarly derived as an extremum of the energy functional. These equations are

$$\phi_0 + \frac{\kappa_3 g_S}{2M}\phi_0^2 + \frac{\kappa_4 g_S^2}{6M^2}\phi_0^3 = \frac{g_S}{m_S^2}\rho_S \tag{4.13}$$

$$V_0 = \frac{g_V}{m_V^2}\rho_B \tag{4.14}$$

where the scalar density is given by

$$\rho_S = \frac{4}{(2\pi)^3}\int_0^{k_F} d^3k \frac{M^*}{(k^2 + M^{*2})^{1/2}} \tag{4.15}$$

The solution to these equations is discussed in section 4.3.

We now turn our attention to *finite nucleon systems*. We retain the spherically

symmetric spatial variations in the meson fields and therefore require the full energy density in Eq. (4.9). The meson field equations, acquired in the same manner as above, are

$$\left(\nabla^2 - m_S^2\right)\phi_0 - \frac{\kappa_3 g_S m_S^2}{2M}\phi_0^2 - \frac{\kappa_4 g_S^2 m_S^2}{6M^2}\phi_0^3 = -g_S \rho_S \tag{4.16}$$

$$\left(\nabla^2 - m_V^2\right)V_0 = -g_V \rho_B \tag{4.17}$$

Note that for spherically symmetric systems, the laplacian becomes

$$\nabla^2 = \frac{\partial^2}{\partial r^2} + \frac{2}{r}\frac{\partial}{\partial r} \tag{4.18}$$

Using a Green's function, the solution to Eq. (4.17) is

$$g_V V_0 = \frac{g_V^2}{4\pi}\int d^3y\, \rho_B(\vec{y})\frac{e^{-m_V|\vec{x}-\vec{y}|}}{|\vec{x}-\vec{y}|} \tag{4.19}$$

$$= \frac{g_V^2}{x m_V}\int y\, dy\, \rho_B(y)\sinh(m_V x_<)e^{-m_V x_>} \tag{4.20}$$

where the angular dependence has now been integrated out. Since the contribution of the laplacian in Eq. (4.17) is small compared with that of the vector meson mass, to a first approximation it can be neglected [5, 20],

$$g_V V_0 = \frac{g_V^2}{m_V^2}\rho_B \tag{4.21}$$

However, the omitted term produces a small, but important, contribution to the vector field; this can have a significant effect on the total energy and baryon number. It is then convenient to express the vector field as

$$g_V V_0 = \frac{g_V^2}{m_V^2}\rho_B + \delta W_0 \tag{4.22}$$

with $\delta W_0 \equiv g_V \delta V_0$. Substituting this into Eq. (4.20) and rearranging, one obtains an explicit expression for δW_0 in terms of the baryon density

$$\delta W_0(r) = \frac{g_V^2}{4\pi} \int d^3 y \rho_B(\vec{y}) \frac{e^{-m_V |\vec{x}-\vec{y}|}}{|\vec{x}-\vec{y}|} - \frac{g_V^2}{m_V^2} \rho_B(r) \qquad (4.23)$$

Minimization of the total energy with respect to the local Fermi wave number now yields the GS of the system. A Lagrange multiplier is used to incorporate the constraint of fixed B such that

$$\delta E(k_F, \phi_0, V_0) - \mu \delta B(k_F) = 0 \qquad (4.24)$$

Since the variations of the energy density with respect to both the scalar and vector fields vanish, they can be held constant in the variation of k_F, the result of which is the constraint equation

$$\mu = g_V V_0(r) + [k_F^2(r) + M^{*2}(r)]^{1/2} \qquad (4.25)$$

where the Lagrange multiplier, μ, is the chemical potential and is constant throughout the nucleus.

On the surface ($r = r_0$), the baryon density vanishes. The constraint equation at the surface then yields the first boundary condition

$$M^*(r_0) = \mu - \delta W_0(r_0) \qquad (4.26)$$

where Eq. (4.22) has now been employed.

To determine the second boundary condition, consider the solution to the linear

homogeneous scalar field equation

$$\phi_0 = \phi_c \frac{e^{-(r-r_0)m_S}}{r/r_0} \tag{4.27}$$

The constant $g_S\phi_c = M - \mu + \delta W_0(r_0)$ is determined at the surface. Differentiating Eq. (4.27) with respect to r and then evaluating at the surface, we acquire the second boundary condition

$$\left[\frac{\partial M^*(r)}{\partial r}\right]_{r_0} = [M + \delta W_0(r_0) - \mu]\left(\frac{1 + m_S r_0}{r_0}\right)(1 + \epsilon) \tag{4.28}$$

The solution to the scalar field equation in Eq. (4.27) no longer holds when the nonlinear terms are included; therefore, a small correction ϵ has been included to compensate. In the nonlinear case, the scalar field equation is integrated outward from r_0, and ϵ in Eq. (4.28) is varied until the solution vanishes for large r. Once this correction is determined, the meson field equations are integrated inward from the surface, solving Eq. (4.25) at each point for k_F and varying μ until the fields are flat at the origin. The methodology used to solve this system is discussed in detail in section 4.3.

The calculated binding energy and baryon number of a series of nuclei with different radii can be fit with a SEMF of the form

$$\frac{E}{B} = a_1 + a_2 B^{-1/3} \tag{4.29}$$

where only the bulk and surface terms have been retained. The bulk constant, a_1, is determined by the binding energy of infinite nuclear matter. Then, after calculating a number of finite nuclei, the surface energy, a_2, can be obtained by plotting the calculated energies per baryon against the calculated values of $B^{-1/3}$. The results of numerical methods for these finite systems are discussed in later sections.

We now extend our theory to consider *systems of nucleons and hyperons.* First we investigate uniform matter composed of n, p, Ξ^0, and Ξ^-, subject to the conditions

$$Q = 0 \tag{4.30}$$

$$|S|/B = 1 \tag{4.31}$$

where Q and S are the total charge and strangeness respectively. These systems shall be subsequently referred to as *cascade-nucleon* (ΞN) matter. Equation (4.30) restricts the system to equal numbers of p and Ξ^-; similarly, Eq. (4.31) forces the numbers of n and Ξ^0 to be equal. Therefore the system is now characterized by two Fermi wave numbers, k_{Fp} and k_{Fn}. For simplicity we employ an average cascade mass $M_\Xi = (M_{\Xi^0} + M_{\Xi^-})/2$. Since the energy density is now symmetric under the interchange of k_{Fp} and k_{Fn}, the minimum binding energy always occurs such that $k_{Fp} = k_{Fn}$. As a result, we can further restrict this system to a single Fermi wave number, k_F. It is a consequence of these arguments that equilibrium is imposed upon the reaction

$$n + \Xi^0 \rightleftharpoons p + \Xi^- \tag{4.32}$$

and the system is described by only one chemical potential. Again we mention that the ρ-mesons do not contribute here for similar reasons to the *nucleon* case.

Next, we must make some assumptions about the cascade couplings. Since the baryon current is conserved, the vector coupling is taken to be universal, $g_V = g_{V\Xi}$. However, an independent scalar coupling for the cascades, $g_{S\Xi}$, is assumed.

Consider the case of *infinite ΞN matter.* The addition of hyperons to the theory

requires only the addition of new source terms. A source term of the form

$$\delta\mathcal{E} = \frac{\gamma}{(2\pi)^3} \int_0^{k_F} d^3k (k^2 + M_\Xi^{*2})^{1/2} \tag{4.33}$$

is added to the energy density in Eq. (4.12) where

$$M_\Xi^* = M_\Xi - g_{s\Xi}\phi_0 \tag{4.34}$$

In addition, a new term is included in the baryon density

$$\delta\rho_B = \frac{\gamma}{(2\pi)^3} \int_0^{k_F} d^3k \tag{4.35}$$

Here $\gamma = 4$ for (Ξ^0, Ξ^-) with spin up and down. Except for the additional source terms, the meson field equations remain unchanged. The new term added to the source in the scalar field Eq. (4.13) is

$$\delta\rho_S = \frac{4s}{(2\pi)^3} \int_0^{k_F} d^3k \frac{M_\Xi^*}{(k^2 + M_\Xi^{*2})^{1/2}} \tag{4.36}$$

where

$$s \equiv g_{s\Xi}/g_s \tag{4.37}$$

Equation (4.35) is incorporated into the source in the vector field Eq. (4.14). The solution to these equations is also discussed in section 4.3.

We now examine the case of *finite ΞN matter*. The source terms in Eqs. (4.33) and (4.35) are incorporated into the energy density in Eq. (4.9). Next the terms in Eqs. (4.36) and (4.35) are added to meson field equations in Eqs. (4.16) and (4.17) respectively. Then a new constraint equation is produced in the same manner as

before

$$\mu = g_V V_0 + \frac{1}{2} \left[(k_F^2 + M^{*2})^{1/2} + (k_F^2 + M_\Xi^{*2})^{1/2} \right] \tag{4.38}$$

Similarly, the boundary conditions are now

$$M^*(r_0) = \frac{1}{1+s} [2\mu - 2\delta W_0(r_0) - M_\Xi + sM] \tag{4.39}$$

$$\left[\frac{\partial M^*(r)}{\partial r} \right]_{r_0} = \frac{1}{1+s} [2\delta W_0(r_0) - 2\mu + M_\Xi + M] \left(\frac{1 + m_s r_0}{r_0} \right) (1 + \epsilon) \tag{4.40}$$

Consider again the SEMF in Eq. (4.29). The conditions imposed on ΞN matter in Eqs. (4.30) and (4.31) now justify the elimination of the Coulomb and symmetry terms. Then a_1 is taken to be the binding energy of infinite ΞN matter; next, proceeding as before, the surface energy, a_2, can be extracted.

Finally, we investigate a class of matter in which Λ's are added to the ΞN matter described above. These systems are referred to as *lambda-cascade-nucleon ($\Lambda\Xi N$) matter*. The previous restrictions do not relate the number of Λ's to the number of N's and Ξ's; therefore a second Fermi wave number, $k_{F\Lambda}$, is needed. Again the vector coupling is taken to be universal and an independent scalar coupling, $g_{s\Lambda}$, is employed. Now equilibrium is imposed on the reactions

$$n + \Xi^0 \rightleftharpoons \Lambda + \Lambda \tag{4.41}$$

$$p + \Xi^- \rightleftharpoons \Lambda + \Lambda \tag{4.42}$$

as well as on Eq. (4.32). As before, the system is then characterized by a single chemical potential. The source terms required for the inclusion of Λ's in both

infinite and finite ΞN matter are

$$\delta \mathcal{E} = \frac{2}{(2\pi)^3} \int_0^{k_{F\Lambda}} d^3k (k^2 + M_\Lambda^{*2})^{1/2} \tag{4.43}$$

$$\delta \rho_{\text{B}} = \frac{2}{(2\pi)^3} \int_0^{k_{F\Lambda}} d^3k \tag{4.44}$$

$$\delta \rho_{\text{S}} = \frac{2t}{(2\pi)^3} \int_0^{k_{F\Lambda}} d^3k \frac{M_\Lambda^*}{(k^2 + M_\Lambda^{*2})^{1/2}} \tag{4.45}$$

where

$$M_\Lambda^* = M_\Lambda - g_{S\Lambda} \phi_0 \tag{4.46}$$

and

$$t \equiv g_{S\Lambda}/g_S \tag{4.47}$$

In the case of finite $\Lambda \Xi N$ matter, there are now two constraint equations

$$\mu = g_V V_0 + \frac{1}{2} \left[(k_F^2 + M^{*2})^{1/2} + (k_F^2 + M_\Xi^{*2})^{1/2} \right] \tag{4.48}$$

$$\mu = g_V V_0 + (k_{F\Lambda}^2 + M_\Lambda^{*2})^{1/2} \tag{4.49}$$

The Λ density begins interior to the surface r_0; this allows the ΞN boundary conditions to be used in the $\Lambda \Xi N$ case.

4.3 Methodology

In this section we develop a methodology for solving the systems of equations discussed in section 4.2. In the case of nucleon matter the parameters g_S, g_V, m_S, m_V, M, κ_3, and κ_4 must first be specified. The vector meson mass is defined to be the mass of the ω meson and M $\equiv$ 939 MeV. The remaining constants are given by the three coupling sets in Table 4.2; to determine these sets the theory was fit to
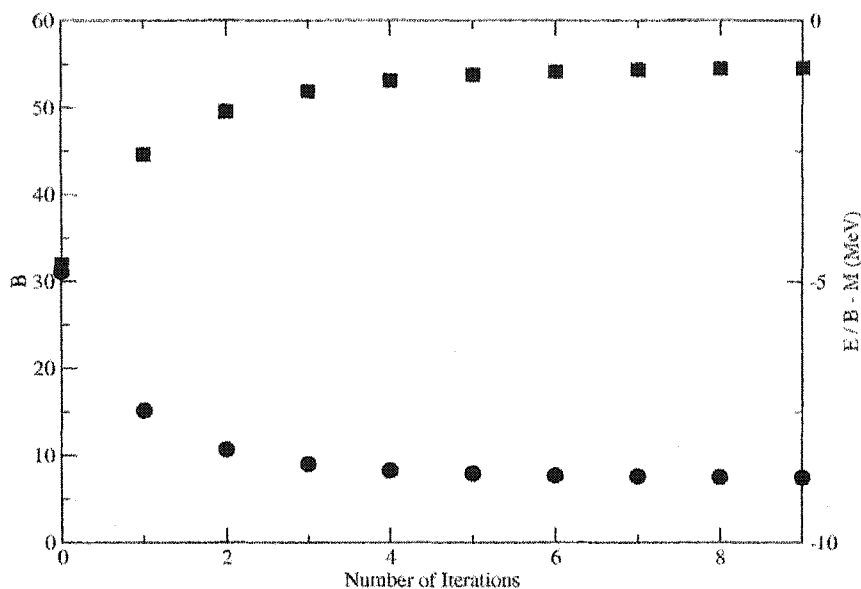
FIG. 4.1: Convergence of the baryon number and binding energy per baryon (boxes and circles respectively) after 9 iterations for an ordinary nucleus of $r_0 = 15/m_S$, N = Z, and using the L2 parameter set.

	g_S^2	g_V^2	m_S	m_V	κ_3	κ_4	$g_{S\Lambda}/g_S$
L2	109.63	190.43	520	783	0	0	0.88660
NLC	95.11	148.93	500.8	783	1.9195	-7.3928	0.88190
Q1	103.67	164.70	504.57	782	1.6582	-6.6045	0.88403

TABLE 4.2: Parameter sets taken from [1, 2]. m_S and m_V are in MeV. $g_{S\Lambda}/g_S$ is fit to reproduce the binding energy of a single Λ in nuclear matter.

reproduce various properties of ordinary nuclear matter [1, 2]. The simplest set, L2, includes only linear terms in the scalar field. The sets NLC and Q1 both expand the theory to include nonlinear terms. As a result, these sets must be fit to more properties of nuclear matter than L2.

To extend the theory to systems of nucleons and hyperons, specification of the constants $g_{S\Lambda}$, $g_{S\Xi}$, $g_{V\Lambda}$, and $g_{V\Xi}$ is also required. Since the vector meson is coupled to the conserved baryon current, we assume a universal vector coupling, $g_V = g_{V\Lambda} = g_{V\Xi}$. The scalar couplings, on the other hand, are adjusted to reproduce

$g_{S\Xi}/g_S$	$\delta\mathcal{E}/\delta\rho_B - M_\Xi$
1.0	-68.9
0.95	-51.6
0.9	-34.3

TABLE 4.3: Values of the binding energy (in MeV) of a single Ξ in nuclear matter for various Ξ coupling ratios and the parameter set NLC.

the binding energies of single hyperons in nuclear matter. For instance, the Λ scalar coupling is designed to reproduce the binding energy of a single Λ in nuclear matter, experimentally determined to be -28 MeV [26]. The values of $g_{S\Lambda}/g_S$ are also shown in Table 4.2. Unfortunately data on the binding energy of a single Ξ in nuclear matter is uncertain. Therefore, a range of Ξ scalar couplings is investigated; the values used are $g_{S\Xi}/g_S = 1.0$, 0.95, and 0.9. These values correspond to the binding energies listed in Table 4.3.

Consider the case of infinite nucleon matter. To obtain the solution to this system, first one must specify k_F. Both Eqs. (4.13) and (4.14) are now solved for their respective meson fields. Then, using the meson fields and k_F, one calculates the energy density in Eq. (4.12). This is in turn used to evaluate the binding energy per baryon, $BE(k_F) \equiv \mathcal{E}/\rho_B - M$. In RMFT the medium saturates and $BE(k_F)$ has a minimum; this equilibrium value, BE_0, serves as the bulk term in the SEMF, a_1. This procedure is also applicable to infinite ΞN and $\Lambda \Xi N$ systems provided the appropriate source terms are included.

Now we discuss the methodology used for all finite systems. First the scalar field Eq. (4.16) is converted into a pair of coupled first-order finite difference equations for $[\phi_0(r), \phi_0'(r)]$; these equations are solved using a shooting method. To accomplish this, one fixes μ and r_0; now the boundary conditions are uniquely determined. Since $k_F(r_0) = 0$, we can solve the finite difference equations for $\phi_0(r)$ and $\phi_0'(r)$ one step in. These solutions are substituted back into the constraint equation from which

$k_F(r)$, one step in, is determined. In this manner we iterate in from the surface, evaluating $\rho_B(r)$ and $\mathcal{E}(r)$ at every point. This process is repeated until ρ_B and ϕ_0 become constant as r approaches the origin (or equivalently $\rho'_B = \phi'_0 = 0$ at $r = 0$); we achieve this by adjusting the chemical potential.[5] Note that initially, ϵ and δW_0 are ignored.

Now we incorporate the two correction terms. In order to discuss the role of ϵ, let us examine the second boundary condition. When nonlinear terms are introduced, the small parameter, ϵ, is included to compensate. Iterating the finite difference equations *out* from the surface, ϵ in Eq. (4.28) is adjusted such that the scalar field vanishes for large r. The newly corrected boundary condition is then used to resolve the finite system by integrating *in* as described above.

Next, the correction term δW_0 is added to the vector field. Initially Eq. (4.21) was employed; however, this is accurate only in the limit of a large m_V. A small, but important, contribution to the vector field was omitted; therefore, the term δW_0, defined by Eq. (4.23) and calculated from the previous $\rho_B(r)$, is included. Then the entire process is repeated again. After successive iterations on the vector field, B and BE $\equiv E/B - M$ both converge to their full solutions. This convergence is illustrated in Fig. 4.1 for ordinary nucleon matter; here, the parameter set L2 was used, a radius of $r_0 = 15m_0^{-1}$ was assumed, and 9 iterations on the vector field have been carried out. Similar convergence was found in all cases studied here.

Finally, we consider the SEMF in Eq. (4.29) where a_1 is defined as the BE_0 of infinite matter. The calculated values of BE and $B^{-1/3}$ of the finite systems are plotted against each other for nuclei of various radii. Then using this SEMF as a linear fit, the surface energy, a_2, is determined. The above approach to finite systems

---

[5]We mention that better convergence is obtained by decreasing the step size. Step sizes as small as $dr = 0.0001m_S^{-1}$ are considered here at which the quantities BE and B appear to have converged to better than 0.5%.
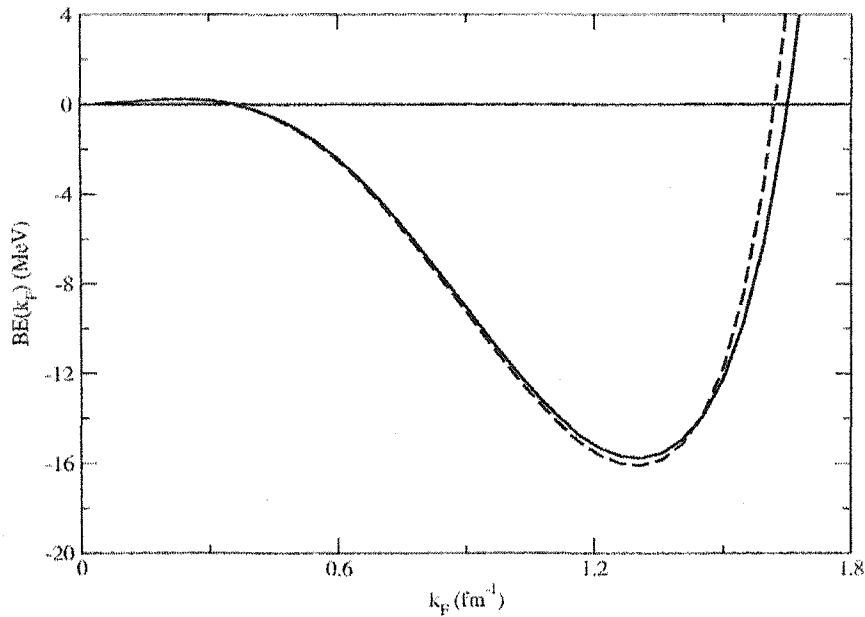
FIG. 4.2: Binding energy per baryon for infinite nuclear matter with N = Z as a function of Fermi wave number. These results are for the coupling sets NLC (solid line) and Q1 (dashed line).

is first calibrated by the *nucleon* matter case; then it is extended to investigate the ΞN and $\Lambda \Xi N$ systems detailed in section 4.2.

4.4 Results and Discussion

In this section, we discuss the application of the above methodologies. First we consider the results of our infinite matter calculations, starting with nucleon systems. Table 4.4 shows the equilibrium values of k_F, M^*/M, and BE_0 obtained for infinite nucleon matter using the L2, NLC, and Q1 parameter sets. The values calculated here reproduce those in [2, 20]. Then $BE(k_F)$ is plotted for both the NLC and Q1 sets in Fig. 4.2. The minimum, BE_0, in Fig. 4.2 is taken to be a_1 in the SEMF for each coupling set. This is in good agreement with the empirical bulk term [5].

We now turn our attention to infinite systems of nucleons and hyperons; these

	k_F	M^*/M	$\mathcal{E}/\rho_B - M$
L2	1.301	0.5409	-15.758
NLC	1.301	0.6313	-15.768
Q1	1.299	0.5975	-16.099

TABLE 4.4: Calculated equilibrium values of the Fermi momentum (in fm^{-1}), effective mass, and the BE_0 (in MeV) for infinite nucleon matter are shown using the coupling sets in Table 4.2. These numbers reproduce the results in [2, 20].

	$g_{s\Xi}/g_s$	k_F	M^*/M	$\mathcal{E}/\rho_B - M_\Lambda$
NLC	1.0	1.363	0.1391	-41.343
	0.95	1.351	0.1686	-22.747
	0.9	1.326	0.2232	-4.741
Q1	1.0	1.320	0.1372	-42.728
	0.95	1.310	0.1643	-24.013
	0.9	1.290	0.2104	-5.812

TABLE 4.5: Calculated equilibrium values of the Fermi momentum (in fm^{-1}), effective mass, and the BE_0 (in MeV) for infinite ΞN matter are shown using the coupling sets NLC and Q1 in Table 4.2 and a range of values for $g_{s\Xi}/g_s$.

investigations are conducted using only the nonlinear cases, NLC and Q1. We begin by investigating infinite ΞN matter for the range of Ξ scalar couplings mentioned above. Since the lowest mass state of separated baryons under the conditions Eqs. (4.30) and (4.31) consists entirely of Λ's, $BE(k_F)$ for infinite cascade-nucleon matter is defined by $BE(k_F) \equiv \mathcal{E}/\rho_B - M_\Lambda$. The calculated equilibrium values for this type of matter are given in Table 4.5. Notice that $|BE_0|$ decreases as the Ξ coupling grows weaker while the equilibrium k_F remains fairly constant. Graphs of $BE(k_F)$ for the NLC set and each Ξ scalar coupling ratio shown in Fig. 4.3 illustrate this point. Although the equilibrium k_F is roughly the same here as in the nucleon case, these systems contain twice as many baryons; as a result, the baryon density is much higher than in infinite nucleon matter. Also, the effective mass is considerably smaller, on the order of a third the value of the nucleon case. Again a_1 in the SEMF for each coupling ratio is taken to be the minimum (BE_0) of the corresponding
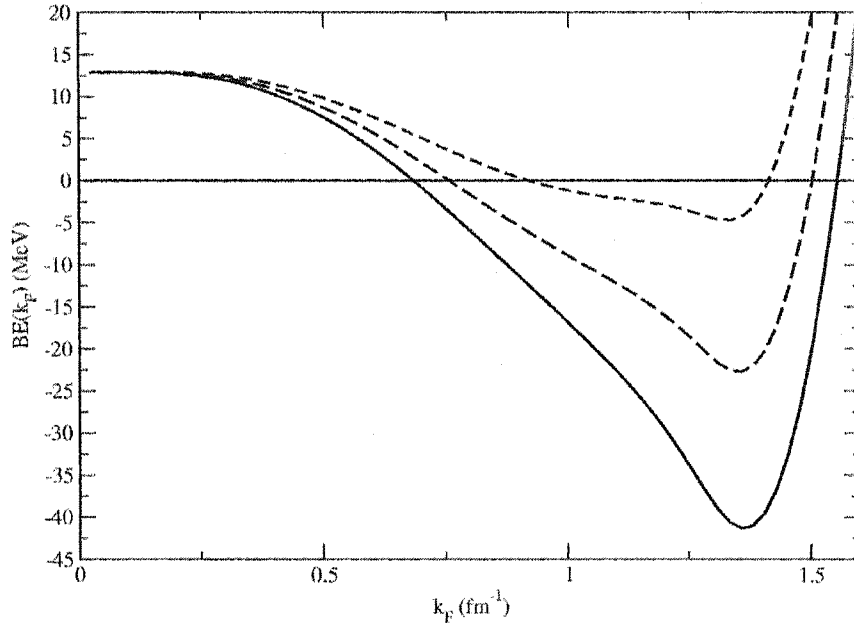
FIG. 4.3: Binding energies per baryon for infinite cascade-nucleon matter computed relative to isolated lambdas (the lowest energy free baryon state for $|S|/B = 1$) as a function of the Fermi wave number using NLC. Note the left hand intercept is $(M_\Xi + M_N)/2 - M_\Lambda$. The solid, long dashed, and short dashed lines correspond to $g_{s\Xi}/g_s = 1.0$, 0.95, and 0.9 respectively.

	$g_{s\Xi}/g_s$	k_F	$k_{F\Lambda}$	M^*/M	$\mathcal{E}/\rho_B - M_\Lambda$
NLC	1.0	1.343	0.8665	0.1202	-42.229
	0.95	1.319	1.026	0.1321	-24.704
	0.9	1.288	1.159	0.1511	-8.100
Q1	1.0	1.302	0.8141	0.1213	-43.457
	0.95	1.278	0.9831	0.1325	-25.792
	0.9	1.247	1.124	0.1495	-9.095

TABLE 4.6: Calculated equilibrium values of the Fermi momenta (in fm^{-1}), effective mass, and the BE_0 (in MeV) for infinite $\Lambda\Xi N$ matter are shown using the coupling sets NLC and Q1 in Table 4.2 and a range of values for $g_{s\Xi}/g_s$.

curve in Fig. 4.3. We also mention that the value of $g_{S\Xi}/g_S = 0.886$ is the lowest Ξ coupling ratio for which infinite ΞN matter was still bound.

Next, we consider infinite $\Lambda\Xi N$ systems using the same range of Ξ scalar couplings quoted above. Note that as in the ΞN case, $BE(k_F) \equiv \mathcal{E}/\rho_B - M_\Lambda$. This investigation produced the equilibrium values shown in Table 4.6. Here the equilibrium values of k_F, M^*/M, and BE_0 differ little from the ΞN results for large Ξ coupling; however, the difference becomes more pronounced as the Ξ coupling decreases. In our formulation, a second Fermi wave number, $k_{F\Lambda}$, was included for the Λ's; as one might expect, $k_{F\Lambda}$ grows, and consequently the proportion of Λ's increases, as the gap between $g_{S\Xi}$ and $g_{S\Lambda}$ narrows. The smallest value of the Ξ scalar coupling for which infinite $\Lambda\Xi N$ matter was still bound was $g_{S\Xi}/g_S = 0.875$.

Now we examine the results of the finite matter investigation. To begin with, we consider the finite nucleon matter system. The calculated values of μ, B, $BE = E/B - M$ as a function of r_0 for this type of matter using the L2, NLC, and Q1 sets are shown in Table 4.7. As stated above, 9 iterations on the vector field were conducted on nuclei calculated using the L2 set; this demonstrated the convergence of the system. Subsequent finite nucleon matter results were obtained using 5 iterations which gave results for B and BE to better than 1%. The radii used here, $r_0 = 15$, 20, and 25 in units of m_S^{-1}, include nuclei spanning a range of $B \sim 50 - 400$. As an example, $\rho_B(r)$ and $\phi_0(r)$ for a nucleus with $r_0 = 20m_S^{-1}$ calculated with the NLC set are displayed in Fig. 4.4. The interior of the nucleus is roughly constant in both $\rho_B(r)$ and $\phi_0(r)$. Then the effective mass increases to near unity and the baryon density drops to zero at r_0; this is a typical example of the surface structure for finite nucleon systems.

Next using the NLC set the calculated values of BE are plotted vs. $B^{-1/3}$ in Fig. 4.5 for nuclei of various radii. Notice that the infinite matter value, BE_0, has also been included. A SEMF of the form Eq. (4.29) is used as a linear fit in Fig.
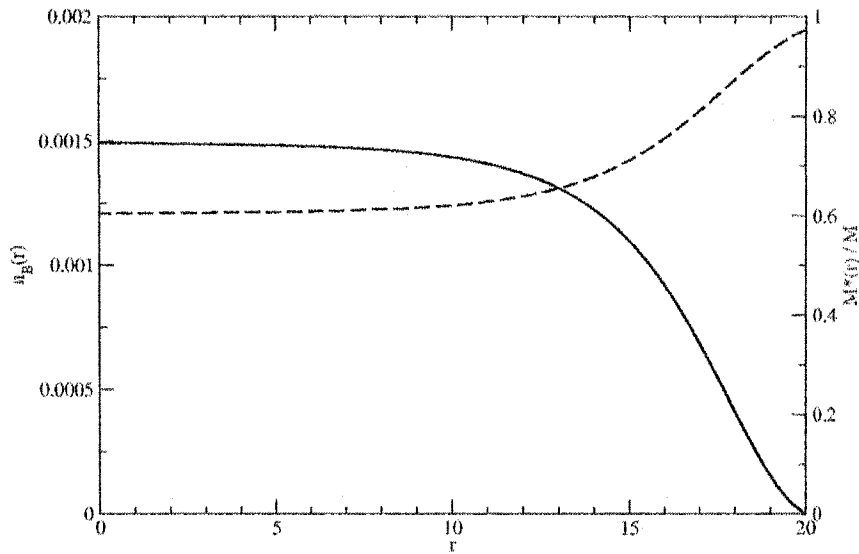
FIG. 4.4: The baryon density $n_B(r) = \rho_B(r)/M^3$ (solid line) and effective mass $M^*(r)/M$ (dashed line) vs. r (in units of m_S^{-1}) for an ordinary finite nucleus with $N = Z$, $B = 188.87$, $r_0 = 20/m_S$, and using the NLC parameter set.

4.5; the slope of this fit is the surface energy, in this case $a_2 = 18.0$ MeV. The surface energies for the various coupling sets are given in Table 4.8 along with the experimentally determined value [5]; the values of a_2 for both NLC and Q1 show good agreement with experiment.

The agreement between the values calculated with the more realistic interactions and the empirical result for the surface energy of ordinary nucleon matter using this effective lagrangian and density functional approach gives us some confidence in our exploratory study of the surface structure of strange superheavy nuclei.

Now we investigate finite ΞN matter for the values of $g_{s\Xi}/g_s$ quoted above. Since the best fit to both infinite and finite nucleon matter was obtained with NLC, we use this set exclusively in the following discussion. The values of μ, B, and $BE = E/B - M_\Lambda$ obtained for finite ΞN matter are given in Table 4.9. For the same reasons as in the infinite ΞN case, the binding energy per baryon is redefined as $BE \equiv E/B - M_\Lambda$. Note that due to a slower rate of convergence, these systems
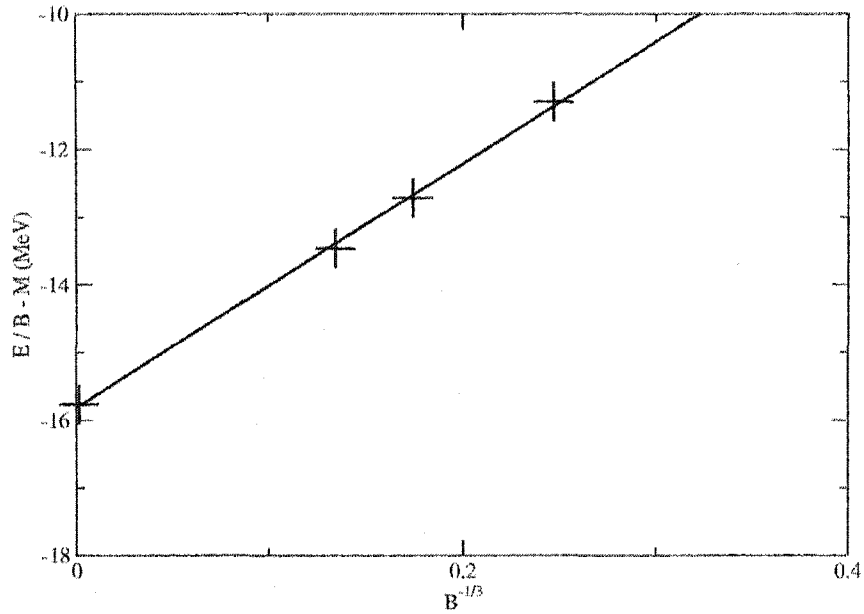
FIG. 4.5: Fit to the calculated SEMF for ordinary nuclear matter with N = Z and the NLC couplings. The surface energy is given by the slope of the curve, here $a_2 = 18.0$ MeV.

	r_0	μ	B	$E/B - M$
L2	15	4.7055924	54.568	-8.7527
	20	4.69755554	160.72	-10.939
NLC	15	4.6968452	66.438	-11.297
	20	4.69165108	188.87	-12.719
	25	4.68905238	408.43	-13.464
Q1	15	4.6965099	62.581	-11.262
	20	4.69083149	179.76	-12.808
	25	4.68800689	390.77	-13.615

TABLE 4.7: Results of finite nucleon matter for the L2, NLC, and Q1 parameter sets and various radii. Calculations with L2 used 9 iterations on the vector field while 5 were used with NLC and Q1. The radii are in m_s^{-1}, the chemical potential is in fm^{-1}, and $E/B - M$ is in MeV.

	a_2
L2	26.51
NLC	18.01
Q1	19.11
Expt.	17.8

TABLE 4.8: Calculated values of the surface energy (in MeV) for nucleon matter using the parameter sets in Table 4.2. The experimental value is also included [5].

were calculated using 9 iterations on the vector field. Also the radii, $r_0 = 10$ and 15 in units of m_S^{-1}, were used here; this includes nuclei with baryon numbers ranging from $B \sim 30 - 200$ depending on the Ξ coupling. It is also important to mention that for the coupling ratio $g_{s\Xi}/g_s = 0.9$, the nuclei were unbound for our choice of radii. For one nucleus of this type, Fig. 4.6 shows the plots of both $\rho_B(r)$ and $\phi_0(r)$; this is for a nucleus with $g_{s\Xi}/g_s = 1.0$ and $r_0 = 15 m_S^{-1}$. Notice that the baryon densities in the interior of the nucleus are much larger than those in nucleon matter; also, the effective mass drops to less than a third of the nucleon matter value in the interior. The result is a much higher total B for a fixed r_0. Another feature of note is the surface structure; here the width of the surface has decreased relative to the previous case. For each of the Ξ scalar coupling ratios, the calculated values of BE are plotted vs. $B^{-1/3}$; these plots are overlaid in Fig. 4.7. The infinite matter values are also included. As in nucleon matter, the SEMF is used as a linear fit, one for each Ξ coupling ratio, from which the surface energy is determined. The values of a_2 are given in Table 4.10.

As mentioned in section 4.2, precise data on the binding energy for a single Ξ in nuclear matter is unavailable. The values appearing in the literature range from -14 to -40 MeV. This necessitated that a number of Ξ scalar couplings be investigated. Now that the surface energies have been acquired for the Ξ couplings, they are plotted vs. these coupling ratios in Fig. 4.8. A linear interpolation is used between
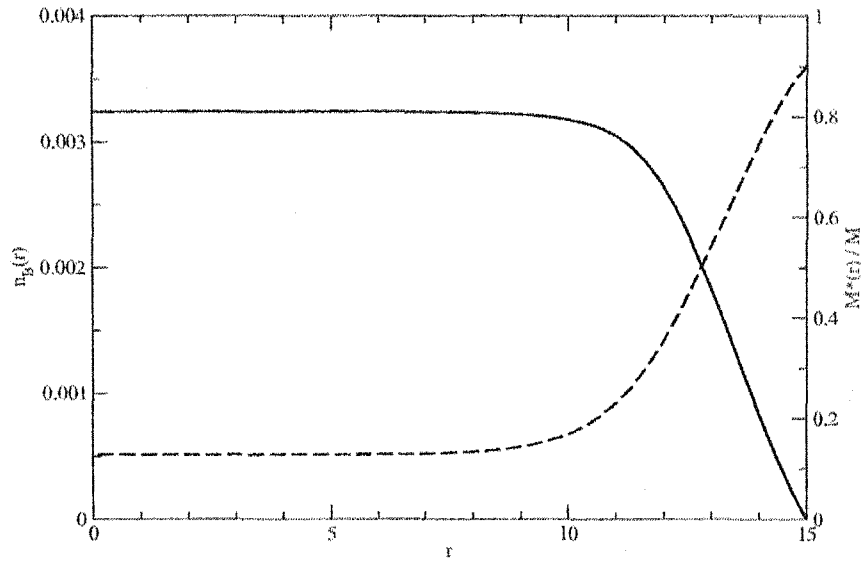
FIG. 4.6: The baryon density $n_B(r) = \rho_B(r)/M^3$ (solid line) and effective mass $M^*(r)/M$ (dashed line) vs. r (in units of m_S^{-1}) for a nucleus composed of nucleons and cascades with $r_0 = 15/m_S$, $B = 164.92$, and $g_{s\Xi}/g_S = 1.0$ subject to the constraints $Q = 0$ and $|S|/B = 1$. These results were obtained using the NLC parameter set.
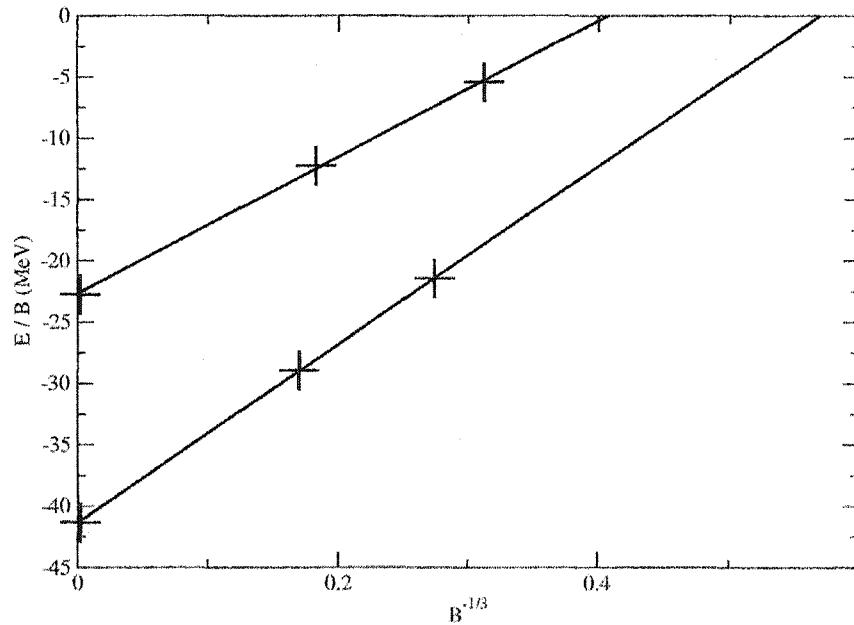
FIG. 4.7: Binding energy vs. $B^{-1/3}$ for matter composed of equal numbers of cascades and nucleons for the NLC coupling set. The upper and lower curves correspond to $g_{s\Xi}/g_S = 0.95$ and 1.0 respectively. The surface energy is just the slope of these lines.

	$g_{S\Xi}/g_S$	r_0	μ	B	$E/B - M_\Lambda$
NLC	1.0	10	1.1604726	48.459	-21.416
		15	1.154255303	204.64	-28.944
	0.95	10	1.178092	32.866	-5.4176
		15	1.17206095	164.92	-12.241

TABLE 4.9: Results for finite ΞN matter for the NLC parameter set and a number of radii. These calculations used 9 iterations on the vector field. The radii are in m_S^{-1}, the chemical potential is in units of M, and $E/B - M_\Lambda$ is in MeV.

	$g_{S\Xi}/g_S$	a_2
NLC	1.0	72.69
	0.95	55.64

TABLE 4.10: Values of the surface energy (in MeV) for ΞN matter using the NLC parameter set from Table 4.2.

the points; this is extended by extrapolation into the region which corresponds to values of the binding energy of a single Ξ appearing in the literature. We feel confident in the neglect of the Λ's over this region because preliminary investigations of finite $\Lambda\Xi N$ matter show that the BE and B change little from ΞN matter. In Fig. 4.9 the baryon density of a $\Lambda\Xi N$ nucleus of $r_0 = 10 m_S^{-1}$ is shown; notice that the Λ density begins interior to the surface and is comparatively much smaller.

A preliminary calculation was also conducted with a Φ meson coupled to the conserved strangeness current. This simulates a repulsion between like strange particles. In order to test the size of this interaction which could be tolerated, the Φ coupling was increased until the system was no longer bound. The values for which this occurred for infinite ΞN matter are $g_\Phi/g_\rho = 0.6839$, 0.5090, and 0.2353 corresponding to $g_{S\Xi}/g_S = 1.0$, 0.95, and 0.9 respectively.[6]

It should be mentioned that the conditions Q = 0 and $|S|/B = 1$ were intro-

---

[6]To include the Φ meson in infinite ΞN matter, we add two terms to the lagrangian, $\delta\mathcal{L} = -2ig_\Phi\bar{\Xi}\gamma_\mu\Xi\Phi_\mu + \frac{1}{2}m_\Phi^2\Phi_\mu\Phi_\mu$. Here $m_\Phi = 1020$ MeV.
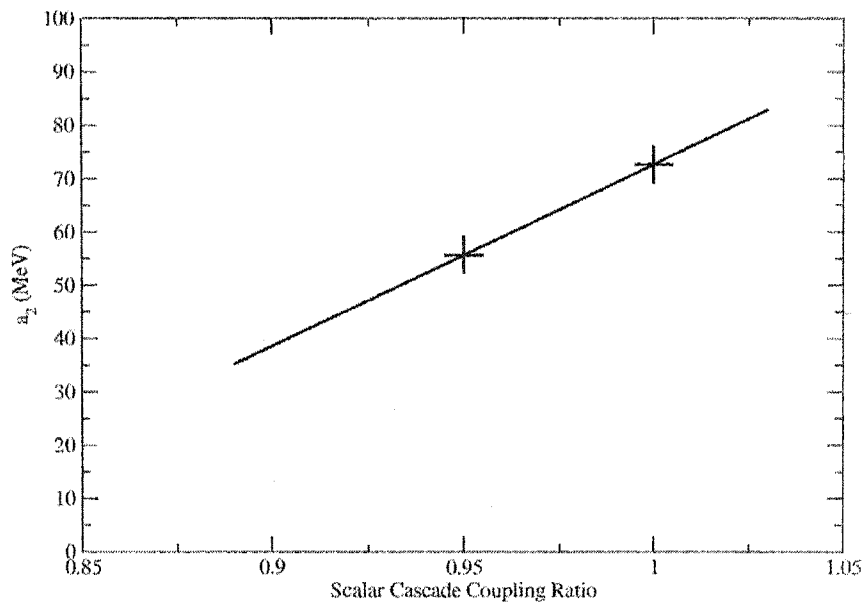
FIG. 4.8: Linear fit to the surface energy, a_2, vs. scalar cascade coupling ratio ($g_{s\Xi}/g_s$) for cascade-nucleon matter assuming $Q = 0$, $|S|/B = 1$, and neglecting Λ's.
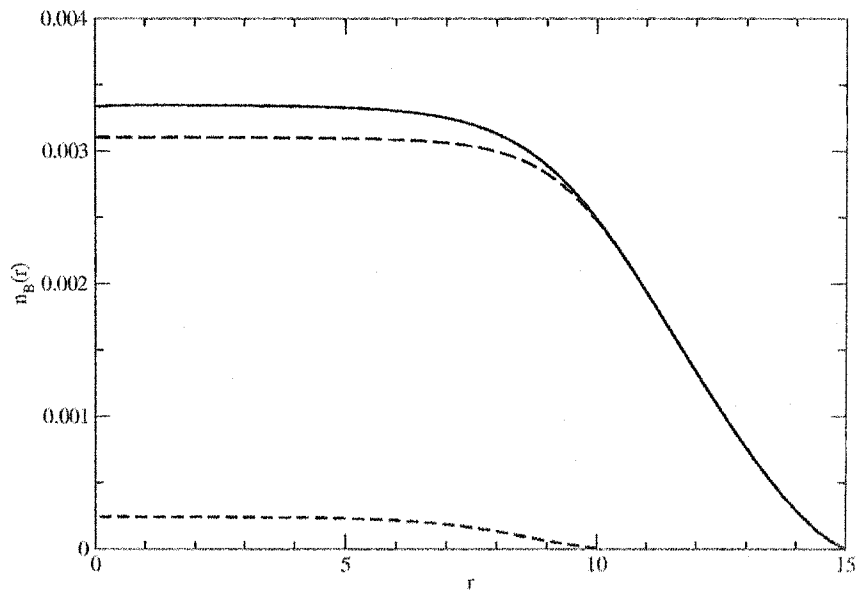
FIG. 4.9: Baryon densities for a finite system of nucleons, cascades, and lambdas with B = 146.25 for the NLC coupling set and $g_{s\Xi}/g_s = 1.0$. The total baryon density, the total density of cascades and nucleons, and the lambda density are shown by the solid, long dashed, and short dashed curves respectively. Notice that the lambda density is finite only interior to the surface.

duced to eliminate the coulomb and symmetry terms from the SEMF. Since both charge and strangeness are conserved quantities in the strong interaction, these conditions are unaffected by strong (and electromagnetic) reactions in the system. As a result, this is an intrinsically interesting case and the calculation is simplified by the need for only a single Fermi wave number. Of course, experimental processes could produce an arbitrary Q and $|S|/B$. Therefore it is of interest to estimate how much our results might be modified as these conditions are relaxed.

The SEMF has been generalized to include both nucleons and hyperons in [35, 62, 63]. The generalized SEMF proposed by Dover and Gal contains additional contributions to the bulk and symmetry energies [35]. Their SEMF, with their parameter set I, can be used to estimate how much the quantity E/B changes as one moves away from the conditions $Q = 0$ and $|S|/B = 1$. The additional terms result in $|\delta E/B| < 5$ MeV for the range $1/2 < |S|/B < 5/4$ and arbitrary Q. If one makes the rough assumption that the calculated energy could change by this amount, the surface energy extracted from plotting E/B vs. $B^{-1/3}$ could change by up to 30% (this is undoubtedly an overestimate). Calculations with arbitrary Q and $|S|/B$ are more difficult. Work is in progress to examine some of these systems.

It is also of some interest to consider the experimental manifestations of these nuclei. A number of experimental searches for strange matter have been conducted, examples of which are [51, 52, 53, 54]; all have yielded negative results. Characteristically, the systems considered here are stable against strong decay but unstable against weak decay. Therefore, their lifetimes are on the order of the weak interaction timescale, or $\sim 10^{-8}$ s. They will experience strangeness changing weak decays, such as the decay modes $\Lambda + N \rightarrow N + N$ and $\Xi + N \rightarrow \Lambda + N$. We expect relativistic heavy ion collisions or supernovae to be possible production sources for these systems. Of course, multistrange baryon systems would have to make transitions to the GS for the present calculations to be applicable. The actual rate of production

of nuclei of the type considered here is a question that goes well beyond the scope of the present paper.

One physical consequence of our results is that the *minimum* size of these objects is predicted. This value is obtained by setting $E/B = 0$ in the SEMF and then solving for B. The minimum baryon numbers derived from our calculations are 5.4 and 14.6 for $g_{s\Xi}/g_s = 1.0$ and 0.95 respectively. However, shell structure becomes more important in the region of small E/B. As a result, Hartree calculations are more reliable here. Research is in progress to more accurately estimate this number.

The purpose of the present thesis was to test the approach of FST beyond the valley of stability, specifically in the region of nonzero strangeness. The content of chapter 4 provides a successful application of this approach to strange superheavy nuclei. The following two chapters are devoted to a second application of this methodology in the strangeness sector, single Λ-hypernuclei.

CHAPTER 5

Single Λ-hypernuclei

5.1 Introduction

In this chapter, as a second application of the effective field theory approach of FST to the strangeness sector, we model single Λ-hypernuclei. This type of nuclei has a number of interesting features. As we have seen previously, a single Λ in the nucleus is stable against strong decay. This is due to the fact that the Λ, by virtue of its nature, carries a non-zero strangeness. Thus, a single Λ-hypernucleus will decay on the timescale of the weak interaction. This property enhances the potential for their detection experimentally. Also, the Λ and the nucleon are distinguishable particles.[1] These hypernuclei provide a probe into certain aspects of the strong interaction, such as the tensor force. In addition, this class of nuclei present a test case for the extension of our theoretical model outside the valley of stability as they are accessible by current experiments. Production of single Λ-hypernuclei has been achieved via the reactions (π^+, K^+) and (K^-, π^-) [8, 9, 10, 40]. However,

---

[1]The Λ and the nucleon are distinguishable particles here because no interaction is included in this theory which could convert a Λ into a nucleon or vice versa. If, for instance, kaon exchange was included, the Λ and the nucleon could no longer be considered distinguishable.

the resolution obtained here is fairly low. Recently, new processes capable of higher resolution than the above reactions have become available. One such process utilizes forward scattering from the reaction $(e, e' K^+)$ [11, 12]. Also, γ-ray coincidence experiments have been used to access this sector with high resolution [13].

To model single Λ-hypernuclei, we directly use the approach of FST outlined in chapter 2 by adding a new degree of freedom, a single, isoscalar Λ. We then construct a new Λ-lagrangian, consistent with their methodology, as an extension of the full interacting lagrangian of FST. This Λ-lagrangian contains a series of free parameters, which are determined by least-squares fits to experimental data. Various levels of sophistication in the Λ-lagrangian are investigated. This lagrangian can be used to predict other properties of single Λ-hypernuclei once the free parameters have been fixed.

5.2 Theoretical Description of Single Λ-hypernuclei

The specific phenomena that we seek to investigate here are GS binding energies (i.e. chemical potentials), densities, single-particle spectra, and particle-hole states of single Λ-hypernuclei. To this end we add a single, isoscalar Λ to the theory. Note that the Λ is also a chiral singlet because it is invariant under the full $SU(2)_L \otimes SU(2)_R$ transformation. Then, we construct our effective Λ-lagrangian as an additional contribution to the full $\nu = 4$ lagrangian of FST, utilizing their methodology. This lagrangian is of the form

$$\mathcal{L} = \mathcal{L}_{FST} + \mathcal{L}_\Lambda \tag{5.1}$$

Here we restrict ourselves to the mesons already incorporated into the theory by

FST; therefore, no new terms are needed for the meson sector. As a result, the Λ-lagrangian is confined to the fermion sector. First, we consider all possible contributions up to order $\nu = 2$, consistent with this approach. Our effective Λ-lagrangian now takes the form

$$\mathcal{L}_\Lambda^{(2)} = -\bar{\Lambda}\left[\gamma_\mu\left(\frac{\partial}{\partial x_\mu} - ig_{V\Lambda}V_\mu\right) + (M_\Lambda - g_{S\Lambda}\phi)\right]\Lambda \tag{5.2}$$

Notice that the coupling constants, $g_{S\Lambda}$ and $g_{V\Lambda}$, are free parameters and are different from those used in the nucleon case. Single Yukawa rho and pion couplings to the Λ are absent as they do not conserve isospin. Also, no electromagnetic coupling is retained to this order as $Q = 0$ for the Λ. Four-fermion terms are discussed in appendix D.

However, this lagrangian, to order $\nu = 2$, fails to reproduce the small experimental spin-orbit splitting of the p-states, as in $^{13}_\Lambda$C [38]. It was proposed in the literature that tensor couplings of order $\nu = 3$ be introduced to correct for this limitation [36, 37]. We add tensor couplings to the vector and photon fields, shown by

$$\mathcal{L}_\Lambda^{(T)} = \frac{g_{T\Lambda}g_V}{4M}\bar{\Lambda}\sigma_{\mu\nu}V_{\mu\nu}\Lambda + \frac{e}{4M}\bar{\Lambda}\lambda_\Lambda\sigma_{\mu\nu}F_{\mu\nu}\Lambda \tag{5.3}$$

The constant $g_{T\Lambda}$ is a free parameter. Here $\lambda_\Lambda = -0.613$ is the anomalous magnetic moment of the Λ. Since we want to make a full expansion in our Λ-lagrangian to order $\nu = 3$, consistent with this approach, we must also include three additional terms, shown by the following

$$\mathcal{L}_\Lambda^{(N)} = \mu_1\frac{g_S^2}{2M}\bar{\Lambda}\Lambda\phi^2 + \mu_2\frac{g_V^2}{2M}\bar{\Lambda}\Lambda V_\mu V_\mu + i\mu_3\frac{g_Sg_V}{M}\bar{\Lambda}\gamma_\mu\Lambda\phi V_\mu \tag{5.4}$$

where μ_1, μ_2, and μ_3 are three more free parameters. In the nucleon case, the terms comparable to these last three were regrouped through redefinition of the meson

fields. However, in the Λ case this is no longer possible unless additional mesons are added to the theory. A more complete description of how the terms in the Λ-lagrangian are chosen is contained in appendix D. Now our Λ-lagrangian, complete to order $\nu = 3$, is

$$\mathcal{L}_\Lambda = \mathcal{L}_\Lambda^{(2)} + \mathcal{L}_\Lambda^{(T)} + \mathcal{L}_\Lambda^{(N)} \tag{5.5}$$

Note that our lagrangian in Eq. (5.1) includes all possible terms up to $\nu = 4$ in the nucleon and meson sectors as well.[2]

In the Hartree formalism, we add a new wave function for each new baryon, given here for the Λ by

$$\psi_\Lambda(\vec{x}) = \frac{1}{r} \left(\begin{array}{c} i G_\Lambda(r) \Phi_{\kappa m} \\ -F_\Lambda(r) \Phi_{-\kappa m} \end{array} \right) \tag{5.6}$$

Plugging this wave function into the Dirac equation yields the following new pair of Hartree equations

$$\left[\frac{\partial}{\partial r} + \frac{\kappa}{r} \right] G_\Lambda(r) - [E_\Lambda - U_4 + U_5] F_\Lambda(r) - U_6 G_\Lambda(r) = 0 \tag{5.7}$$

$$\left[\frac{\partial}{\partial r} - \frac{\kappa}{r} \right] F_\Lambda(r) + [E_\Lambda - U_4 - U_5] G_\Lambda(r) + U_6 F_\Lambda(r) = 0 \tag{5.8}$$

---

[2]It is of potential interest to consider coupling additional scalar and vector mesons, such as the f_0 and the Φ, to the strangeness density and conserved strangeness current respectively. This allows one to eliminate the terms in $\mathcal{L}_\Lambda^{(N)}$ using the equations of motion and redefinitions of the new fields. However, the number of additional terms, and their accompanying free parameters, introduced to $\nu = 3$, three in the fermion lagrangian and at least four in the meson sector, makes this approach more complex than the present framework. Fortunately, the point is relatively unimportant for the single Λ-hypernuclei considered here as these new mesons are self-fields of the Λ. If they are included, they would appear only in the energy functional and have no effect on the energy eigenvalues; as the last eigenvalue in this approach is equivalent to the total binding energy per baryon for the GS, they have no effect on the cases of interest here.

where the Λ single-particle potentials are

$$U_4 = \frac{g_{V\Lambda}}{g_V}W - \frac{\mu_3}{M}\Phi W \tag{5.9}$$

$$U_5 = M_\Lambda - \frac{g_{S\Lambda}}{g_S}\Phi + \frac{\mu_1}{2M}\Phi^2 - \frac{\mu_2}{2M}W^2 \tag{5.10}$$

$$U_6 = \frac{g_{T\Lambda}}{2M}\frac{\partial W}{\partial r} + \frac{\lambda_\Lambda}{2M}\frac{\partial A}{\partial r} \tag{5.11}$$

Since all our additional terms are in the fermion lagrangian, the only change to the meson equations are added contributions to the source terms. The new contributions to the source terms arising from the Λ-lagrangian are

$$\delta\rho_S = \frac{1}{4\pi r^2}\left(G_\Lambda^2(r) - F_\Lambda^2(r)\right)\left(\frac{g_{S\Lambda}}{g_S} + \frac{\mu_1}{M}\Phi\right)$$
$$- \frac{1}{4\pi r^2}\left(G_\Lambda^2(r) + F_\Lambda^2(r)\right)\frac{\mu_3}{M}W \tag{5.12}$$

$$\delta\rho_B = \frac{1}{4\pi r^2}\left(G_\Lambda^2(r) + F_\Lambda^2(r)\right)\left(\frac{g_{V\Lambda}}{g_V} - \frac{\mu_3}{M}\Phi\right)$$
$$- \frac{1}{4\pi r^2}\left(G_\Lambda^2(r) - F_\Lambda^2(r)\right)\frac{\mu_2}{M}W \tag{5.13}$$

$$\delta\rho_B^T = \frac{1}{4\pi r^2}2G_\Lambda(r)F_\Lambda(r)\frac{g_{T\Lambda}}{f_V} \tag{5.14}$$

$$\delta\rho_a^T = \frac{1}{4\pi r^2}2\lambda_\Lambda G_\Lambda(r)F_\Lambda(r) \tag{5.15}$$

The new energy functional is identical in form to the one used by FST, with only one additional energy eigenvalue, E_Λ. The numerical solution to the extended set of coupled, local, nonlinear differential equations was obtained by extension of a program developed by Huertas [16, 21]. Here we use the parameter sets of FST for the nucleon and meson parameters. There are six new parameters in our Λ-lagrangian: $g_{S\Lambda}$, $g_{V\Lambda}$, $g_{T\Lambda}$, μ_1, μ_2, and μ_3. They are fit to a series of experimentally known Λ single-particle levels. These least-squares fits are conducted at various levels of truncation in our Λ-lagrangian, while maintaining the full lagrangian of FST to order $\nu = 4$. Now this lagrangian can be used to *predict* other properties

of single Λ-hypernuclei. One application we investigate in the next chapter is $s_{1/2}$-splittings.

5.3 Parameter Fits

The methodology with which the parameter fits are conducted is described in this section. As discussed in section 5.2, the full lagrangian contains a number of free parameters. To use this lagrangian for predictive purposes, these parameters must be determined. Those constants which lie in the nucleon and meson sectors are fixed by the G2 parameter set. This set was developed by FST [1] and is given in Table 2.1. Notice that it contains all possible terms to order $\nu = 4$ in both the nucleon and meson sectors of the lagrangian. FST determine these parameters by conducting a least-square χ^2 fit, of the form shown in Eq. (2.40), to experimental data from along the valley of stability. This process is described in detail in [1] and reviewed in chapter 2.

Now if we consider the full lagrangian in Eq. (5.1), we will notice that the parameters in the Λ sector are still unconstrained. In fact, a total of six parameters remain undetermined to order $\nu = 3$. Fits are conducted at various levels of truncation in the underlying Λ-lagrangian to fix the relevant constants. The fits performed here are entirely separate from the one which determined the G2 parameter set; however, the framework which FST used to conduct their fits is identical to the one employed here. Consequently, experimental data from single Λ-hypernuclei is utilized to constrain the parameters in the Λ-lagrangian. This data, which is listed in Table 5.1, consists of three types of observables: GS binding energies, Λ s-p shell excitation energies, and spin-orbit splittings of the p-states.[3] Now we use the

---

[3]Appendix E provides an alternative potential-based examination of the consistency of the experimental GS binding energies.

	Experimental Data			M2 Calculation
GS E/B	$^{13}_{\Lambda}$C	-11.69 ± 0.12	[40]	-11.08
	$^{16}_{\Lambda}$O	-12.50 ± 0.35	[8]	-12.22
	$^{28}_{\Lambda}$Si	-17.70 ± 0.29	[9]	-17.63
	$^{32}_{\Lambda}$S	-17.50 ± 0.5	[9]	-18.22
	$^{40}_{\Lambda}$Ca	-18.70 ± 1.1	[8]	-18.89
	$^{208}_{\Lambda}$Pb	-27.0 ± 1.0	[10]	-28.08
E_{SO}	$^{13}_{\Lambda}$C	0.15 ± 0.09	[38]	0.150
E_{SP}	$^{13}_{\Lambda}$C	10.83 ± 0.03	[38]	8.975
	$^{16}_{\Lambda}$O	10.6 ± 0.3	[39]	8.414
	$^{40}_{\Lambda}$Ca	7.70 ± 1.0	[8]	7.920

TABLE 5.1: The experimental data used in the parameter fits. This includes six GS binding energies (E/B), one spin-orbit splitting of the p-states ($E_{SO} = E_{1p_{1/2}} - E_{1p_{3/2}}$), and three Λ s-p shell excitation energies ($E_{SP} = E_{1p_{3/2}} - E_{1s_{1/2}}$). The calculated values of these observables, using the M2 set, are also shown. The values are given in MeV.

framework outlined in chapter 2 and section 5.2 to calculate these same observables for some initial guess of the parameters. The calculated and experimental values are both substituted into the equation

$$\chi^2_N = \sum_i \sum_X \left[\frac{X^{(i)}_{exp} - X^{(i)}_{th}}{W^{(i)}_X X^{(i)}_{exp}} \right]^2 \qquad (5.16)$$

where N is the number of data points. The parameters are varied such that the theoretical and experimental values converge. The constants are fixed at the values that produce a global minimum in χ^2_N.

To conduct fits of this type, the degree of truncation in the lagrangian must first be determined. This will define the number of free parameters which are varied in the fit. Our underlying Λ-lagrangian is truncated at four different levels and separate parameter fits are conducted at each. First, we consider the simplest possible case; only terms to order $\nu = 2$ are retained in the Λ-lagrangian, which corresponds to $\mathcal{L}^{(2)}_\Lambda$. This Λ-lagrangian has a total of two free parameters, g_{SA} and g_{VA}. In this

	M1	M2	M3-1	M3-2	M4
g_{SA}/g_S	0.87357	0.87195	0.87362	0.87154	0.87195
g_{VA}/g_V	1.0	0.97873	0.97766	0.98055	0.97873
$g_{TA}/4$		-0.885	-0.890	-0.879	-0.885
μ_1			-0.1214	0.1565	0.0774
μ_2			-0.1971	0.2542	0.3440
μ_3					0.0774

TABLE 5.2: The five parameter sets constructed here. Note that all the constants are natural and that these sets represent different levels of sophistication in the Λ-lagrangian.

	M2	M3-1	M3-2	M4
$\chi^2_{10}(UW) \times 100$	0.147	0.126		
$\chi^2_{10}(W) \times 10$	0.337		0.249	0.229

TABLE 5.3: The χ^2 values for both the unweighted and weighted fits, UW and W respectively, relative to the χ^2 of the M1 set. Here χ^2 is determined from Eq. (5.16) using 10 pieces of data.

case, the vector coupling is assumed to be universal, as it is coupled to the conserved baryon current, and the scalar coupling is fit to reproduce the binding energy of a single Λ in nuclear matter, which is about -28 MeV [26]. These assumptions are in keeping with the previous work in [34] and chapter 4. The parameters determined here are shown in Table 5.2 as the M1 set. This set reproduces the GS binding energies fairly well, but is unable to simulate either the correct spin-orbit splitting in the p-states or the s-p shell excitation energies in light Λ-hypernuclei.

In order to obtain a better fit to the data, we increase the level of truncation. Therefore, tensor couplings to both the vector and photon fields are included, which correspond to the terms in $\mathcal{L}_\Lambda^{(T)}$. As a result, a third free parameter, g_{TA}, is introduced. This fit is performed using seven pieces of experimental data: the six GS binding energies and the spin-orbit splitting given in Table 5.1. In this particular case, the weights in Eq. (5.16) are all taken to be equal. The resulting parameters
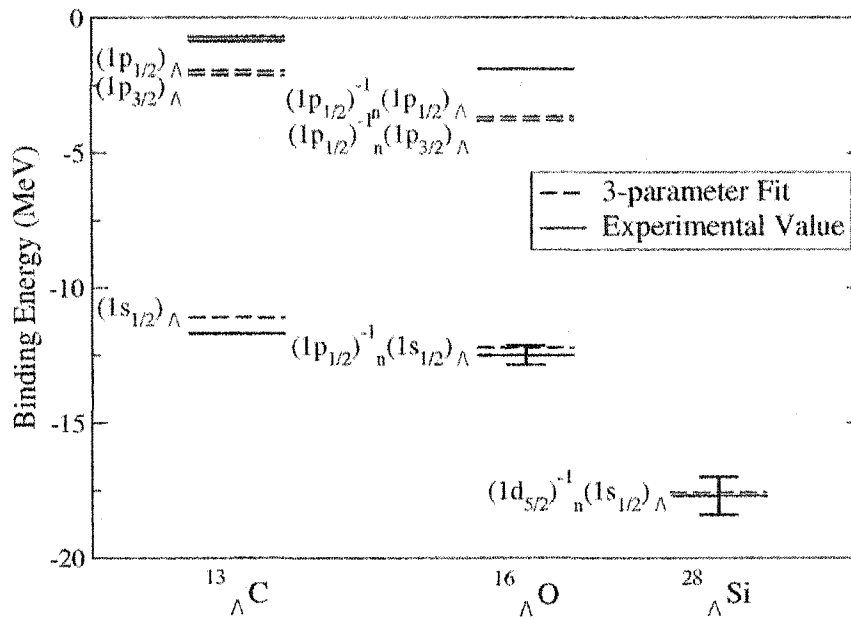
FIG. 5.1: Results of the unweighted 3-parameter fit, along with Fig. 5.2, to a series of experimental data. The G2 parameter set of FST is used for both the nucleon and meson sectors [1].
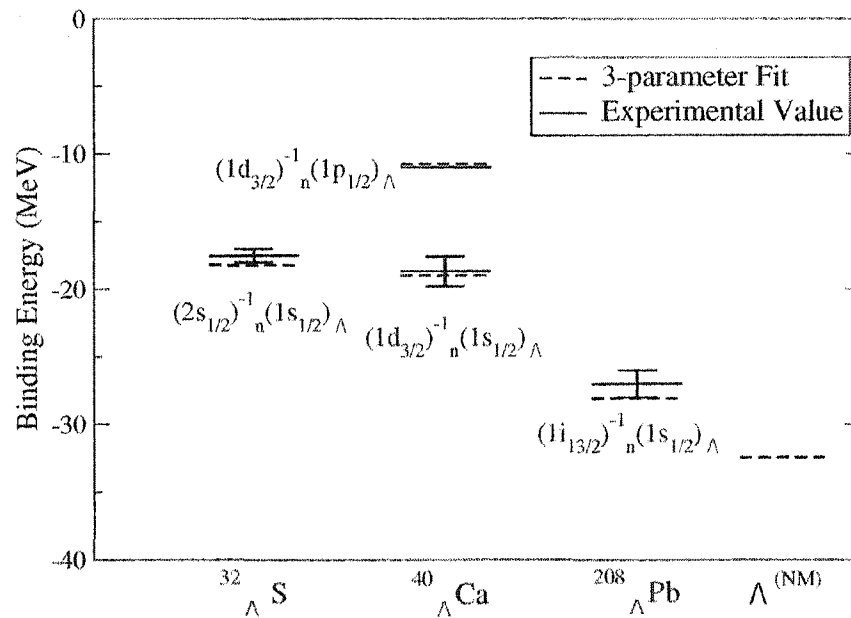
FIG. 5.2: Results of the unweighted 3-parameter fit, along with Fig. 5.1, to a series of experimental data. The G2 parameter set of FST is used for both the nucleon and meson sectors [1]. The calculated binding energy of a single Λ in infinite nuclear matter is also shown.

are given in Table 5.2 as the M2 set. These constants all satisfy the assumption of naturalness. Table 5.1 also outlines the numerical results of this 3-parameter fit. The outcome of this fit is shown graphically in Figs. 5.1 and 5.2. One can see that both the GS binding energies and the small spin-orbit splitting in the p-states are reproduced well. The calculated s-p shell excitation energies fail to duplicate the experimental values of these observables for the lightest Λ-hypernuclei; however, it is correctly given by the time one gets to $^{40}_{\Lambda}$Ca. In Fig. 5.2, the value of -32.4 MeV is given as the calculated binding energy of a single Λ in nuclear matter. This M2 parameter set will be used in the subsequent calculation of the $s_{1/2}$-splittings in chapter 6.

Plots of the proton, neutron, and Λ densities for the GS's of $^{16}_{\Lambda}$N and $^{40}_{\Lambda}$Ca calculated using this M2 set are shown in Figs. 5.3 and 5.4 respectively. A graph of the Hartree spinors from the Λ wave function, $G_{\Lambda}(r)$ and $F_{\Lambda}(r)$, for the GS of $^{40}_{\Lambda}$Ca using the M2 set is given in Fig. 5.5. Notice that the magnitude of the lower spinor is very small; this indicates that the Λ is essentially behaving as a non-relativistic particle in the nuclear potential.

Next, the two terms nonlinear in the scalar and vector field, shown in $\mathcal{L}_{\Lambda}^{(N)}$, are retained. This brings the number of unconstrained parameters up to five. For this 5-parameter fit, ten pieces of experimental data are used; in addition to the data utilized in the 3-parameter fit, the three Λ s-p shell excitation energies listed in Table 5.1 are also included. Two versions of the 5-parameter fit were conducted here: one unweighted and one weighted. In the former case, all of the weights are equal. For the latter, the weighting scheme is as follows:

- $W_X^{(i)} = 1.0$ for GS binding energies;

- $W_X^{(i)} = 10.0$ for Λ s-p shell excitation energies;

- and $W_X^{(i)} = 40.0$ for the spin-orbit splitting.
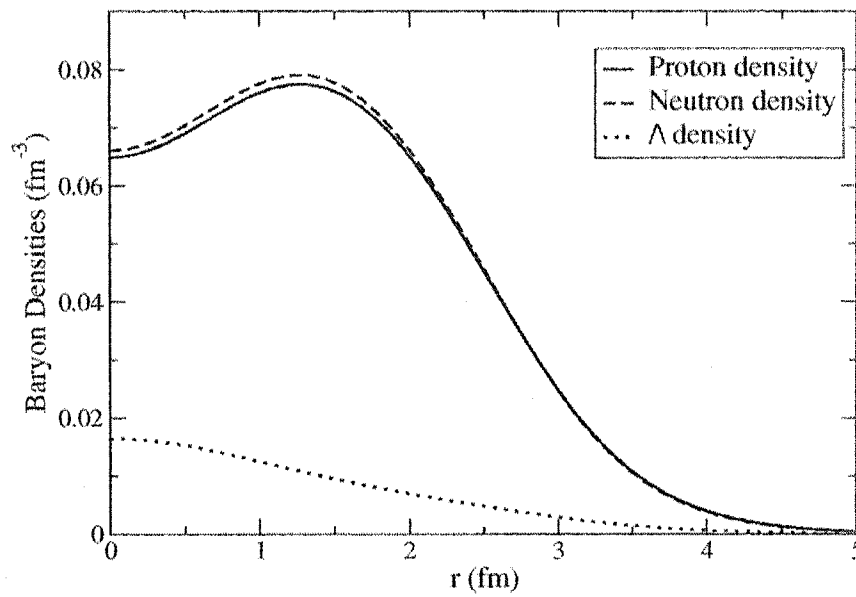
FIG. 5.3: Plot of the proton, neutron, and Λ densities for the GS of $^{16}_{\Lambda}$N. Here the M2 parameter set was used.
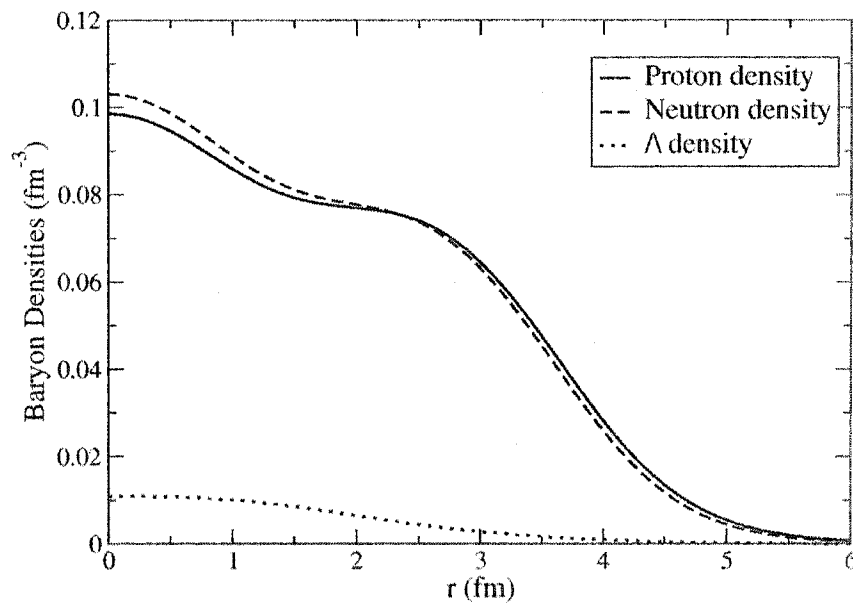
FIG. 5.4: Plot of the proton, neutron, and Λ densities for the GS of $^{40}_{\Lambda}$Ca. Here the M2 parameter set was used.
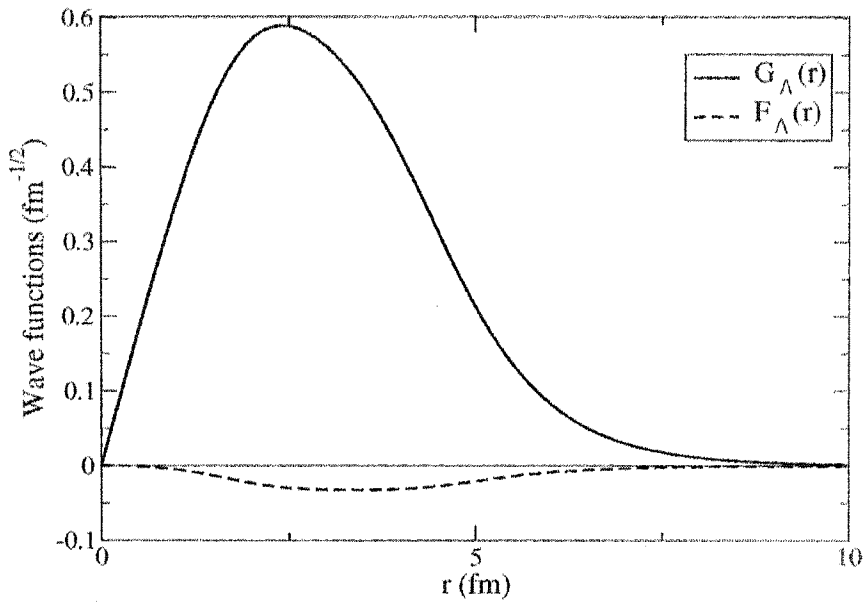
FIG. 5.5: Radial wave functions of the Λ in the $(1s_{1/2})$ state for the GS of $^{40}_{\Lambda}$Ca. Here the M2 parameter set was used.

Some justification for the selection of these weights can be gleaned from [104]. The formula $W_X^{(i)} = f_i(\Delta E_{exp}/E_{exp})$ was used where f_i is an arbitrary factor chosen to prevent any observable from dominating the fit. However, not enough data was available to constrain the two new parameters individually. As a result, we initially restrict these parameters with the relation

$$\frac{\mu_2}{\mu_1} = \left(\frac{g_S\phi_0}{g_V V_0}\right)^2_{n.m.} = 1.624 \qquad (5.17)$$

where n.m. denotes the nuclear matter values, which are found in [2]. However, the new parameters are not very well determined and fail to significantly improve the fit in either the unweighted or weighted case, as can be seen from Table 5.3. Therefore, we leave the constraint of Eq. (5.17) intact. The results of both 5-parameter fits are shown in Table 5.2; the M3-1 and M3-2 sets denote the unweighted and weighted schemes respectively. Again notice that the parameters are all essentially natural.

Lastly, to include all possible terms up to order $\nu = 3$ in the Λ-lagrangian, all three terms in $\mathcal{L}_\Lambda^N$ are retained. Again, not enough data was available to individually constrain the new parameters; therefore, we restrict these parameters with the relation

$$\mu_1 = \mu_3 = 0.225\mu_2 \tag{5.18}$$

and fix the remaining constants using the M2 set. These ratios were chosen because they tend to concentrate the effects of the new contributions in the surface of the nucleus, i.e. the additional contributions now essentially vanish for uniform nuclear matter. This will have a greater effect on the s-p shell excitations than on the GSs. The weighting scheme described above was used. The resulting parameters are listed in Table 5.2 as the M4 set. Again, as seen in Table 5.3 the improvement in the overall fit is negligible. The M3-2 and M4 sets both improve the fit to the GSs but do worse with respect to the s-p shell excitations; the M3-1 set has the opposite effect.

CHAPTER 6

$s_{1/2}$-splittings

6.1 Introduction

Consider nuclei like $^{16}_{\Lambda}O$; the GS's of such systems are, in fact, particle-hole states. One process by which nuclei of this type are created is the reaction (π^+, K^+) on target nuclei with closed proton and neutron shells [8, 9, 10]. During the course of this reaction a neutron is converted into a Λ. As a result, a neutron hole is also created which, for the GS, inhabits the outermost neutron shell. The angular momentum of the Λ and the neutron hole couple to form a multiplet. However, due to the fact that in the GS the Λ occupies the $1s_{1/2}$ shell, there are only two states in these multiplets. It is these configurations that we refer to as $s_{1/2}$-doublets. The reaction $(e, e' K^+)$ is another process used to create nuclei of this type [11, 12]. This process differs in that a proton hole is created here and that greater resolution is possible.

An inspection of Figs. 5.1 and 5.2 reveals that many of the GSs are actually $s_{1/2}$-doublets. This chapter is devoted to the development of a systematic method to calculate these splittings. To this end, we utilize the analysis described in [19] and

97

reviewed in appendix F. This system defines a particle-hole matrix element as the sum of Dirac two-body matrix elements. These Dirac matrix elements are reduced to two dimensional radial integrals via angular momentum relations [45]. We express these integrals in terms of the Hartree spinors determined from the single-particle analysis of the preceding chapter. The effective interaction used here follows directly from our effective lagrangian. For the $\Lambda - N$ case, this corresponds to simple Yukawa scalar and neutral vector meson exchange. Isospin requirements prevent rho meson and single Yukawa pion exchange from contributing. Furthermore, the fact that the nucleon and the Λ are distinguishable particles indicates that no exchange matrix elements need be calculated. As it turns out, only the spatial part of the vector exchange contributes to the $s_{1/2}$-splittings in single Λ-hypernuclei. This component vanishes in the static limit ($M \to \infty$) and hence has no direct interpretation in terms of static two-body potentials. This current-current interaction has an analog in the electromagnetic case, Møller scattering; the spatial components of the currents vanish in the non-relativistic limit [14]. This method is used to calculate the $s_{1/2}$-splittings of every applicable state displayed in the Figs. 5.1 and 5.2.

6.2 Theory of $s_{1/2}$-doublets

In order to calculate the splitting of these doublets, we first consider Dirac two-body matrix elements of the forms [41]

$$\langle (n_1 l_1 j_1)(n_2 l_2 j_2)JM|V(r_{12})|(n_3 l_3 j_3)(n_4 l_4 j_4)J'M'\rangle \qquad (6.1)$$

and

$$\langle (n_1 l_1 j_1)(n_2 l_2 j_2)JM|V(r_{12})\vec{\sigma}^{(1)} \cdot \vec{\sigma}^{(2)}|(n_3 l_3 j_3)(n_4 l_4 j_4)J'M'\rangle \qquad (6.2)$$

where the single-particle wave functions are specified by $\{nlj\}$, corresponding to

either the upper or lower components in Eq. (2.17), and $V(r_{12})$ is some effective interaction. Next, we expand this effective interaction in terms of Legendre polynomials [41]

$$V(r_{12}) = \sum_{k=0}^{\infty} f_k(r_1, r_2) P_k(\cos\theta_{12}) \tag{6.3}$$

$$= \sum_{k=0}^{\infty} f_k(r_1, r_2) C_k(1) \cdot C_k(2) \tag{6.4}$$

where the Racah functions, $C_{kq}(\theta, \phi)$, are defined in appendix A. Inverting Eq. (6.3) yields the expression

$$f_k(r_1, r_2) = \frac{2k+1}{2} \int_{-1}^{1} d(\cos\theta_{12}) P_k(\cos\theta_{12}) V(r_{12}) \tag{6.5}$$

In the case of Eq. (6.2), the effective interaction is coupled to Pauli matrices. Therefore, Eq. (6.3) is modified to

$$V(r_{12})\vec{\sigma}^{(1)} \cdot \vec{\sigma}^{(2)} = \sum_{k\lambda} (-1)^{k+1-\lambda} f_k(r_1, r_2) \chi_\lambda^{(k,1)}(1) \cdot \chi_\lambda^{(k,1)}(2) \tag{6.6}$$

Here $\chi_{\lambda\mu}^{(k,1)}$ are C_{kq} coupled to Pauli matrices, shown by

$$\chi_{\lambda\mu}^{(k,1)} = \sum_{qq'} C_{kq}\sigma_{1q'} \langle kq1q'|k1\lambda\mu\rangle \tag{6.7}$$

Now we introduce a specific type of effective interaction. The form we use here follows directly from the effective lagrangian in the preceding chapter and to lowest order, corresponds to simple Yukawa couplings of both the scalar and vector fields, given by

$$V(r_{12}) = \gamma_4^{(1)}\gamma_4^{(2)} \left[\frac{-g_S g_{SA}}{4\pi} \frac{e^{-m_S r_{12}}}{r_{12}} + \gamma_\mu^{(1)}\gamma_\mu^{(2)} \frac{g_V g_{VA}}{4\pi} \frac{e^{-m_V r_{12}}}{r_{12}} \right] \tag{6.8}$$

Here $r_{12} = |\vec{r}_1 - \vec{r}_2|$. This simplistic spatial dependence is possible because retardation in the meson propagators is neglected [41], or

$$\frac{1}{p_\mu^2 + m^2} \rightarrow \frac{1}{\vec{p}^2 + m^2} \tag{6.9}$$

Otherwise the full Lorentz structure is maintained [41]. Couplings to the rho and pion fields are absent as $T = 0$ for the Λ. Also, note that as this effective interaction is isoscalar, it does not distinguish between proton and neutron holes. In this formalism, we can now write

$$f_k(r_1, r_2) = \gamma_4^{(1)}\gamma_4^{(2)} \left[f_k^S(r_1, r_2) + \gamma_\mu^{(1)}\gamma_\mu^{(2)} f_k^V(r_1, r_2) \right] \tag{6.10}$$

where

$$f_k^S(r_1, r_2) = -\frac{g_S g_{S\Lambda}}{4\pi}(2k+1)\frac{2m_S}{\pi}i_k(m_S r_<)k_k(m_S r_>) \tag{6.11}$$

$$f_k^V(r_1, r_2) = \frac{g_V g_{V\Lambda}}{4\pi}(2k+1)\frac{2m_V}{\pi}i_k(m_V r_<)k_k(m_V r_>) \tag{6.12}$$

where $r_<$ ($r_>$) is the smaller (larger) of r_1 and r_2. Here $i_k(mr)$ and $k_k(mr)$ are modified spherical Bessel functions of order k.[1]

The matrix elements in Eqs. (6.1) and (6.2) are actually six dimensional integrals. Treating the γ-matrices as 2×2 block matrices operating on the upper and lower components of the Hartree spinors, these Dirac matrix elements, for each term in the interaction, are actually the sum of four separate integrals. The scalar and vector time ($\mu = 4$) components of the effective interaction take the form of Eq. (6.1); the vector spatial ($\mu = 1, 2, 3$) components take the form of Eq. (6.2). Thankfully, angular momentum relations allow one to integrate out the angular dependence [45].

---

[1] The modified spherical Bessel functions are defined in appendix A.

These integrals, for the scalar and vector time components, become

$$(6.1) = \sum_{k=0}^{\infty} \langle 12|f_k^i(r_1,r_2)|34\rangle (-1)^{j_2+j_3+J} \left\{ \begin{array}{ccc} J & j_2 & j_1 \\ k & j_3 & j_4 \end{array} \right\} \delta_{JJ'}\delta_{MM'}$$

$$\times \langle (l_1\tfrac{1}{2})j_1||C_k(1)||(l_3\tfrac{1}{2})j_3\rangle \langle (l_2\tfrac{1}{2})j_2||C_k(2)||(l_4\tfrac{1}{2})j_4\rangle \qquad (6.13)$$

where $i = S, V$ and (6.1) indicates the quantity in Eq. (6.1). For the vector spatial components, these integrals become

$$(6.2) = \sum_{k=0}^{\infty}\sum_{\lambda} \langle 12|f_k^V(r_1,r_2)|34\rangle (-1)^{k+1-\lambda}(-1)^{j_2+j_3+J} \left\{ \begin{array}{ccc} J & j_2 & j_1 \\ \lambda & j_3 & j_4 \end{array} \right\} \delta_{JJ'}\delta_{MM'}$$

$$\times \langle (l_1\tfrac{1}{2})j_1||\chi_\lambda^{(k,1)}(1)||(l_3\tfrac{1}{2})j_3\rangle \langle (l_2\tfrac{1}{2})j_2||\chi_\lambda^{(k,1)}(2)||(l_4\tfrac{1}{2})j_4\rangle \qquad (6.14)$$

The 6-j symbols limit the possible allowed values of k and λ. The reduced matrix elements are evaluated using [45] and further limit k and λ. Note that as the upper and lower Hartree spinors have different l values, the reduced matrix elements in Eqs. (6.13) and (6.14) must have the corresponding, appropriate l values.

Now consider the remaining two-dimensional radial integrals, where the numbers are a shorthand for all the quantum numbers needed to uniquely specify the radial wave functions [41],

$$\langle 12|f_k^i(r_1,r_2)|34\rangle = \int_0^\infty \int_0^\infty dr_1 dr_2 U_1(r_1)U_2(r_2)f_k^i(r_1,r_2)U_3(r_1)U_4(r_2) \qquad (6.15)$$

Here $R(r) = U(r)/r$ are the appropriate radial Dirac wave functions, in terms of $G_a(r)$ and $F_a(r)$, and again $i = S, V$.

Using the Hartree spinor representation, the particle-hole matrix element is

expressed as a sum of Dirac matrix elements of the types shown above [19], or[2]

$$v_{ab;lm}^{J} = \sum_{J'}(2J'+1)\left\{\begin{array}{ccc} j_m & j_a & J' \\ j_b & j_l & J \end{array}\right\}\langle lbJ'|V|amJ'\rangle \tag{6.16}$$

No exchange term is required, due to the fact that the Λ and the nucleon are distinguishable particles here. For example, the particle-hole matrix element for the vector spatial component of the effective interaction is

$$\begin{aligned}
v_{32;14}^{J}(\text{vs}) &= (-1)^{j_2+j_3+J}\sum_{k}^{\infty}\sum_{\lambda}(-1)^{k}\left\{\begin{array}{ccc} j_2 & j_4 & \lambda \\ j_1 & j_3 & J \end{array}\right\}\int\int dr_1 dr_2 \\
&\times \Big\{ G_1(r_1)F_3(r_1)f_k^{V}(r_1,r_2)G_2(r_2)F_4(r_2) \\
&\times \langle(l_{1A}\tfrac{1}{2})j_1||\chi_{\lambda}^{(k,1)}(1)||(l_{3B}\tfrac{1}{2})j_3\rangle\langle(l_{2A}\tfrac{1}{2})j_2||\chi_{\lambda}^{(k,1)}(2)||(l_{4B}\tfrac{1}{2})j_4\rangle \\
&- G_1(r_1)F_3(r_1)f_k^{V}(r_1,r_2)F_2(r_2)G_4(r_2) \\
&\times \langle(l_{1A}\tfrac{1}{2})j_1||\chi_{\lambda}^{(k,1)}(1)||(l_{3B}\tfrac{1}{2})j_3\rangle\langle(l_{2B}\tfrac{1}{2})j_2||\chi_{\lambda}^{(k,1)}(2)||(l_{4A}\tfrac{1}{2})j_4\rangle \\
&- F_1(r_1)G_3(r_1)f_k^{V}(r_1,r_2)G_2(r_2)F_4(r_2) \\
&\times \langle(l_{1B}\tfrac{1}{2})j_1||\chi_{\lambda}^{(k,1)}(1)||(l_{3A}\tfrac{1}{2})j_3\rangle\langle(l_{2A}\tfrac{1}{2})j_2||\chi_{\lambda}^{(k,1)}(2)||(l_{4B}\tfrac{1}{2})j_4\rangle \\
&+ F_1(r_1)G_3(r_1)f_k^{V}(r_1,r_2)F_2(r_2)G_4(r_2) \\
&\times \langle(l_{1B}\tfrac{1}{2})j_1||\chi_{\lambda}^{(k,1)}(1)||(l_{3A}\tfrac{1}{2})j_3\rangle\langle(l_{2B}\tfrac{1}{2})j_2||\chi_{\lambda}^{(k,1)}(2)||(l_{4A}\tfrac{1}{2})j_4\rangle \Big\}
\end{aligned} \tag{6.17}$$

Here l_{iA} and l_{iB} are the l values corresponding to the upper and lower Hartree spinors respectively for the ith wave function where $i = 1,..4$. Now the splitting, for a $s_{1/2}$-doublet, is just the difference between the particle-hole matrix elements of

---

[2]These particle-hole matrix elements are developed in appendix F.

the two available states, or

$$\delta\epsilon = v_{n\Lambda;n\Lambda}^{J=j_1+j_2} - v_{n\Lambda;n\Lambda}^{J=|j_1-j_2|} \tag{6.18}$$

The substitutions used to acquire the appropriate indices for this case are $n = 1, 3$ and $\Lambda = 2, 4$. The solution to the Hartree equations yields a single-particle energy level for the GS, E_Λ. As previously mentioned, for the cases under consideration this level is in fact a doublet; however, Eq. (6.18) evaluates only the size of the *splitting*. In order to determine the position of the doublet relative to E_Λ, one needs the relation[3]

$$\sum_J (2J + 1)\,\delta\epsilon = 0 \tag{6.19}$$

We now have a framework with which to calculate the size of the $s_{1/2}$-splittings of the single Λ-hypernuclei of interest here and to determine their location relative to E_Λ. The problem is reduced to Slater integrals and some algebra; the 6-j and 9-j symbols are determined using [105, 106]. The Dirac wave functions needed to solve the radial integrals are taken as the solutions to the Hartree equations from the previous section. Once all the parameters in the underlying lagrangian are fixed, the splitting is completely determined in this approach as there are no additional constants fit to excited state properties [41]. We also mention that this approach is applicable to excited states and multiplets for this class of nuclei.

To calibrate this approach, we apply it to *ordinary nuclei*. Two modifications to our framework are required here. First, an exchange term is included because the proton and neutron are indistinguishable particles. As a result, the particle-hole

---

[3]The proof of this relation is contained in appendix G.

matrix element becomes the following [19]:[2]

$$
v_{ab;lm}^{J} = \sum_{J'} (2J' + 1) \left\{ \begin{matrix} j_m & j_a & J' \\ j_b & j_l & J \end{matrix} \right\} \left[\langle lbJ'|V|amJ' \rangle - (-1)^{j_a+j_m+J'} \langle lbJ'|V|maJ' \rangle \right]
$$

(6.20)

Second, the effective interaction is also modified, requiring additional couplings to the rho and pion fields [41]

$$
\begin{aligned}
V(r_{12}) &= \gamma_4^{(1)}\gamma_4^{(2)} \left[\frac{-g_S^2}{4\pi} \frac{e^{-m_S r_{12}}}{r_{12}} + \gamma_\mu^{(1)}\gamma_\mu^{(2)} \frac{g_V^2}{4\pi} \frac{e^{-m_V r_{12}}}{r_{12}} \right. \\
&\left. + \gamma_\mu^{(1)}\gamma_\mu^{(2)} \frac{\tilde{\tau}^{(1)} \cdot \tilde{\tau}^{(2)}}{4} \frac{g_\rho^2}{4\pi} \frac{e^{-m_\rho r_{12}}}{r_{12}} + \gamma_5^{(1)}\gamma_5^{(2)} \tilde{\tau}^{(1)} \cdot \tilde{\tau}^{(2)} \frac{g_\pi^2}{4\pi} \frac{e^{-m_\pi r_{12}}}{r_{12}} \right]
\end{aligned}
$$

(6.21)

These alterations make the ordinary nuclear matter case considerably more complicated than the case of single Λ-hypernuclei.

6.3 Results and Discussion of the $s_{1/2}$-splittings

In this section we discuss the calculation of the $s_{1/2}$-splittings in Λ-hypernuclei and the results obtained from these calculations. Following the methodology established in section 6.2, one needs to evaluate $\delta\epsilon$ from Eq. (6.18) to determine the size of these doublets. It is possible to separate $\delta\epsilon$ into contributions from each portion of the effective interaction, or

$$
\delta\epsilon = \delta\epsilon(s) + \delta\epsilon(vt) + \delta\epsilon(vs)
$$

(6.22)

where s, vt, and vs represent the scalar, vector time, and vector spatial components respectively. As it turns out, the scalar and vector time components each cancel in the splitting, shown by

$$
\delta\epsilon(s) = \delta\epsilon(vt) = 0
$$

(6.23)

Therefore, the $s_{1/2}$-splittings are entirely determined from the vector spatial term in the effective interaction, or

$$\delta\epsilon = \delta\epsilon(\text{vs}) \qquad (6.24)$$

This is true for any system in which either the Λ or the nucleon hole has $j = 1/2$.[4] It is interesting to note that this calculation tests a different sector of the underlying lagrangian than the mean field analysis and that, as there is no corresponding interpretation in the static limit ($M \rightarrow \infty$), it is here an entirely relativistic effect. Now, to determine the splitting we only need to evaluate the particle-hole matrix element in Eq. (6.17) for the two appropriate J values. These matrix elements have been reduced to two-dimensional radial integrals and some algebra [45]; the 6-j and 9-j symbols are evaluated using [105, 106]. The integrals are solved using the Hartree spinors, $G_a(r)$ and $F_a(r)$, calculated in the single-particle analysis. Notice that the integrals in the vector spatial contribution mix the upper and lower components of the Hartree wave functions. Numerically, the integration is performed using Simpson's method.

The results of this analysis are contained in Table 6.1. The splittings with a neutron hole listed in Table 6.1 all correspond to single-particle levels which were used in the fits of the preceding discussion, as shown in Figs. 5.1 and 5.2. The $s_{1/2}$-splittings for $^{16}_{\Lambda}$O and $^{28}_{\Lambda}$Si are graphed in Fig. 6.1; the GS doublets for $^{32}_{\Lambda}$S and $^{40}_{\Lambda}$Ca are plotted in Fig. 6.2.

Notice that the splittings in Figs. 6.1 and 6.2 are all within the experimental error bars on the GS binding energies.

The appropriate level orderings are shown. It should be mentioned that the three excited states with neutron holes shown in Table 6.1 will overlap with other states of the same J value. Therefore in these cases one must diagonalize the hamil-

---

[4]The proof of this statement is contained in appendix H.

Nucleus	State	Levels	$\lvert \delta\epsilon \rvert$
$^{12}_{\Lambda}\mathrm{B}$	$(1\mathrm{p}_{3/2})_\mathrm{p}^{-1}(1\mathrm{s}_{1/2})_\Lambda$	$2^-_\mathrm{GS},\ 1^-$	430
$^{16}_{\Lambda}\mathrm{N}$	$(1\mathrm{p}_{1/2})_\mathrm{p}(1\mathrm{s}_{1/2})_\Lambda$	$1^-_\mathrm{GS},\ 0^-$	481
	$(1\mathrm{p}_{3/2})_\mathrm{p}^{-1}(1\mathrm{s}_{1/2})_\Lambda$	$2^-_\mathrm{LL},\ 1^-$	318
$^{16}_{\Lambda}\mathrm{O}$	$(1\mathrm{p}_{1/2})_\mathrm{n}(1\mathrm{s}_{1/2})_\Lambda$	$1^-_\mathrm{GS},\ 0^-$	489
	$(1\mathrm{p}_{1/2})_\mathrm{n}(1\mathrm{p}_{3/2})_\Lambda$	$2^+_\mathrm{LL},\ 1^+$	128
	$(1\mathrm{p}_{1/2})_\mathrm{n}(1\mathrm{p}_{1/2})_\Lambda$	$1^+_\mathrm{LL},\ 0^+$	668
$^{28}_{\Lambda}\mathrm{Si}$	$(1\mathrm{d}_{5/2})_\mathrm{n}^{-1}(1\mathrm{s}_{1/2})_\Lambda$	$3^+_\mathrm{GS},\ 2^+$	293
$^{32}_{\Lambda}\mathrm{S}$	$(2\mathrm{s}_{1/2})_\mathrm{n}(1\mathrm{s}_{1/2})_\Lambda$	$1^+_\mathrm{GS},\ 0^+$	220
$^{40}_{\Lambda}\mathrm{Ca}$	$(1\mathrm{d}_{3/2})_\mathrm{n}^{-1}(1\mathrm{s}_{1/2})_\Lambda$	$2^+_\mathrm{GS},\ 1^+$	310
	$(1\mathrm{d}_{3/2})_\mathrm{n}^{-1}(1\mathrm{p}_{1/2})_\Lambda$	$2^-_\mathrm{LL},\ 1^-$	394
$^{208}_{\Lambda}\mathrm{Pb}$	$(1\mathrm{i}_{13/2})_\mathrm{n}^{-1}(1\mathrm{s}_{1/2})_\Lambda$	$7^+_\mathrm{GS},\ 6^+$	24

TABLE 6.1: $\mathrm{s}_{1/2}$-splittings, and some excited states, are shown with their respective configurations, level orderings, and doublet magnitudes. Here LL denotes lower level and $\lvert \delta\epsilon \rvert$ is in keV.
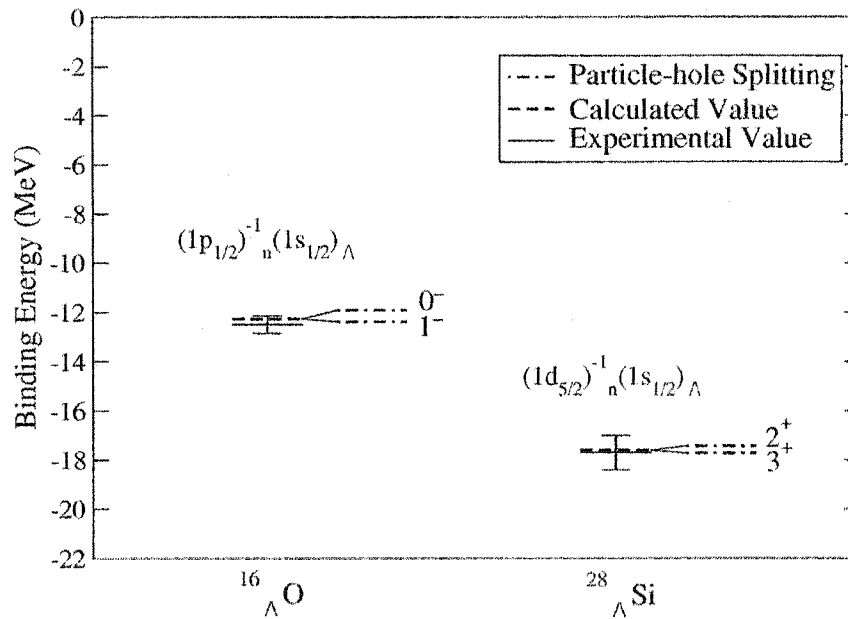
FIG. 6.1: Graph of GS particle-hole splittings and their respective level orderings for $^{16}_{\Lambda}\mathrm{O}$ and $^{28}_{\Lambda}\mathrm{Si}$. The single-particle calculations were conducted using the M2 parameter set and are plotted alongside the experimental values [8, 10]. Notice that the splittings lie within the experimental error bars in both cases.

107
107
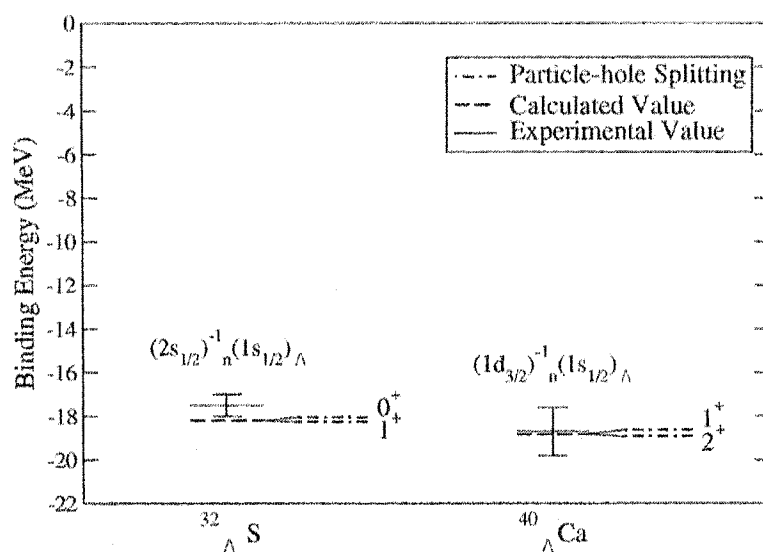
FIG. 6.2: Graph of GS particle-hole splittings and their respective level orderings for $^{32}_{\Lambda}$S and $^{40}_{\Lambda}$Ca. The single-particle calculations were conducted using the M2 parameter set and are plotted alongside the experimental values [8, 9]. Notice that the splittings lie within the experimental error bars in both cases.

tonian to determine the correct splitting and level ordering. The remaining doublets in Table 6.1, those with proton holes, are for predicted Λ single-particle levels. These three are shown in Fig. 6.3; here, in addition to the GS splittings for both $^{12}_{\Lambda}$B and $^{16}_{\Lambda}$N, the doublet for the first calculated excited state in $^{16}_{\Lambda}$N is also given. These splittings will be measured in an upcoming experiment using the reaction $(e, e'\,K^+)$ with much greater resolution than the (π^+, K^+) reactions [11, 12]. As the effective interaction used here is isoscalar, there is no distinction in this approach between proton and neutron holes. This is apparent when comparing the GS's of $^{16}_{\Lambda}$N and $^{16}_{\Lambda}$O; the slight difference in their splittings, which is only about 10 keV, arises from Coulomb effects. Also note that the splittings for configurations with the holes in the same shell are larger for the smaller j value. For example, the doublet for the GS of $^{12}_{\Lambda}$B, in the $(1p_{3/2})^{-1}_{p}(1s_{1/2})_{\Lambda}$ configuration, is smaller than that of the GS of $^{16}_{\Lambda}$N, in the $(1p_{1/2})^{-1}_{p}(1s_{1/2})_{\Lambda}$ state. Similarly, $|\delta\epsilon|$ for the GS of $^{40}_{\Lambda}$Ca, in the $(1d_{3/2})^{-1}_{p}(1s_{1/2})_{\Lambda}$ state, is greater than $|\delta\epsilon|$ for the GS of $^{28}_{\Lambda}$Si, in the $(1d_{5/2})^{-1}_{p}(1s_{1/2})_{\Lambda}$ configuration.
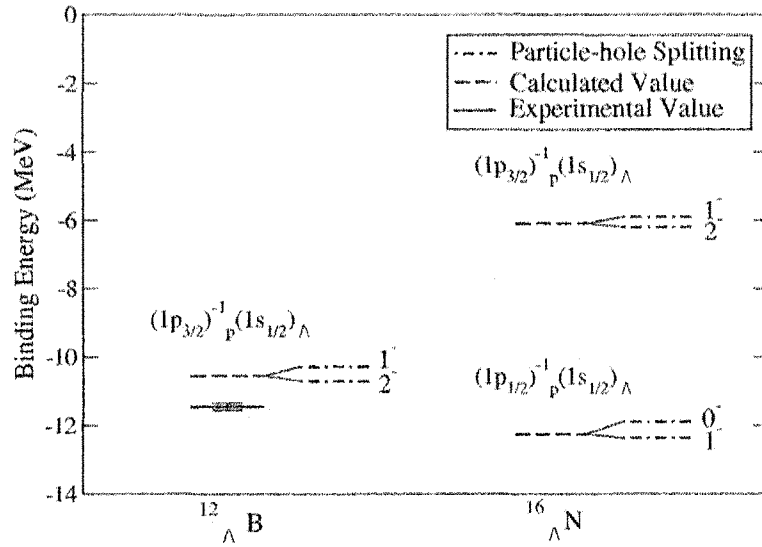
FIG. 6.3: Graph of particle-hole splittings for $^{12}_\Lambda$B and $^{16}_\Lambda$N and their respective level orderings. In addition to the GSs, the first calculated excited state in $^{16}_\Lambda$N is also included. The single-particle calculations were conducted using the M2 parameter set. The experimental value for the GS of $^{12}_\Lambda$B is taken from [107].

The level orderings for each calculated doublet are also given in Table 6.1. Notice that for all of the cases considered here, the state with the higher J value is the GS or, in the case of excited states, the lower level.

Recent gamma-ray spectroscopy experiments [13] (and the experimental error bars on the GS binding energy of $^{12}_\Lambda$B) suggest that the particle-hole splittings are in fact much smaller. As the tensor coupling was important in the spin-orbit splittings, it is reasonable to assume that it may play an important role in the case of the $s_{1/2}$-splittings. Higher order terms in the effective interaction, especially those involving the tensor coupling to the Λ, may be required to obtain a quantitative description of the small $s_{1/2}$-doublet splitting.[5,6] This is left for future work.

[5]A systematic analysis of the effective interaction to all orders, at least in non-relativistic many-body theory, is presented in [19].

[6]The retention of higher diagrams in the effective interaction, particularly those including the tensor coupling to the Λ, is left for future work. Also, it is worth noting that while the kaon makes no contribution at the mean field level, kaon exchange may play a role in the effective interaction. Some idea of the relative contribution of kaon exchange can be obtained from the Nijmegen potentials [42, 43, 44]. An investigation of the effect of kaon exchange on the $s_{1/2}$-
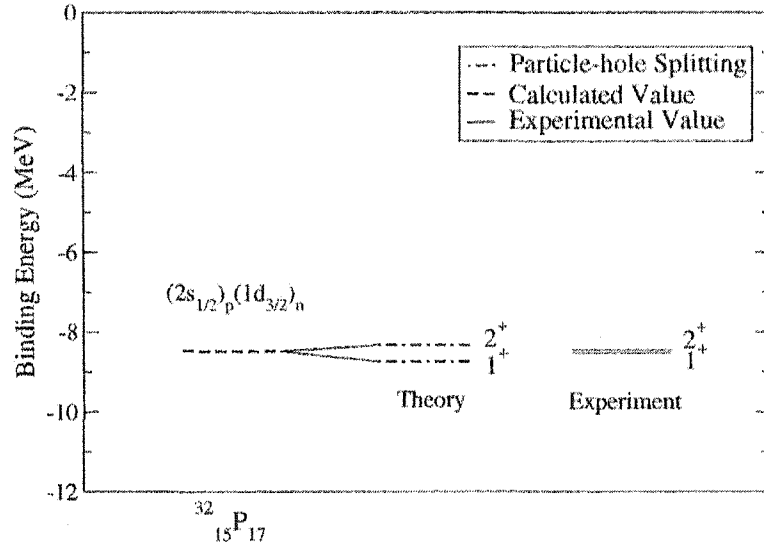
FIG. 6.4: Particle-hole splitting for the GS of $^{32}_{15}P_{17}$. The level orderings and splittings are shown for both theory and experiment. Here the G2 parameter set of FST was used [1].

The present analysis was also extended to the case of *ordinary nuclei*. The necessary modifications to the theory were discussed in section 6.2. We apply this approach to the case of $^{32}_{15}P_{17}$ in the $(2s_{1/2})_p(1d_{3/2})_n$ state. As noted before, this calculation will require direct and exchange contributions from the scalar, vector, rho, and pion terms in the effective interaction. Fortunately, the statement of Eq. (6.23) holds here for the direct term and can be extended to include the direct rho time component as well. The result of our calculation is 413 keV; the observed value is 77 keV [46]. This is shown graphically in Fig. 6.4; notice that the correct magnitude and level ordering is obtained. However, it should be noted that this calculation is considerably more complicated than the Λ-N case.

splittings in effective field theory is also left to future work.

CHAPTER 7

Conclusion

The effective field theory approach of FST was developed to solve the nuclear many-body problem. Formulated in terms of hadrons as generalized coordinates, it has the great advantage of incorporating all the important general principles of physics: quantum mechanics, Lorentz covariance, microscopic causality, spontaneously broken chiral symmetry, and the underlying symmetry structure of QCD. This approach is part of a continuing effort to describe and understand nuclei. It has been applied with great success to nuclei in the valley of stability [1, 2]. The central work of the present thesis is the extension of this framework to the region of nonzero strangeness. The main contributions of the current work are divided into three sections below.

1. In chapter 4, we consider the application of the FST approach to strange superheavy nuclei. The new contributions to this subject are:

   - the coupled, nonlinear field equations following from Eqs. (1.28) and (1.31) - (1.35) are solved numerically with appropriate boundary conditions for ordinary finite nuclei;

110

- the resulting baryon density and scalar field provide a picture of the size and shape of the surface of ordinary nuclei;

- the surface energy of ordinary nuclei is extracted by fitting to the SEMF and is in agreement with experiment. This successfully calibrates the approach;

- cascade-nucleon (ΞN) matter subject to the constraints $Q = 0$ and $|S|/B = 1$ is then similarly studied for a range of Ξ scalar couplings;

- the determined densities again give a picture of the size and shape of the surface of ΞN nuclei;

- the surface energy is also acquired by fitting to the SEMF of ΞN nuclei;

- with the Λ scalar coupling fit to experiment, the inclusion of Λ's has little effect on the results.

2. In chapter 5, we consider single Λ-hypernuclei using the methodology of FST. The following are a list of the main new contributions of the present work:

- a minimalist extension is made to the strangeness $S = -1$ sector in which an isoscalar Λ is included in the full FST effective lagrangian;

- Huertas' program to solve the relativistic Hartree equations of FST [16] is appropriately extended and modified;

- parameter fits to experimental data are conducted at various levels of truncation in the new Λ-lagrangian;

- it is found that the 3-parameter fit obtains excellent overall agreement with the experimental data;

- it is also determined that the inclusion of more parameters does not significantly improve the fit;

- the resulting effective lagrangian is used to predict the GS binding energies, densities, and single-particle spectra of other single Λ-hypernuclei.

3. Chapter 6 is dedicated to a specific phenomena of single Λ-hypernuclei, $s_{1/2}$-splittings. The new contributions of the present work are:

   - the effective particle-hole interaction is derived from the previously determined effective lagrangian;

   - it is discovered that the only term that contributes to the $s_{1/2}$-splittings is the spatial part of the neutral vector exchange;

   - it is also found that the GS doublet splittings of all the Λ-hypernuclei used in the fitting procedure lie within current experimental error on the GS binding energies;

   - predictions are made for the $s_{1/2}$-splittings in $^{12}_{\Lambda}$B and $^{16}_{\Lambda}$N which will be measured in an upcoming experiment at the Thomas Jefferson National Accelerator Facility [11, 12];[1]

   - the $s_{1/2}$-splitting in a comparable ordinary nucleus $^{32}_{15}$P$_{17}$ successfully calibrates the approach; however, this calculation is more complicated as isovector interactions and exchange contributions are now required.

The methodology which FST have constructed was designed to reproduce the characteristics of nuclei in the valley of stability. The present work, by successfully expanding their formalism to the strangeness sector, indicates that this theory is more robust. Coupled with other recent applications of this framework outside the

---

[1]The retention of higher diagrams in the effective interaction, particularly those including the tensor coupling to the Λ, is left for future work. Also, it is worth noting that while the kaon makes no contribution at the mean field level, kaon exchange may play a role in the effective interaction. Some idea of the relative contribution of kaon exchange can be obtained from the Nijmegen potentials [42, 43, 44]. An investigation of the effect of kaon exchange on the $s_{1/2}$-splittings in effective field theory is also left to future work.

region of stability [16, 21], the research presented here implies that the effective field theory approach of FST provides a predictive method for approximating QCD in the strong-coupling, nuclear physics regime.

APPENDIX A

Definitions and Conventions

In this appendix, some useful definitions are listed. This work utilizes the conventions of [5]. Here we use $x_\mu = (\vec{x}, it)$ and repeated Greek indices are summed form 1 to 4. The Pauli matrices are

$$\sigma_1 = \begin{pmatrix} 0 & 1 \\ 1 & 0 \end{pmatrix}; \quad \sigma_2 = \begin{pmatrix} 0 & -i \\ i & 0 \end{pmatrix}; \quad \sigma_3 = \begin{pmatrix} 1 & 0 \\ 0 & -1 \end{pmatrix} \tag{A.1}$$

and they satisfy the relation

$$\sigma_i \sigma_j - \sigma_j \sigma_i = 2i\epsilon_{ijk}\sigma_k \tag{A.2}$$

They are sometimes written as $\vec{\sigma} = (\sigma_1, \sigma_2, \sigma_3) = \vec{\tau}$. The notation $\vec{\sigma}$ and $\vec{\tau}$ are used for spin and isospin respectively.

114

The Dirac matrices are shown by

$$\vec{\alpha} = \begin{pmatrix} 0 & \vec{\sigma} \\ \vec{\sigma} & 0 \end{pmatrix}; \qquad \beta = \begin{pmatrix} 1 & 0 \\ 0 & -1 \end{pmatrix} \tag{A.3}$$

The gamma matrices are constructed from these Dirac matrices and are given by

$$\gamma_\mu = (i\vec{\alpha}\beta, \beta) \tag{A.4}$$

where $\gamma_\mu = \gamma_\mu^\dagger$. In addition, we define the pseudoscalar

$$\gamma_5 \equiv \gamma_1 \gamma_2 \gamma_3 \gamma_4 \tag{A.5}$$

and the second rank tensor

$$\sigma_{\mu\nu} \equiv \frac{-i}{2} \left[\gamma_\mu, \gamma_\nu \right] \tag{A.6}$$

The gamma matrices satisfy the following relations:

$$\gamma_\mu \gamma_\nu + \gamma_\nu \gamma_\mu = 2\delta_{\mu\nu} \tag{A.7}$$

and

$$\gamma_\mu \gamma_5 + \gamma_5 \gamma_\mu = 0 \tag{A.8}$$

The Racah functions are defined as [45]

$$C_{kq}(\theta, \phi) = \left(\frac{4\pi}{2k+1} \right)^{1/2} Y_{kq}(\theta, \phi) \qquad (A.9)$$

where the $Y_{kq}(\theta, \phi)$ are the spherical harmonics. We also define $\chi_{\lambda\mu}^{(k,1)}$ as C_{kq} coupled to Pauli matrices, shown by

$$\chi_{\lambda\mu}^{(k,1)} = \sum_{qq'} C_{kq} \sigma_{1q'} \langle kq1q' | k1\lambda\mu \rangle \qquad (A.10)$$

The modified spherical Bessel functions are

$$
\begin{aligned}
i_n(z) &= \sqrt{\frac{\pi}{2z}} I_{n+1/2}(z) \\
&= z^n \left(\frac{1}{z} \frac{d}{dz} \right)^n \frac{\sinh z}{z} \qquad (A.11) \\
k_n(z) &= \sqrt{\frac{\pi}{2z}} K_{n+1/2}(z) \\
&= (-1)^n \frac{\pi}{2} \left[i_{-(n+1)}(z) - i_n(z) \right] \\
&= (-1)^n \frac{\pi}{2} \left[z^n \left(\frac{1}{z} \frac{d}{dz} \right)^n \frac{\cosh z}{z} - z^n \left(\frac{1}{z} \frac{d}{dz} \right)^n \frac{\sinh z}{z} \right] \\
&= (-z)^n \frac{\pi}{2} \left(\frac{1}{z} \frac{d}{dz} \right)^n \frac{e^{-z}}{z} \qquad (A.12)
\end{aligned}
$$

The following angular momentum relations are useful in this work [45]:

$$(-1)^{j_2+j_3+J} = \left\{ \begin{array}{ccc} J & j_2 & j_3 \\ 0 & j_3 & j_2 \end{array} \right\} [(2j_2 + 1)(2j_3 + 1)]^{1/2} \qquad (A.13)$$

$$\sum_j (2j+1)(2j''+1) \begin{Bmatrix} j_1 & j_2 & j' \\ j_3 & j_4 & j \end{Bmatrix} \begin{Bmatrix} j_3 & j_2 & j \\ j_1 & j_4 & j'' \end{Bmatrix} = \delta_{j'j''} \tag{A.14}$$

and

$$\sum_{j_{23}} (-1)^{j_{23}+j_{31}+j_{12}} (2j_{23}+1) \begin{Bmatrix} j_1 & j_2 & j_{12} \\ j_3 & j & j_{23} \end{Bmatrix} \begin{Bmatrix} j_2 & j_3 & j_{23} \\ j_1 & j & j_{31} \end{Bmatrix} = \begin{Bmatrix} j_3 & j_1 & j_{31} \\ j_2 & j & j_{12} \end{Bmatrix} \tag{A.15}$$

The scalar product of two commuting tensor operators given by is [45]

$$\langle \gamma' j_1' j_2' J'M' | T(K) \cdot U(K) | \gamma j_1 j_2 JM \rangle = (-1)^{j_1+j_2'+J} \delta_{J'J} \delta_{M'M} \begin{Bmatrix} J & j_2' & j_1' \\ K & j_1 & j_2 \end{Bmatrix}$$

$$\times \sum_{\gamma''} \langle \gamma' j_1' || T(K) || \gamma'' j_1 \rangle \langle \gamma'' j_2' || U(K) || \gamma j_2 \rangle \tag{A.16}$$

For the purposes of this work, the Racah functions will take the place of T(K) and U(K). The reduced matrix elements relevant here are

$$\langle (l' \tfrac{1}{2}) j' || C_k || (l \tfrac{1}{2}) j \rangle = (-1)^{j'+1/2} \left[(2j'+1)(2j+1) \right]^{1/2}$$

$$\times \begin{pmatrix} j' & k & j \\ -\tfrac{1}{2} & 0 & \tfrac{1}{2} \end{pmatrix} \left[\frac{1+(-1)^{l'+l+k}}{2} \right] \tag{A.17}$$

and

$$\langle (l'\tfrac{1}{2})j'||\chi_\lambda^{(k,1)}||(l\tfrac{1}{2})j\rangle = [(2j'+1)(2j+1)(2\lambda+1)]^{1/2}$$

$$\times \begin{Bmatrix} l' & l & k \\ \tfrac{1}{2} & \tfrac{1}{2} & 1 \\ j' & j & \lambda \end{Bmatrix} \langle l'||C_k||l\rangle \langle \tfrac{1}{2}||\sigma_1||\tfrac{1}{2}\rangle \quad (A.18)$$

To determine Eq. (A.18), we must also specify the following reduced matrix elements [45]:

$$\langle l'||C_k||l\rangle = (-1)^{l'}[(2l'+1)(2l+1)]^{1/2} \begin{pmatrix} l' & k & l \\ 0 & 0 & 0 \end{pmatrix} \quad (A.19)$$

and

$$\langle \tfrac{1}{2}||\sigma_1||\tfrac{1}{2}\rangle = \sqrt{6} \quad (A.20)$$

APPENDIX B

Ordering the Terms in the

Lagrangian

In order to conduct a systematic expansion in our lagrangian we require some method for ordering the terms. To accomplish this, FST use a system that involves both naive dimensional analysis (NDA) and relativistic mean field theory (RMFT). In this framework, higher order terms are successively smaller. This will allow one to truncate the lagrangian in a meaningful fashion.

B.1 Naive Dimensional Analysis

NDA states that once all the appropriate dimensional factors have been absorbed in a given term, what remains is a dimensionless constant [17]. Furthermore, this constant is of order unity, an assumption which is known as "naturalness." The

119

following expression is used to identify all of the dimensional factors associated with the specific components in any given term

$$g\frac{1}{m!n!}f_\pi^2 M^2 \left(\frac{\bar{N}N}{f_\pi^2 M}\right)^k \left(\frac{\phi}{f_\pi}\right)^m \left(\frac{V}{f_\pi}\right)^n \left(\frac{\partial}{M}\right)^p \qquad (B.1)$$

Here g is the generic dimensionless constant, f_π is the pion-decay constant, and M is the chiral symmetry breaking scale [1]. Note that this expression can be expanded to include additional baryons and mesons. As examples, examine the terms

$$g_A \bar{N}\gamma_\mu \gamma_5 a_\mu N \qquad (B.2)$$

$$g_S \bar{N}\phi N$$

$$g_V \bar{N}\gamma_\mu V_\mu N$$

Using Eq. (B.1), we see that the constants are

$$g_A \sim 1 \qquad (B.3)$$

$$g_S, g_V \sim \frac{M}{f_\pi} \leq 4\pi \qquad (B.4)$$

The pion couplings, v_μ and a_μ, already have a factor of $1/f_\pi$ associated with them; consequently, they are treated as derivatives [1]. Next, consider a more complicated term

$$\bar{N}\sigma_{\mu\nu}V_{\mu\nu}N \qquad (B.5)$$

Eq. (B.1) tells us that the following factor must accompany this term

$$\frac{f_V}{4f_\pi} = \frac{f_V g_V}{4M} \tag{B.6}$$

Here the substitution of Eq. (B.4) was used and the constant was labeled $g = f_V/4$ for future convenience. All the terms in the lagrangians used or developed in this work have been treated using this methodology.

B.2 Relativistic Mean Field Theory

RMFT allows one to remove some of the complexity associated with the quantum fields from the nuclear many-body problem. Imagine a box with a volume V and containing a fixed number of baryons, B. If the volume of the box shrinks, then the baryon density must increase. If the baryon density becomes large enough, then the source terms in the equations of motion can be replaced by their expectation values [5]. Furthermore, the meson fields can also be replaced by their expectation values. In this case, these are just their classical fields

$$\phi(x_\mu) \rightarrow \langle\phi\rangle = \phi_0(r)$$

$$V_\mu(x_\mu) \rightarrow \langle V_\mu\rangle = i\delta_{\mu 4}V_0(r)$$

$$\rho_\mu(x_\mu) \rightarrow \langle\rho_\mu\rangle = i\delta_{\mu 4}b_0(r)$$

$$A_\mu(x_\mu) \rightarrow \langle A_\mu\rangle = i\delta_{\mu 4}A_0(r) \tag{B.7}$$

which are time independent. Since there is no spatial direction in the problem for a uniform system at rest, the vector fields can only develop their fourth component [5]. For the purposes of this work, we restrict ourselves to spherical symmetry. Note that the pion has no mean field in a spherically symmetric system; as a result, all the pion couplings drop out. The conditions under which RMFT applies exist in the regime of low-energy nuclear physics.

The mean meson fields, when scaled with their respective coupling constants, shown by

$$\Phi = g_S\phi_0; \qquad W = g_V V_0; \qquad R = g_\rho b_0; \qquad A = eA_0 \tag{B.8}$$

are large. However, they are small when compared to the chiral symmetry breaking scale, M. The Fermi wave number, which is related to the size of the derivatives, is also small compared to M, or[1]

$$\frac{\Phi}{M}, \frac{W}{M} \sim \frac{1}{3}; \qquad \frac{k_F}{M} \sim \frac{1}{4} \tag{B.9}$$

If the naturalness assumption of NDA holds, then it follows from RMFT that terms with increasing powers of the meson fields (and derivatives) will become successively smaller. Therefore, truncation of the lagrangian can now be conducted in a meaningful fashion.

---

[1]The spatial variations of the meson fields and baryon densities are observed to occur on the scale of the nuclear surface [3]. k_F provides a characteristic inverse length scale for the nuclear surface. As a result, we can now employ the relation $\nabla \propto k_F$.

APPENDIX C

Hartree Formalism

Consider a simple single-particle hamiltonian

$$h(\vec{x}) = -i\vec{\alpha} \cdot \vec{\nabla} + g_V V_0(r) + \beta \left[M - g_S \phi_0(r) \right] \qquad (C.1)$$

which satisfies the Dirac equation

$$h(\vec{x}) \psi_n(\vec{x}) = E_n \psi_n(\vec{x}) \qquad (C.2)$$

where E_n is the energy eigenvalue. Note that the following discussion also holds for the full $h(\vec{x})$ in chapter 2 as well. The solutions to Eq. (C.2) are of the form

$$\psi_n(\vec{x}) = \begin{pmatrix} \psi_\alpha(\vec{x}) \\ \psi_\beta(\vec{x}) \end{pmatrix} \qquad (C.3)$$

123

where ψ_α and ψ_β are two component Hartree spinors and n is the radial quantum number [5].

The total angular momentum is defined as the sum of the orbital and spin angular momenta, or

$$\vec{J} = \vec{L} + \vec{S} \tag{C.4}$$

Using $\vec{L} = \vec{r} \times \vec{p}$ and

$$\vec{\Sigma} = \begin{pmatrix} \vec{\sigma} & 0 \\ 0 & \vec{\sigma} \end{pmatrix} \tag{C.5}$$

we re-express Eq. (C.4) as

$$\vec{J} = i\vec{r} \times \vec{\nabla} + \vec{\Sigma}/2 \tag{C.6}$$

Next, we define the operator

$$\begin{aligned} K &\equiv \beta(\vec{\Sigma} \cdot \vec{L} + 1) \\ &= \beta(\vec{\Sigma} \cdot \vec{J} + 1/2) \end{aligned} \tag{C.7}$$

When the following commutators are examined, one discovers that

$$[h, \vec{J}^2] = [h, \vec{S}^2] = [h, K] = [h, J_i] = 0 \tag{C.8}$$

This implies that the eigenvalues of these four operators, $\{j, s, -\kappa, m_j\}$ respectively, are all good quantum numbers and that they characterize the states ψ_α and ψ_β [5]. A few examples of the respective quantum numbers of different states are shown in

state	n	κ	j	l_A	l_B
$(1s_{1/2})$	1	-1	1/2	0	1
$(1p_{3/2})$	1	-2	3/2	1	2
$(1p_{1/2})$	1	1	1/2	1	0
$(1d_{3/2})$	1	2	3/2	2	1
$(2s_{1/2})$	2	-1	1/2	0	1

TABLE C.1: Some examples of different states and their respective quantum numbers.

Table C.1. Note that states with the same $\{j, s, -\kappa, m_j\}$ are denoted by different n and that $s = 1/2$ for all of the cases considered in this work. The square of the operator K is

$$
\begin{aligned}
K^2 &= \vec{L}^2 + \vec{\Sigma}^2 \cdot \vec{L} + 1 \\
&= \vec{J}^2 + 1/4
\end{aligned}
\tag{C.9}
$$

It follows from Eq. (C.9) that $\kappa = \pm(j + 1/2)$.

The commutator of the hamiltonian with $\vec{L}^2$ does not vanish, or

$$
\left[h, \vec{L}^2 \right] \neq 0
\tag{C.10}
$$

Consequently the eigenvalue l is not a good quantum number of the system. However, while ψ_n is not an eigenstate of $\vec{L}^2$, both ψ_α and ψ_β separately are. This is

manifest by the relations

$$\vec{L}^2\psi_\alpha \;=\; \left[(j+1/2)^2 + \kappa\right]\psi_\alpha \;=\; l_A(l_A+1)\psi_\alpha \tag{C.11}$$

$$\vec{L}^2\psi_\beta \;=\; \left[(j+1/2)^2 - \kappa\right]\psi_\beta \;=\; l_B(l_B+1)\psi_\beta \tag{C.12}$$

where κ is expressed in terms of l_A and l_B by

$$\kappa = \begin{cases} l_A \\ \\ l_B + 1 \end{cases} \kappa > 0$$

$$\kappa = \begin{cases} -l_A - 1 \\ \\ -l_B \end{cases} \kappa < 0$$

Note that the eigenvalues l_A and l_B always differ by one and, as their parity is $(-1)^l$, the upper and lower components of ψ_n always have opposite parity [41].

Next, it is assumed that the radial and angular parts of the Hartree spinors are independent. For the angular contribution, we construct the spin spherical harmonics, given for the upper component of Eq. (C.3) by

$$\Phi_{\kappa m}(\theta,\phi) \;=\; \sum_{m_{l_A} m_s} \langle l_A m_{l_A}, \tfrac{1}{2}m_s | l_A \tfrac{1}{2} jm \rangle \, Y_{l_A m_{l_A}}(\theta,\phi)\chi_{m_s} \tag{C.13}$$

where Y_{lm} are the spherical harmonics and χ_{m_s} are two component Pauli spinors. By replacing $l_A \rightarrow l_B$ and $\kappa \rightarrow -\kappa$, one arrives at the spin spherical harmonic for

the lower component. The solutions to the Dirac equation now take the form

$$\psi_n(\vec{x}) = \frac{1}{r} \begin{pmatrix} iG_n(r)\Phi_{\kappa m} \\ -F_n(r)\Phi_{-\kappa m} \end{pmatrix} \zeta_t \qquad (C.14)$$

Here t labels the isospin projection: $t = +1/2 \ (-1/2)$ for protons (neutrons) [5]. Substituting Eq. (C.14) into Eq. (C.2), we acquire the radial Hartree equations, or [5]

$$\left[\frac{\partial}{\partial r} + \frac{\kappa}{r} \right] G_n(r) - [E_n - g_V V_0(r) + M - g_S \phi_0(r)] \, F_n(r) = 0 \qquad (C.15)$$

$$\left[\frac{\partial}{\partial r} - \frac{\kappa}{r} \right] F_n(r) + [E_n - g_V V_0(r) - M + g_S \phi_0(r)] \, G_n(r) = 0 \qquad (C.16)$$

The radial meson equations are

$$\frac{\partial^2}{\partial r^2} \phi_0(r) + \frac{2}{r}\frac{\partial}{\partial r} \phi_0(r) - m_S^2 \phi_0(r) \;=\; -g_S \rho_S(r) \qquad (C.17)$$

$$\frac{\partial^2}{\partial r^2} V_0(r) + \frac{2}{r}\frac{\partial}{\partial r} V_0(r) - m_V^2 V_0(r) \;=\; -g_V \rho_B(r) \qquad (C.18)$$

The source terms can now be expressed in terms of the Hartree spinors, or

$$\rho_S(r) \;=\; \bar{\psi}\psi = \sum_n \left(\frac{2j_n + 1}{4\pi r^2} \right) \left[G_n{}^2(r) - F_n{}^2(r) \right] \qquad (C.19)$$

$$\rho_B(r) \;=\; \psi^\dagger \psi = \sum_n \left(\frac{2j_n + 1}{4\pi r^2} \right) \left[G_n{}^2(r) + F_n{}^2(r) \right] \qquad (C.20)$$

Equations (C.15) - (C.20) form a system of equations that must now be solved self-consistently [5]. Modification of this system to incorporate a more complicated $h(\vec{x})$, such as the one in Eq. (2.16), is straightforward.

APPENDIX D

Analysis of All Possible Terms in

the Λ-lagrangian

In this appendix, we discuss the selection of the terms in our Λ-lagrangian to order $\nu = 3$. It is straightforward to see which terms are retained to order $\nu = 2$, with the exception of the four fermion terms. Therefore, the following is a list of all remaining possible combinations of the fields to order $\nu = 3$, consistent with this approach, and a short discussion of each.

- Four fermion terms in the nuclear case, such as $\bar{N}N\bar{N}N$, are eliminated by substituting the meson equations of motion into the lagrangian. Under normal circumstances this is not feasible; however, this is allowed when the system is already in equilibrium. Here we want to extend the framework of FST to single Λ-hypernuclei with no additional mesons. In this case, either $\bar{N}N\bar{\Lambda}\Lambda$ or $\bar{\Lambda}\Lambda\bar{\Lambda}\Lambda$ can be eliminated using this method, but not both simultaneously. Fortunately, the

128

second term involves self-fields of the Λ and consequently, can be discarded. This scheme also applies to terms with more than four fermion fields.[1]

- The term $\bar{\Lambda}\sigma_{\mu\nu}V_{\mu\nu}\Lambda$ is consistent with this framework.

- The terms $\bar{\Lambda}\Lambda\phi^2$ and $\bar{\Lambda}\Lambda V_\mu{}^2$ are also retained. In the nucleon sector, terms of this variety were regrouped using meson field redefinitions. Here the terms have different constants than in the nucleon case; therefore, these terms cannot simply be regrouped, unless additional mesons are included.

- The term $\bar{\Lambda}\gamma_\mu\Lambda\phi V_\mu$ is consistent with this framework. In the nuclear case, it was eliminated via the Dirac equation, but this is not possible here.

- Next, the following term is consistent with this methodology, but can be rewritten as

$$\bar{\Lambda}\gamma_\mu\Lambda\frac{\partial\phi}{\partial x_\mu} = \frac{\partial}{\partial x_\mu}\left(\bar{\Lambda}\gamma_\mu\Lambda\phi\right) - \left[\frac{\partial}{\partial x_\mu}\left(\bar{\Lambda}\gamma_\mu\Lambda\right)\right]\phi \qquad \text{(D.1)}$$

The second term is a total derivative, which does not change the lagrangian, and the third term is a four derivative of a conserved current, which is zero. Therefore this term can be neglected.

---

[1]An equivalent approach to the traditional meson-baryon effective field theories is the point coupling model, which contains only the baryon fields in a local lagrangian [108]. In the point coupling case, the energy functional is an explicit functional of the densities; thus, the energy functional can be minimized to determine the exact GS density directly. In contrast, the energy functional in the meson-nucleon theories is an implicit functional of the density. In order to minimize the energy functional, one must first show that the variational derivatives of the energy functional with respect to the meson fields are zero. However, the meson-baryon approach does have the advantage of focusing more explicitly on the interaction mechanism.

- Consider the following terms

$$\bar{\Lambda}\gamma_\mu\phi\frac{\partial}{\partial x_\mu}\Lambda \tag{D.2}$$

$$\bar{\Lambda}\gamma_\mu\gamma_\nu V_\mu\frac{\partial}{\partial x_\nu}\Lambda \tag{D.3}$$

$$\bar{\Lambda}\gamma_\mu\gamma_\nu\frac{\partial}{\partial x_\mu}\frac{\partial}{\partial x_\nu}\Lambda \tag{D.4}$$

The Dirac equation for the Λ can be substituted into each of these to convert them into a type of term already considered.

- Lastly, all of the contributions with A_μ are absorbed into other terms in the same manner as like terms with V_μ. However, the terms $\bar{\Lambda}\gamma_\mu\Lambda A_\mu$ and $\bar{\Lambda}\Lambda A_\mu^2$ can be discarded as $Q = 0$ for the Λ. Therefore, the only remaining electromagnetic term is $\bar{\Lambda}\sigma_{\mu\nu}F_{\mu\nu}\Lambda$.

Note that the constants in front of each term have yet to be determined. When the terms are regrouped, the free parameters can be redefined to suit our purposes.

APPENDIX E

Check on the Consistency of the

Experimental Data

In this appendix, we conduct a simple check on the consistency of the experimental binding energies. Here, we use a square-well potential of depth U_0 and range $R = r_0 B^{1/3}$ to approximate the nucleus. In this case, the binding energy of a Λ particle in this nucleus, B_Λ, is given by the solution to the equation [19, 109]

$$s = (1-x)^{-1/2} \cot^{-1} \left[-\left(\frac{x}{1-x}\right)^{1/2} \right] \tag{E.1}$$

where $x = B_\Lambda / U_0$,

$$s = \left[\left(\frac{2\mu_\Lambda R^2}{\hbar^2}\right) U_0 \right]^{1/2} \tag{E.2}$$

131
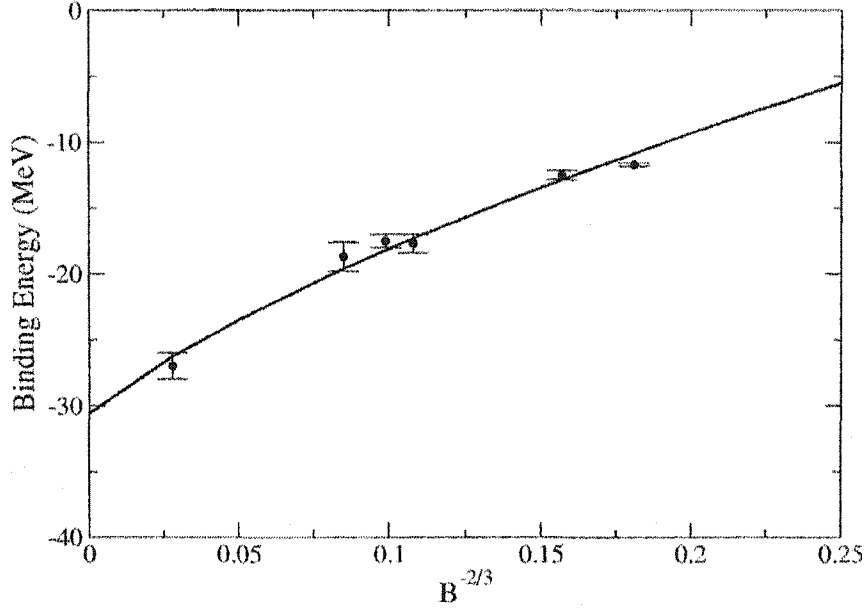
FIG. E.1: Fit, using Eq. (E.5), to the experimental GSs of single Λ-hypernuclei given in Table 6.1. Here 10 terms have been retained. In the limit that B $\to \infty$, we acquire the result $U_0 = -30.56$ MeV.

and

$$\frac{1}{\mu_\Lambda} = \frac{1}{m_\Lambda} + \frac{1}{Am_N} \tag{E.3}$$

Here m_Λ and m_N are the masses of the Λ and nucleon respectively. A denotes the number of nucleons, $(B - 1)$. The following equation is a solution to Eq. (E.1) as $s \to \infty$

$$B_\Lambda = U_0 - \frac{\hbar^2 \pi^2}{2\mu_\Lambda R^2} \left(1 - \frac{2}{s} + \frac{3}{s^2} + \cdots \right) \tag{E.4}$$

If one rewrites Eq. (E.2) as $1/s^2 = \gamma B^{-2/3}$, where γ is some free parameter, and substitutes it into Eq. (E.4), we arrive at

$$B_\Lambda = U_0 \left[1 - \pi^2 \gamma B^{-2/3} \left(1 - 2\sqrt{\gamma B^{-2/3}} + 3\gamma B^{-2/3} + \cdots \right) \right] \tag{E.5}$$

In Fig. E.1, a least-squares fit to the experimental GSs of single Λ-hypernuclei was performed using Eq. (E.5), where 10 terms have been retained. The values of the parameters that produced this fit were $U_0 = -30.56$ and $\gamma = 0.6525$. Here U_0 corresponds to the binding energy of a single Λ in nuclear matter; this is in good agreement with values given in the literature, -28 MeV [26], and the number determined in section 5.3, -32.4 MeV. Combining the expressions $R = r_0 B^{1/3}$, $1/s^2 = \gamma B^{-2/3}$, and Eq. (E.2), we acquire the result

$$r_0 = \left(\frac{\hbar^2}{2\mu_\Lambda \gamma |U_0|} \right)^{1/2} \tag{E.6}$$

Furthermore, we notice that for large B, Eq. (E.3) becomes $\mu_\Lambda \simeq m_\Lambda$. Therefore, we can rewrite Eq. (E.6) as

$$r_0 = \left(\frac{\hbar^2}{2m_N} \frac{m_N}{m_\Lambda} \frac{1}{\gamma |U_0|} \right)^{1/2} = 0.926 \text{ fm} \tag{E.7}$$

This result compares favorably with the value given in [5], $r_0 = 1.07$ fm. The analysis of this appendix gives us confidence that the data is consistent, except for shell effects, which are calculated in this work.

APPENDIX F

Particle-Hole Matrix Elements

This appendix outlines the theoretical techniques used to calculate the particle-hole matrix elements used in chapter 6. This discussion is taken from [19].

F.1 Particle-Hole Operators

Assume the GS of the core is a set of completely filled single-particle levels. In a spherically symmetric system, these states can be characterized by

$$|\alpha\rangle = |n l s j m_j\rangle = |a, m_j\rangle \tag{F.1}$$

where $s = 1/2$, $j = |l \pm 1/2|$, and the parity of these states is determined by $(-1)^l$.

Now we define the particle and hole creation operators as

$$a_\alpha^\dagger \equiv C_\alpha^\dagger \qquad \alpha > F$$

$$b_\alpha^\dagger \equiv S_{-\alpha} C_{-\alpha} \quad \alpha < F$$

where $C^\dagger$ and C are the fermion creation and destruction operators respectively. F is a number that lies between the last filled state and the first unfilled state [19]. Here

$$S_\alpha = (-1)^{j_\alpha - m_\alpha} \tag{F.2}$$

is a phase convention. The C's obey the anti-commutation relations

$$\left\{ C_\alpha, C_{\alpha'}^\dagger \right\} = \delta_{\alpha\alpha'} \tag{F.3}$$

$$\left\{ C_\alpha, C_{\alpha'} \right\} = \left\{ C_\alpha^\dagger, C_{\alpha'}^\dagger \right\} = 0 \tag{F.4}$$

Therefore, the particle and hole operators satisfy the following relations

$$\left\{ a_\alpha, a_{\alpha'}^\dagger \right\} = \left\{ b_\alpha, b_{\alpha'}^\dagger \right\} = \delta_{\alpha\alpha'} \tag{F.5}$$

$$\left\{ a_\alpha, a_{\alpha'} \right\} = \left\{ a_\alpha^\dagger, a_{\alpha'}^\dagger \right\} = \left\{ b_\alpha, b_{\alpha'} \right\} = \left\{ b_\alpha^\dagger, b_{\alpha'}^\dagger \right\} = 0 \tag{F.6}$$

Lastly, we define the particle-hole pair creation operator as the combination

$$\zeta_{\alpha\beta}^\dagger \equiv a_\alpha^\dagger b_\beta^\dagger \tag{F.7}$$

F.2 Tamm-Dancoff Approximation

Consider the matrix element

$$\langle \psi_n | \left[H, \zeta_{\alpha\beta}^\dagger \right] | \psi_0 \rangle = \langle \psi_n | \left(H \zeta_{\alpha\beta}^\dagger - \zeta_{\alpha\beta}^\dagger H \right) | \psi_0 \rangle$$

$$= (E_n - E_0) \langle \psi_n | \zeta_{\alpha\beta}^\dagger | \psi_0 \rangle \tag{F.8}$$

where the hamiltonian is $H = H_0 + H_1 + H_2$. The components of this hamiltonian are given by

$$H_0 = \sum_{\alpha < F} (T_\alpha - \frac{1}{2} V_\alpha) \tag{F.9}$$

$$H_1 = \sum_{\alpha > F} \epsilon_\alpha a_\alpha^\dagger a_\alpha - \sum_{\alpha < F} \epsilon_\alpha b_{-\alpha}^\dagger b_{-\alpha} \tag{F.10}$$

$$H_2 = \frac{1}{2} \sum_{\alpha\beta\gamma\delta} \langle \alpha\beta | V | \gamma\delta \rangle N(C_\alpha^\dagger C_\beta^\dagger C_\delta C_\gamma) \tag{F.11}$$

The states $|\psi_0\rangle$ and $|\psi_n\rangle$ are the exact GS and an exact excited state respectively, given by

$$|\psi_0\rangle \equiv |0\rangle \tag{F.12}$$

$$|\psi_n\rangle \equiv \sum_{\alpha\beta} \psi_{\alpha\beta}^{(n)*} \zeta_{\alpha\beta}^\dagger |0\rangle \tag{F.13}$$

where the matrix element is

$$\langle \psi_n | \zeta_{\alpha\beta}^\dagger | \psi_0 \rangle \equiv \psi_{\alpha\beta}^{(n)} \tag{F.14}$$

N is the normal ordered product, which places all the creation operators, particle and hole, to the left. Next, we calculate the matrix element in Eq. (F.8) by explicitly evaluating the commutators of Eqs. (F.9) - (F.11) with Eq. (F.7)

$$\left[H_0, \zeta_{\alpha\beta}^\dagger\right] = 0 \tag{F.15}$$

$$\left[H_1, \zeta_{\alpha\beta}^\dagger\right] = (\epsilon_\alpha - \epsilon_{-\beta})\zeta_{\alpha\beta}^\dagger \tag{F.16}$$

To evaluate the third commutator, we must first note that the particle and hole destruction operators operating on $|0\rangle$ are

$$a_\alpha |0\rangle = b_\alpha |0\rangle = 0 \tag{F.17}$$

Now we consider the commutator of H_2, shown by

$$\left[H_2, \zeta_{\alpha\beta}^\dagger\right] = \frac{1}{2} \sum_{\lambda\sigma\mu\nu} \langle\lambda\sigma|V|\mu\nu\rangle \left[N(C_\lambda^\dagger C_\sigma^\dagger C_\nu C_\mu), \zeta_{\alpha\beta}^\dagger\right] \tag{F.18}$$

where

$$C_{-\alpha} = \theta(\alpha - F)a_\alpha + \theta(F - \alpha)S_\alpha b_{-\alpha}^\dagger \tag{F.19}$$

First we evaluate the normal ordered product

$$N(C_\lambda^\dagger C_\sigma^\dagger C_\nu C_\mu) = 2(S_\mu S_\sigma a_\lambda^\dagger b_\mu^\dagger b_{-\sigma} a_\nu - S_\nu S_\sigma a_\lambda^\dagger b_\nu^\dagger b_{-\sigma} a_\mu) \tag{F.20}$$

where the symmetry $\langle\lambda\sigma|V|\mu\nu\rangle = \langle\sigma\lambda|V|\nu\mu\rangle$ was used. The commutator becomes

$$\left[N(C_\lambda^\dagger C_\sigma^\dagger C_\nu C_\mu), \zeta_{\alpha\beta}^\dagger\right] = 2\left(S_\mu S_\sigma a_\lambda^\dagger b_\mu^\dagger \delta_{-\sigma\beta}\delta_{\nu\alpha} - S_\nu S_\sigma a_\lambda^\dagger b_{-\nu}^\dagger \delta_{-\sigma\beta}\delta_{\mu\alpha}\right) \qquad \text{(F.21)}$$

Here only terms with the combinations $a^\dagger b^\dagger$ were retained as all others vanish in the matrix element. Equation (F.18) now becomes

$$\left[H_2, \zeta_{\alpha\beta}^\dagger\right] = \sum_{\lambda\mu} S_{-\mu} S_{-\beta}\left(\langle\lambda - \beta|V|-\mu\alpha\rangle - \langle\lambda - \beta|V|\alpha - \mu\rangle\right)\zeta_{\lambda\mu}^\dagger \qquad \text{(F.22)}$$

Substituting Eqs. (F.15), (F.16), and (F.22) into Eq. (F.8) and then rearranging, one arrives at the result

$$\left[(E_0 + \epsilon_\alpha - \epsilon_{-\beta}) - E_n\right]\psi_{\alpha\beta}^{(n)} + \sum_{\lambda\mu} v_{\alpha\beta;\lambda\mu}\psi_{\lambda\mu}^{(n)} = 0 \qquad \text{(F.23)}$$

where

$$v_{\alpha\beta;\lambda\mu} \equiv S_{-\mu}S_{-\beta}\left(\langle\lambda - \beta|V|-\mu\alpha\rangle - \langle\lambda - \beta|V|\alpha - \mu\rangle\right) \qquad \text{(F.24)}$$

Next, we briefly consider a calculation of the transition matrix element of some multipole operator,

$$T = \sum_{\alpha\beta} C_\alpha^\dagger \langle\alpha|T|\beta\rangle C_\beta \qquad \text{(F.25)}$$

between one of the collective excitations and the GS. In the Tamm-Dancoff approx-

imation, only the terms with the combinations $a^\dagger b^\dagger$ will contribute, or

$$T = \sum_{\alpha\beta} \langle \alpha|T|-\beta\rangle S_{-\beta} \zeta^\dagger_{\alpha\beta} \tag{F.26}$$

$$\langle \psi_n|T|\psi_0\rangle = \sum_{\alpha\beta} \langle \alpha|T|-\beta\rangle S_\beta \psi^{(n)}_{\alpha\beta} \tag{F.27}$$

Therefore, it is just the sum of single-particle matrix elements weighted by the coefficients $\psi^{(n)}_{\alpha\beta}$ which are determined from above.

F.3 Reduction of the Basis

The dimension of Eq. (F.23) can be reduced by noting that J is a good quantum number. We define the following irreducible tensor of rank J

$$\zeta^\dagger(abJM) \equiv \sum_{m_\alpha m_\beta} \langle j_\alpha m_\alpha j_\beta m_\beta | j_\alpha j_\beta JM\rangle \zeta^\dagger_{\alpha\beta} \tag{F.28}$$

Next, we further define the matrix element

$$\begin{aligned}
\psi^{(n)}_J(ab) &\equiv \langle \psi^n_{JM}|\zeta^\dagger(abJM)|\psi_0\rangle \\
&= \sum_{m_\alpha m_\beta} \langle j_\alpha m_\alpha j_\beta m_\beta | j_\alpha j_\beta JM\rangle \psi^{(n)}_{\alpha\beta}
\end{aligned} \tag{F.29}$$

Using the Wigner-Eckart Theorem, Eq. (F.26) is rewritten as

$$
\begin{aligned}
T_{JM} &= \frac{1}{(2J+1)^{1/2}} \sum_{\alpha\beta} S^2_{-\beta} \langle j_\alpha m_\alpha j_\beta - m_\beta | j_\alpha j_\beta JM \rangle \langle a || T_J || b \rangle \zeta^\dagger_{\alpha\beta} \\
&= \frac{1}{(2J+1)^{1/2}} \sum_{ab} \langle a || T_J || b \rangle \zeta^\dagger(abJM)
\end{aligned}
\tag{F.30}
$$

and from this it follows that

$$
\langle \psi^n_J || T_J || \psi_0 \rangle = \sum_{ab} \langle a || T_J || b \rangle \psi^{(n)}_J(ab)
\tag{F.31}
$$

The basis in Eq. (F.23) can be reduced by summing with the Clebsch-Gordon coefficients in Eq. (F.29). For a spherically symmetric system, we use the relation

$$
\epsilon_\alpha - \epsilon_{-\beta} = \epsilon_a - \epsilon_b
\tag{F.32}
$$

Next, consider the following matrix element,

$$
\begin{aligned}
\langle \lambda - \beta | V | - \mu\alpha \rangle &= \langle j_\lambda m_\lambda j_\beta - m_\beta | V | j_\mu j_\beta JM \rangle \\
&= \sum_{JM} \sum_{J'M'} \langle j_\lambda m_\lambda j_\beta - m_\beta | j_\lambda j_\beta J'M' \rangle \\
&\quad \times \langle j_\lambda j_\beta J'M' | V | j_\mu j_\alpha JM \rangle \langle j_\mu j_\alpha JM | j_\mu - m_\mu j_\alpha m_\alpha \rangle
\end{aligned}
\tag{F.33}
$$

Since the Clebsch-Gordon coefficients are real, one can write

$$
\langle j_\mu j_\alpha JM | j_\mu - m_\mu j_\alpha m_\alpha \rangle = \langle j_\mu - m_\mu j_\alpha m_\alpha | j_\mu j_\alpha JM \rangle
\tag{F.34}
$$

Also, as V is rotationally invariant, the following relation holds

$$\langle j_\lambda j_\beta J'M' | V | j_\mu j_\alpha JM \rangle = \langle j_\lambda j_\beta J'M' | V | j_\mu j_\alpha J'M' \rangle \delta_{JJ'} \delta_{MM'} \qquad (F.35)$$

As this is now independent of M, we rewrite it in the shorthand

$$= \langle lbJ' | V | maJ' \rangle \qquad (F.36)$$

In consequence of Eqs. (F.34) - (F.36), it follows that Eq. (F.33) now becomes

$$\langle \lambda - \beta | V | - \mu \alpha \rangle = \sum_{JM} \sum_{J'M'} \langle j_\lambda m_\lambda j_\beta - m_\beta | j_\lambda j_\beta J'M' \rangle$$
$$\times \langle j_\mu - m_\mu j_\alpha m_\alpha | j_\mu j_\alpha J'M' \rangle \langle lbJ' | V | maJ' \rangle \qquad (F.37)$$

Similarly the exchange matrix element is

$$\langle \lambda - \beta | V | \alpha - \mu \rangle = \sum_{JM} \sum_{J'M'} (-1)^{j_\alpha + j_\mu - J} \langle j_\lambda m_\lambda j_\beta - m_\beta | j_\lambda j_\beta J'M' \rangle$$
$$\times \langle j_\mu j_\alpha JM | j_\mu - m_\mu j_\alpha m_\alpha \rangle \langle lbJ' | V | amJ' \rangle \qquad (F.38)$$

Substituting Eqs. (F.37) and (F.38) into Eq. (F.24) yields

$$v_{\alpha\beta;\lambda\mu} = \sum_{J'M'} S_{-\mu} S_{-\beta} \langle j_\lambda m_\lambda j_\beta - m_\beta | j_\lambda j_\beta J'M' \rangle \langle j_\mu - m_\mu j_\alpha m_\alpha | j_\mu j_\alpha J'M' \rangle$$
$$\times \left[\langle lbJ' | V | maJ' \rangle - (-1)^{j_\alpha + j_\mu - J'} \langle lbJ' | V | amJ' \rangle \right] \qquad (F.39)$$

To simplify this further we next consider the relation

$$\sum_{m_\alpha m_\beta M'} S_{-\beta} \langle j_\alpha m_\alpha j_\beta m_\beta | j_\alpha j_\beta JM \rangle \langle j_\mu - m_\mu j_\alpha m_\alpha | j_\mu j_\alpha J'M' \rangle \langle j_\lambda m_\lambda j_\beta - m_\beta | j_\lambda j_\beta J'M' \rangle$$

(F.40)

Using identities from [45], this can be rewritten as

$$= (-1)^{J'-j_\beta-j_\lambda} \left(\frac{2J'+1}{2J+1} \right)^{1/2} \sum_{m_\alpha m_\beta M'} \langle j_\alpha m_\alpha j_\beta m_\beta | j_\alpha j_\beta JM \rangle$$
$$\times \langle j_\mu - m_\mu j_\alpha m_\alpha | j_\mu j_\alpha J'M' \rangle \langle J'M' j_\beta m_\beta | J' j_\beta j_\lambda m_\lambda \rangle$$

(F.41)

Using a 6-J symbol and the orthogonality of the Clebsch-Gordon coefficients, Eq. (F.41) is further reduced to

$$= S_{-\mu} \langle j_\lambda m_\lambda j_\mu m_\mu | j_\lambda j_\mu JM \rangle (-1)^{J'+j_\alpha+j_\mu} (2J'+1) \left\{ \begin{array}{ccc} j_\mu & j_\alpha & J' \\ \\ j_\beta & j_\lambda & J \end{array} \right\}$$

(F.42)

This relation allows one to rewrite Eq. (F.39) in the following fashion

$$\sum_{m_\alpha m_\beta} \langle j_\alpha m_\alpha j_\beta m_\beta | j_\alpha j_\beta JM \rangle v_{\alpha\beta;\lambda\mu} = v_{ab;lm}^J \langle j_\lambda m_\lambda j_\mu m_\mu | j_\lambda j_\mu JM \rangle$$

(F.43)

where the particle-hole matrix element is

$$v_{ab;lm}^J = -\sum_{J'} (2J'+1) \left[\langle lbJ'|V|amJ' \rangle - (-1)^{j_\alpha+j_\mu+J'} \langle lbJ'|V|maJ' \rangle \right]$$
$$\times \left\{ \begin{array}{ccc} j_\mu & j_\alpha & J' \\ \\ j_\beta & j_\lambda & J \end{array} \right\}$$

(F.44)

Furthermore, Eq. (F.23) now becomes

$$[(E_a + \epsilon_a - \epsilon_b) - E_n]\,\psi_J^{(n)}(ab) + \sum_{lm} v_{ab;lm}^J \psi_J^{(n)}(lm) = 0 \qquad (F.45)$$

where Eqs. (F.31), (F.32), and (F.43) have been used.

APPENDIX G

Relative Position of the Splitting

This appendix is dedicated to determining the position of the doublet splittings relative to their energy eigenvalue calculated from the relativistic Hartree equations. Each term in the particle-hole matrix element (scalar, vector, rho, and pion) has a similar J dependence. For example, the J dependence of the scalar contribution to the direct term is of the form[1]

$$(-1)^{j_2+j_3+J} \begin{Bmatrix} j_2 & j_4 & k \\ j_1 & j_3 & J \end{Bmatrix} \tag{G.1}$$

and the J dependence of the scalar contribution to the exchange term is

$$\frac{1}{2J+1}\delta_{Jk} \tag{G.2}$$

---

[1]The full formulae for the splittings are contained in appendix I.

144

Multiplying $v_{32;14}^J(s)$, the scalar component of the particle-hole matrix element, by $(2J+1)$ and then summing over J, one arrives at the result

$$\sum_J (2J+1)v_{32;14}^J(s) = \sum_J (2J+1)(-1)^{j_2+j_3+J} \begin{Bmatrix} j_2 & j_4 & k \\ j_1 & j_3 & J \end{Bmatrix} \alpha_1(r_1, r_2)$$
$$+ \sum_{Jk} (2J+1)\frac{1}{2J+1}\delta_{Jk}\alpha_2(r_1, r_2) \qquad \text{(G.3)}$$

where $\alpha_1(r_1, r_2)$ and $\alpha_2(r_1, r_2)$ are the parts of $v_{32;14}^J(s)$ which are independent of J for the direct and exchange terms respectively. The phase in Eq. (G.3) is converted into a 6-J symbol using the identity Eq. (A.13). Substituting this in, Eq. (G.3) becomes

$$= \sum_J (2J+1) \begin{Bmatrix} J & j_2 & j_3 \\ 0 & j_3 & j_2 \end{Bmatrix} \begin{Bmatrix} j_2 & j_4 & k \\ j_1 & j_3 & J \end{Bmatrix} [(2j_2+1)(2j_3+1)]^{1/2}\alpha_1(r_1, r_2)$$
$$+ \sum_{Jk} \delta_{Jk}\alpha_2(r_1, r_2) \qquad \text{(G.4)}$$

For the direct term, we use the substitutions $j_1 = j_3$ and $j_4 = j_2$. We conclude that the 6J symbols are orthonormal from Eq. (A.14) and as a result, Eq. (G.4) is now

$$= [(2j_2+1)(2j_3+1)]^{1/2}\delta_{k0}\alpha_1(r_1, r_2) + \sum_{Jk} \delta_{Jk}\alpha_2(r_1, r_2) \qquad \text{(G.5)}$$

The particle-hole splitting for the scalar contribution only is defined as

$$\delta\epsilon(s) \equiv v_{ab;lm}^{J=j_1+j_2}(s) - v_{ab;lm}^{J=|j_1-j_2|}(s) \qquad \text{(G.6)}$$

Note that $\alpha_1(r_1, r_2)$ and $\alpha_2(r_1, r_2)$ are common factors, for the direct and exchange terms respectively, in Eq. (G.6). After multiplying $\delta\epsilon(s)$ by $(2J+1)$ and taking the sum over J, the following result is obtained

$$
\begin{aligned}
\sum_J (2J+1)\delta\epsilon(s) \\
&= \left\{ [(2j_2+1)(2j_3+1)]^{1/2}\delta_{k0} - [(2j_2+1)(2j_3+1)]^{1/2}\delta_{k0} \right\} \alpha_1(r_1, r_2) \\
&\quad + \sum_{Jk} (\delta_{Jk} - \delta_{Jk}) \alpha_2(r_1, r_2) \\
&= 0
\end{aligned}
\tag{G.7}
$$

This approach is easily extended to the other terms in $\delta\epsilon$, as their J dependence is of the same form. Note that for the spatial vector and rho components, λ takes the place of k in this derivation.

APPENDIX H

Cancellation of Terms in the

Splitting

In this appendix, we consider only the direct term in the particle-hole matrix element. We will prove that the $k = 0$ terms in the scalar, the vector and rho time, and the pion contributions vanish in the splitting (and the $\lambda = 0$ terms for the spatial vector and rho contributions). Consider only the direct term in the scalar component of the splitting

$$
\delta\epsilon(\mathrm{ds}) = v_{32;14}^{J=j_1+j_2}(\mathrm{ds}) - v_{32;14}^{J=|j_1-j_2|}(\mathrm{ds})
$$

$$
= \left[(-1)^{j_1+j_2} \begin{Bmatrix} j_2 & j_4 & 0 \\ j_1 & j_3 & j_1+j_2 \end{Bmatrix} \right.
$$

$$
\left. - (-1)^{|j_1-j_2|} \begin{Bmatrix} j_2 & j_4 & 0 \\ j_1 & j_3 & |j_1-j_2| \end{Bmatrix} \right] \beta(r_1, r_2) \qquad (\mathrm{H.1})
$$

147

Here $\beta(r_1, r_2)$ is the common part of $\delta\epsilon(ds)$ for $k = 0$.[1] Since we are only interested in the direct term, we use the substitutions $j_3 = j_1$ and $j_4 = j_2$ to arrive at the following

$$= \left[(-1)^{j_1+j_2} \left\{ \begin{array}{ccc} j_2 & j_2 & 0 \\ j_1 & j_1 & j_1+j_2 \end{array} \right\} - (-1)^{|j_1-j_2|} \left\{ \begin{array}{ccc} j_2 & j_2 & 0 \\ j_1 & j_1 & |j_1-j_2| \end{array} \right\} \right] \beta(r_1, r_2)$$

(H.2)

$$= \left[(-1)^{j_1+j_2} \left\{ \begin{array}{ccc} j_1+j_2 & j_1 & j_2 \\ 0 & j_2 & j_1 \end{array} \right\} - (-1)^{|j_1-j_2|} \left\{ \begin{array}{ccc} |j_1-j_2| & j_1 & j_2 \\ 0 & j_2 & j_1 \end{array} \right\} \right] \beta(r_1, r_2)$$

(H.3)

The identity in Eq. (A.13) [45] reduces Eq. (H.3) to

$$= \frac{(-1)^{j_1+j_2}}{[(2j_1+1)(2j_2+1)]^{1/2}} \left[(-1)^{2(j_1+j_2)} - (-1)^{2(|j_1-j_2|)} \right] \beta(r_1, r_2)$$

(H.4)

Since j_1 and j_2 are both half integer, $j_1 + j_2$ and $|j_1 - j_2|$ are both integer. This allows us to conclude that

$$= \frac{(-1)^{j_1+j_2}}{[(2j_1+1)(2j_2+1)]^{1/2}} [1 - 1] \beta(r_1, r_2)$$

$$= 0$$

(H.5)

This proof is readily expandable to the $k = 0$ terms of the vector and rho time, and the pion contributions as well as to the $\lambda = 0$ terms of the vector and rho spatial contributions. Note that this applies only to the direct term in the splittings.

---

[1] The full formulae for the splittings are contained in appendix I.

APPENDIX I

Formulae for the Splittings

In this appendix, all the formulae for the $s_{1/2}$-splittings are listed. These formulae were derived in [110]. In order to calculate particle-hole splittings, we must calculate the particle-hole matrix elements of Eq. (F.44). These are sums of Dirac two-body matrix elements, of the types in Eq. (6.1) and (6.2); these are reduced via Eq. (A.16) to two dimensional integrals and some algebra. The relevant matrix element for the scalar term in the effective interaction is

$$
\begin{aligned}
\langle (12)\mathrm{J}|\gamma_4^{(1)}\gamma_4^{(2)}\frac{-\mathrm{g}_\mathrm{S}^2}{4\pi}\frac{\mathrm{e}^{-\mathrm{m_S r_{12}}}}{\mathrm{r}_{12}}|(34)\mathrm{J}\rangle &= (-1)^{\mathrm{j_2+j_3+J}}\sum_k^\infty \left\{ \begin{matrix} \mathrm{J} & \mathrm{j_2} & \mathrm{j_1} \\ k & \mathrm{j_3} & \mathrm{j_4} \end{matrix} \right\} \\
&\times \langle (l_{1\mathrm{A}}\tfrac{1}{2})\mathrm{j_1}||\mathrm{C}_k(1)||(l_{3\mathrm{A}}\tfrac{1}{2})\mathrm{j_3}\rangle\langle (l_{2\mathrm{A}}\tfrac{1}{2})\mathrm{j_2}||\mathrm{C}_k(2)||(l_{4\mathrm{A}}\tfrac{1}{2})\mathrm{j_4}\rangle \\
&\times \int\int \mathrm{dr_1 dr_2}\,[\mathrm{G}_1(\mathrm{r}_1)\mathrm{G}_3(\mathrm{r}_1) - \mathrm{F}_1(\mathrm{r}_1)\mathrm{F}_3(\mathrm{r}_1)]\,f_k^\mathrm{S}(\mathrm{r}_1,\mathrm{r}_2) \\
&\times [\mathrm{G}_2(\mathrm{r}_2)\mathrm{G}_4(\mathrm{r}_2) - \mathrm{F}_2(\mathrm{r}_2)\mathrm{F}_4(\mathrm{r}_2)]
\end{aligned}
\tag{I.1}
$$

149

where the substitutions have been used

$$\langle(l_{1A}\tfrac{1}{2})j_1\|C_k(1)\|(l_{3A}\tfrac{1}{2})j_3\rangle = \langle(l_{1B}\tfrac{1}{2})j_2\|C_k(2)\|(l_{3B}\tfrac{1}{2})j_4\rangle \qquad (I.2)$$

$$\langle(l_{2A}\tfrac{1}{2})j_1\|C_k(1)\|(l_{4A}\tfrac{1}{2})j_3\rangle = \langle(l_{2B}\tfrac{1}{2})j_2\|C_k(2)\|(l_{4B}\tfrac{1}{2})j_4\rangle \qquad (I.3)$$

and where

$$
\begin{aligned}
f_k^S(r_1, r_2) &= \frac{-g_S^2}{4\pi}\frac{(2k+1)}{2}\int_{-1}^{1}\frac{e^{-m_S r_{12}}}{r_{12}}P_k(\cos\theta_{12})d(\cos\theta_{12}) \\
&= \frac{-g_S^2}{4\pi}(2k+1)\frac{2m_S}{\pi}i_k(m_S r_<)k_k(m_S r_>) \qquad (I.4)
\end{aligned}
$$

The modified spherical Bessel functions are defined in appendix A. Eq. (I.1) is

the direct matrix element; to acquire the exchange matrix element, we use the

substitution $3 \leftrightarrow 4$. The scalar term of the particle-hole matrix element is

$$
\begin{aligned}
v^{J}_{32;14}(s) = {} & -\sum_{k}^{\infty}(-1)^{j_2+j_3+J+k}
\begin{Bmatrix}
j_2 & j_4 & k \\
j_1 & j_3 & J
\end{Bmatrix} \\
& \times \langle (l_{1A}\tfrac{1}{2})j_1 \| C_k(1) \| (l_{3A}\tfrac{1}{2})j_3 \rangle \langle (l_{2A}\tfrac{1}{2})j_2 \| C_k(2) \| (l_{4A}\tfrac{1}{2})j_4 \rangle \\
& \times \int\int dr_1 dr_2 \left[G_1(r_1)G_3(r_1) - F_1(r_1)F_3(r_1) \right] f^S_k(r_1,r_2) \\
& \times \left[G_2(r_2)G_4(r_2) - F_2(r_2)F_4(r_2) \right] \\
& - (-1)^{j_2+j_3+2j_4}\frac{1}{2J+1}\sum_{k}^{\infty}\delta_{Jk} \\
& \times \langle (l_{1A}\tfrac{1}{2})j_1 \| C_k(1) \| (l_{4A}\tfrac{1}{2})j_4 \rangle \langle (l_{2A}\tfrac{1}{2})j_2 \| C_k(2) \| (l_{3A}\tfrac{1}{2})j_3 \rangle \\
& \times \int\int dr_1 dr_2 \left[G_1(r_1)G_4(r_1) - F_1(r_1)F_4(r_1) \right] f^S_k(r_1,r_2) \\
& \times \left[G_2(r_2)G_3(r_2) - F_2(r_2)F_3(r_2) \right] \left[2(1-T) \right]
\end{aligned}
\tag{I.5}
$$

Note that for the $\Lambda - N$ case, the second term in Eq. (I.5) can be neglected, as can all the subsequent exchange terms in this appendix.

The relevant matrix element for the vector time term in the effective interaction is

$$
\langle (12)J | \frac{g_V^2}{4\pi} \frac{e^{-m_V r_{12}}}{r_{12}} | (34)J \rangle = (-1)^{j_2+j_3+J} \sum_k^{\infty} \begin{Bmatrix} J & j_2 & j_1 \\ k & j_3 & j_4 \end{Bmatrix}
$$

$$
\times \langle (l_{1A}\tfrac{1}{2})j_1 \| C_k(1) \| (l_{3A}\tfrac{1}{2})j_3 \rangle \langle (l_{2A}\tfrac{1}{2})j_2 \| C_k(2) \| (l_{4A}\tfrac{1}{2})j_4 \rangle
$$

$$
\times \int\int dr_1 dr_2 \, [G_1(r_1)G_3(r_1) + F_1(r_1)F_3(r_1)] f_k^V(r_1, r_2)
$$

$$
\times [G_2(r_2)G_4(r_2) + F_2(r_2)F_4(r_2)] \tag{I.6}
$$

where

$$
f_k^V(r_1, r_2) = \frac{g_V^2}{4\pi}(2k+1)\frac{2m_V}{\pi} i_k(m_V r_<) k_k(m_V r_>) \tag{I.7}
$$

The vector time term of the particle-hole matrix element is

$$
v_{32;14}^J(vt) = -\sum_k^{\infty}(-1)^{j_2+j_3+J+k} \begin{Bmatrix} j_2 & j_4 & k \\ j_1 & j_3 & J \end{Bmatrix}
$$

$$
\times \langle (l_{1A}\tfrac{1}{2})j_1 \| C_k(1) \| (l_{3A}\tfrac{1}{2})j_3 \rangle \langle (l_{2A}\tfrac{1}{2})j_2 \| C_k(2) \| (l_{4A}\tfrac{1}{2})j_4 \rangle
$$

$$
\times \int\int dr_1 dr_2 \, [G_1(r_1)G_3(r_1) + F_1(r_1)F_3(r_1)] f_k^V(r_1, r_2)
$$

$$
\times [G_2(r_2)G_4(r_2) + F_2(r_2)F_4(r_2)]
$$

$$
-(-1)^{j_2+j_3+2j_4}\frac{1}{2J+1}\sum_k^{\infty}\delta_{Jk}
$$

$$
\times \langle (l_{1A}\tfrac{1}{2})j_1 \| C_k(1) \| (l_{4A}\tfrac{1}{2})j_4 \rangle \langle (l_{2A}\tfrac{1}{2})j_2 \| C_k(2) \| (l_{3A}\tfrac{1}{2})j_3 \rangle
$$

$$
\times \int\int dr_1 dr_2 \, [G_1(r_1)G_4(r_1) + F_1(r_1)F_4(r_1)] f_k^V(r_1, r_2)
$$

$$
\times [G_2(r_2)G_3(r_2) + F_2(r_2)F_3(r_2)][2(1-T)] \tag{I.8}
$$

The relevant matrix element for the vector space term in the effective interaction is

$$\langle (12)J|\gamma_4^{(1)}\gamma_4^{(2)}\gamma_i^{(1)}\gamma_i^{(2)}\frac{g_V^2}{4\pi}\frac{e^{-m_V r_{12}}}{r_{12}}|(34)J\rangle = (-1)^{j_2+j_3+J}\sum_k^\infty \sum_\lambda (-1)^{k+1-\lambda}$$

$$\times \begin{Bmatrix} J & j_2 & j_1 \\ & & \\ \lambda & j_3 & j_4 \end{Bmatrix} \int\int dr_1 dr_2 \left\{ G_1(r_1)F_3(r_1)f_k^V(r_1,r_2)G_2(r_2)F_4(r_2) \right.$$

$$\times \langle (l_{1A}\tfrac{1}{2})j_1||\chi_\lambda^{(k,1)}(1)||(l_{3B}\tfrac{1}{2})j_3\rangle\langle (l_{2A}\tfrac{1}{2})j_2||\chi_\lambda^{(k,1)}(2)||(l_{4B}\tfrac{1}{2})j_4\rangle$$

$$-G_1(r_1)F_3(r_1)f_k^V(r_1,r_2)F_2(r_2)G_4(r_2)$$

$$\times \langle (l_{1A}\tfrac{1}{2})j_1||\chi_\lambda^{(k,1)}(1)||(l_{3B}\tfrac{1}{2})j_3\rangle\langle (l_{2B}\tfrac{1}{2})j_2||\chi_\lambda^{(k,1)}(2)||(l_{4A}\tfrac{1}{2})j_4\rangle$$

$$-F_1(r_1)G_3(r_1)f_k^V(r_1,r_2)G_2(r_2)F_4(r_2)$$

$$\times \langle (l_{1B}\tfrac{1}{2})j_1||\chi_\lambda^{(k,1)}(1)||(l_{3A}\tfrac{1}{2})j_3\rangle\langle (l_{2A}\tfrac{1}{2})j_2||\chi_\lambda^{(k,1)}(2)||(l_{4B}\tfrac{1}{2})j_4\rangle$$

$$+F_1(r_1)G_3(r_1)f_k^V(r_1,r_2)F_2(r_2)G_4(r_2)$$

$$\times \left. \langle (l_{1B}\tfrac{1}{2})j_1||\chi_\lambda^{(k,1)}(1)||(l_{3A}\tfrac{1}{2})j_3\rangle\langle (l_{2B}\tfrac{1}{2})j_2||\chi_\lambda^{(k,1)}(2)||(l_{4A}\tfrac{1}{2})j_4\rangle \right\}$$ (I.9)

The vector space term of the particle-hole matrix element is

$$
v_{32;14}^{J}(\text{vs}) = (-1)^{j_2+j_3+J} \sum_{k}^{\infty} \sum_{\lambda} (-1)^{k}
$$

$$
\times \begin{Bmatrix} j_2 & j_4 & \lambda \\ j_1 & j_3 & J \end{Bmatrix} \int\int dr_1 dr_2 \left\{ G_1(r_1)F_3(r_1)f_k^{V}(r_1,r_2)G_2(r_2)F_4(r_2) \right.
$$

$$
\times \langle (l_{1A}\tfrac{1}{2})j_1 || \chi_{\lambda}^{(k,1)}(1) || (l_{3B}\tfrac{1}{2})j_3 \rangle \langle (l_{2A}\tfrac{1}{2})j_2 || \chi_{\lambda}^{(k,1)}(2) || (l_{4B}\tfrac{1}{2})j_4 \rangle
$$

$$
- G_1(r_1)F_3(r_1)f_k^{V}(r_1,r_2)F_2(r_2)G_4(r_2)
$$

$$
\times \langle (l_{1A}\tfrac{1}{2})j_1 || \chi_{\lambda}^{(k,1)}(1) || (l_{3B}\tfrac{1}{2})j_3 \rangle \langle (l_{2B}\tfrac{1}{2})j_2 || \chi_{\lambda}^{(k,1)}(2) || (l_{4A}\tfrac{1}{2})j_4 \rangle
$$

$$
- F_1(r_1)G_3(r_1)f_k^{V}(r_1,r_2)G_2(r_2)F_4(r_2)
$$

$$
\times \langle (l_{1B}\tfrac{1}{2})j_1 || \chi_{\lambda}^{(k,1)}(1) || (l_{3A}\tfrac{1}{2})j_3 \rangle \langle (l_{2A}\tfrac{1}{2})j_2 || \chi_{\lambda}^{(k,1)}(2) || (l_{4B}\tfrac{1}{2})j_4 \rangle
$$

$$
+ F_1(r_1)G_3(r_1)f_k^{V}(r_1,r_2)F_2(r_2)G_4(r_2)
$$

$$
\times \langle (l_{1B}\tfrac{1}{2})j_1 || \chi_{\lambda}^{(k,1)}(1) || (l_{3A}\tfrac{1}{2})j_3 \rangle \langle (l_{2B}\tfrac{1}{2})j_2 || \chi_{\lambda}^{(k,1)}(2) || (l_{4A}\tfrac{1}{2})j_4 \rangle \left. \right\}
$$
(I.10)

$$-(-1)^{j_2+j_3+2j_4}\frac{1}{2J+1}\sum_{k}^{\infty}\sum_{\lambda}(-1)^{k+1-\lambda}$$

$$\times\int\int dr_1 dr_2\left\{G_1(r_1)F_4(r_1)f_k^{V}(r_1,r_2)G_2(r_2)F_3(r_2)\right.$$

$$\times\langle(l_{1A}\tfrac{1}{2})j_1||\chi_\lambda^{(k,1)}(1)||(l_{4B}\tfrac{1}{2})j_4\rangle\langle(l_{2A}\tfrac{1}{2})j_2||\chi_\lambda^{(k,1)}(2)||(l_{3B}\tfrac{1}{2})j_3\rangle$$

$$-G_1(r_1)F_4(r_1)f_k^{V}(r_1,r_2)F_2(r_2)G_3(r_2)$$

$$\times\langle(l_{1A}\tfrac{1}{2})j_1||\chi_\lambda^{(k,1)}(1)||(l_{4B}\tfrac{1}{2})j_4\rangle\langle(l_{2B}\tfrac{1}{2})j_2||\chi_\lambda^{(k,1)}(2)||(l_{3A}\tfrac{1}{2})j_3\rangle$$

$$-F_1(r_1)G_4(r_1)f_k^{V}(r_1,r_2)G_2(r_2)F_3(r_2)$$

$$\times\langle(l_{1B}\tfrac{1}{2})j_1||\chi_\lambda^{(k,1)}(1)||(l_{4A}\tfrac{1}{2})j_4\rangle\langle(l_{2A}\tfrac{1}{2})j_2||\chi_\lambda^{(k,1)}(2)||(l_{3B}\tfrac{1}{2})j_3\rangle$$

$$+F_1(r_1)G_4(r_1)f_k^{V}(r_1,r_2)F_2(r_2)G_3(r_2)$$

$$\times\left.\langle(l_{1B}\tfrac{1}{2})j_1||\chi_\lambda^{(k,1)}(1)||(l_{4A}\tfrac{1}{2})j_4\rangle\langle(l_{2B}\tfrac{1}{2})j_2||\chi_\lambda^{(k,1)}(2)||(l_{3A}\tfrac{1}{2})j_3\rangle\right\}$$

$$\times[2(1-T)]\tag{I.11}$$

The relevant matrix element for the rho time term in the effective interaction is

$$\langle (12) J | \frac{\tilde{\tau}^{(1)} \cdot \tilde{\tau}^{(2)}}{4} \frac{g_\rho^2}{4\pi} \frac{e^{-m_\rho r_{12}}}{r_{12}} | (34) J \rangle = (-1)^{j_2+j_3+J} \sum_k^\infty \left\{ \begin{array}{ccc} J & j_2 & j_1 \\ & & \\ k & j_3 & j_4 \end{array} \right\}$$

$$\times \langle (l_{1A} \tfrac{1}{2}) j_1 || C_k(1) || (l_{3A} \tfrac{1}{2}) j_3 \rangle \langle (l_{2A} \tfrac{1}{2}) j_2 || C_k(2) || (l_{4A} \tfrac{1}{2}) j_4 \rangle$$

$$\times \int \int dr_1 dr_2 \, [G_1(r_1) G_3(r_1) + F_1(r_1) F_3(r_1)] f_k^\rho(r_1, r_2)$$

$$\times [G_2(r_2) G_4(r_2) + F_2(r_2) F_4(r_2)] \langle T' | \frac{\tilde{\tau}^{(1)} \cdot \tilde{\tau}^{(2)}}{4} | T' \rangle \qquad (I.12)$$

where

$$f_k^\rho(r_1, r_2) = \frac{g_\rho^2}{4\pi} (2k+1) \frac{2m_\rho}{\pi} i_k(m_\rho r_<) k_k(m_\rho r_>) \qquad (I.13)$$

The rho time term of the particle-hole matrix element is

$$v_{32;14}^J(\rho t) = -\sum_k^\infty (-1)^{j_2+j_3+J+k} \left\{ \begin{array}{ccc} j_2 & j_4 & k \\ & & \\ j_1 & j_3 & J \end{array} \right\}$$

$$\times \langle (l_{1A} \tfrac{1}{2}) j_1 || C_k(1) || (l_{3A} \tfrac{1}{2}) j_3 \rangle \langle (l_{2A} \tfrac{1}{2}) j_2 || C_k(2) || (l_{4A} \tfrac{1}{2}) j_4 \rangle$$

$$\times \int \int dr_1 dr_2 \, [G_1(r_1) G_3(r_1) + F_1(r_1) F_3(r_1)] f_k^\rho(r_1, r_2)$$

$$\times [G_2(r_2) G_4(r_2) + F_2(r_2) F_4(r_2)] \left(\frac{3 - 4T}{4} \right)$$

$$-(-1)^{j_2+j_3+2j_4} \frac{1}{2J+1} \sum_k^\infty \delta_{Jk}$$

$$\times \langle (l_{1A} \tfrac{1}{2}) j_1 || C_k(1) || (l_{4A} \tfrac{1}{2}) j_4 \rangle \langle (l_{2A} \tfrac{1}{2}) j_2 || C_k(2) || (l_{3A} \tfrac{1}{2}) j_3 \rangle$$

$$\times \int \int dr_1 dr_2 \, [G_1(r_1) G_4(r_1) + F_1(r_1) F_4(r_1)] f_k^\rho(r_1, r_2)$$

$$\times [G_2(r_2) G_3(r_2) + F_2(r_2) F_3(r_2)] \left(\frac{2T}{4} \right) \qquad (I.14)$$

The relevant matrix element for the rho space component in the effective interaction is

$$\langle (12) J | \gamma_4^{(1)} \gamma_4^{(2)} \gamma_i^{(1)} \gamma_i^{(2)} \frac{\tilde{\tau}^{(1)} \cdot \tilde{\tau}^{(2)}}{4} \frac{g_\rho^2}{4\pi} \frac{e^{-m_\rho r_{12}}}{r_{12}} | (34) J \rangle$$

$$= (-1)^{j_2 + j_3 + J} \sum_k^\infty \sum_\lambda (-1)^{k+1-\lambda} \left\{ \begin{array}{ccc} J & j_2 & j_1 \\ \\ \lambda & j_3 & j_4 \end{array} \right\}$$

$$\times \int \int dr_1 dr_2 \left\{ G_1(r_1) F_3(r_1) f_k^\rho(r_1, r_2) G_2(r_2) F_4(r_2) \right.$$

$$\times \langle (l_{1A} \tfrac{1}{2}) j_1 || \chi_\lambda^{(k,1)}(1) || (l_{3B} \tfrac{1}{2}) j_3 \rangle \langle (l_{2A} \tfrac{1}{2}) j_2 || \chi_\lambda^{(k,1)}(2) || (l_{4B} \tfrac{1}{2}) j_4 \rangle$$

$$- G_1(r_1) F_3(r_1) f_k^\rho(r_1, r_2) F_2(r_2) G_4(r_2)$$

$$\times \langle (l_{1A} \tfrac{1}{2}) j_1 || \chi_\lambda^{(k,1)}(1) || (l_{3B} \tfrac{1}{2}) j_3 \rangle \langle (l_{2B} \tfrac{1}{2}) j_2 || \chi_\lambda^{(k,1)}(2) || (l_{4A} \tfrac{1}{2}) j_4 \rangle$$

$$- F_1(r_1) G_3(r_1) f_k^\rho(r_1, r_2) G_2(r_2) F_4(r_2)$$

$$\times \langle (l_{1B} \tfrac{1}{2}) j_1 || \chi_\lambda^{(k,1)}(1) || (l_{3A} \tfrac{1}{2}) j_3 \rangle \langle (l_{2A} \tfrac{1}{2}) j_2 || \chi_\lambda^{(k,1)}(2) || (l_{4B} \tfrac{1}{2}) j_4 \rangle$$

$$+ F_1(r_1) G_3(r_1) f_k^\rho(r_1, r_2) F_2(r_2) G_4(r_2)$$

$$\times \left. \langle (l_{1B} \tfrac{1}{2}) j_1 || \chi_\lambda^{(k,1)}(1) || (l_{3A} \tfrac{1}{2}) j_3 \rangle \langle (l_{2B} \tfrac{1}{2}) j_2 || \chi_\lambda^{(k,1)}(2) || (l_{4A} \tfrac{1}{2}) j_4 \rangle \right\}$$

$$\times \langle T' | \frac{\tilde{\tau}^{(1)} \cdot \tilde{\tau}^{(2)}}{4} | T \rangle \tag{I.15}$$

The rho space term of the particle-hole matrix element is

$$
v^J_{32;14}(\rho s) = (-1)^{j_2+j_3+J} \sum_{k}^{\infty} \sum_{\lambda} (-1)^k
$$

$$
\times \left\{ \begin{matrix} j_2 & j_4 & \lambda \\ j_1 & j_3 & J \end{matrix} \right\} \int \int dr_1 dr_2 \, \{ G_1(r_1)F_3(r_1)f^\rho_k(r_1,r_2)G_2(r_2)F_4(r_2)
$$

$$
\times \langle (l_{1A}\tfrac{1}{2})j_1 || \chi^{(k,1)}_\lambda(1) || (l_{3B}\tfrac{1}{2})j_3 \rangle \langle (l_{2A}\tfrac{1}{2})j_2 || \chi^{(k,1)}_\lambda(2) || (l_{4B}\tfrac{1}{2})j_4 \rangle
$$

$$
- G_1(r_1)F_3(r_1)f^\rho_k(r_1,r_2)F_2(r_2)G_4(r_2)
$$

$$
\times \langle (l_{1A}\tfrac{1}{2})j_1 || \chi^{(k,1)}_\lambda(1) || (l_{3B}\tfrac{1}{2})j_3 \rangle \langle (l_{2B}\tfrac{1}{2})j_2 || \chi^{(k,1)}_\lambda(2) || (l_{4A}\tfrac{1}{2})j_4 \rangle
$$

$$
- F_1(r_1)G_3(r_1)f^\rho_k(r_1,r_2)G_2(r_2)F_4(r_2)
$$

$$
\times \langle (l_{1B}\tfrac{1}{2})j_1 || \chi^{(k,1)}_\lambda(1) || (l_{3A}\tfrac{1}{2})j_3 \rangle \langle (l_{2A}\tfrac{1}{2})j_2 || \chi^{(k,1)}_\lambda(2) || (l_{4B}\tfrac{1}{2})j_4 \rangle
$$

$$
+ F_1(r_1)G_3(r_1)f^\rho_k(r_1,r_2)F_2(r_2)G_4(r_2)
$$

$$
\times \langle (l_{1B}\tfrac{1}{2})j_1 || \chi^{(k,1)}_\lambda(1) || (l_{3A}\tfrac{1}{2})j_3 \rangle \langle (l_{2B}\tfrac{1}{2})j_2 || \chi^{(k,1)}_\lambda(2) || (l_{4A}\tfrac{1}{2})j_4 \rangle \}
$$

$$
\times \left(\frac{3-4T}{4} \right)
$$

$$
\text{(I.16)}
$$

$$-(-1)^{j_2+j_3+2j_4}\frac{1}{2J+1}\sum_{k}^{\infty}\sum_{\lambda}(-1)^{k+1-\lambda}$$

$$\times\int\int dr_1 dr_2\{G_1(r_1)F_4(r_1)f_k^{\rho}(r_1,r_2)G_2(r_2)F_3(r_2)$$

$$\times\langle(l_{1A}\tfrac{1}{2})j_1||\chi_{\lambda}^{(k,1)}(1)||(l_{4B}\tfrac{1}{2})j_4\rangle\langle(l_{2A}\tfrac{1}{2})j_2||\chi_{\lambda}^{(k,1)}(2)||(l_{3B}\tfrac{1}{2})j_3\rangle$$

$$-G_1(r_1)F_4(r_1)f_k^{\rho}(r_1,r_2)F_2(r_2)G_3(r_2)$$

$$\times\langle(l_{1A}\tfrac{1}{2})j_1||\chi_{\lambda}^{(k,1)}(1)||(l_{4B}\tfrac{1}{2})j_4\rangle\langle(l_{2B}\tfrac{1}{2})j_2||\chi_{\lambda}^{(k,1)}(2)||(l_{3A}\tfrac{1}{2})j_3\rangle$$

$$-F_1(r_1)G_4(r_1)f_k^{\rho}(r_1,r_2)G_2(r_2)F_3(r_2)$$

$$\times\langle(l_{1B}\tfrac{1}{2})j_1||\chi_{\lambda}^{(k,1)}(1)||(l_{4A}\tfrac{1}{2})j_4\rangle\langle(l_{2A}\tfrac{1}{2})j_2||\chi_{\lambda}^{(k,1)}(2)||(l_{3B}\tfrac{1}{2})j_3\rangle$$

$$+F_1(r_1)G_4(r_1)f_k^{\rho}(r_1,r_2)F_2(r_2)G_3(r_2)$$

$$\times\langle(l_{1B}\tfrac{1}{2})j_1||\chi_{\lambda}^{(k,1)}(1)||(l_{4A}\tfrac{1}{2})j_4\rangle\langle(l_{2B}\tfrac{1}{2})j_2||\chi_{\lambda}^{(k,1)}(2)||(l_{3A}\tfrac{1}{2})j_3\rangle\}$$

$$\times\left(\frac{2T}{4}\right) \tag{I.17}$$

The relevant matrix element for the pion term in the effective interaction is

$$\langle (12) \text{J} | \gamma_4^{(1)} \gamma_4^{(2)} \gamma_5^{(1)} \gamma_5^{(2)} \vec{\tau}^{(1)} \cdot \vec{\tau}^{(2)} \frac{g_\pi^2}{4\pi} \frac{e^{-m_\pi r_{12}}}{r_{12}} | (34) \text{J} \rangle = (-1)^{j_2 + j_3 + J + 1}$$

$$\times \sum_k^\infty \left\{ \begin{array}{ccc} \text{J} & j_2 & j_1 \\ & & \\ k & j_3 & j_4 \end{array} \right\} \langle (l_{1\text{A}} \tfrac{1}{2}) j_1 \| C_k(1) \| (l_{3\text{B}} \tfrac{1}{2}) j_3 \rangle \langle (l_{2\text{A}} \tfrac{1}{2}) j_2 \| C_k(2) \| (l_{4\text{B}} \tfrac{1}{2}) j_4 \rangle$$

$$\times \int \int d r_1 d r_2 \, [G_1(r_1) F_3(r_1) + F_1(r_1) G_3(r_1)] \frac{M^*(r_1)}{M} f_k^\pi(r_1, r_2) \frac{M^*(r_2)}{M}$$

$$\times [G_2(r_2) F_4(r_2) + F_2(r_2) G_4(r_2)] \langle T' | \vec{\tau}^{(1)} \cdot \vec{\tau}^{(2)} | T' \rangle \tag{I.18}$$

where

$$f_k^\pi(r_1, r_2) = \frac{g_\pi^2}{4\pi} (2k+1) \frac{2 m_\pi}{\pi} i_k(m_\pi r_<) k_k(m_\pi r_>) \tag{I.19}$$

The pion-nucleon vertex is given by $(f_\pi / m_\pi) \gamma_5 q_\mu \gamma_\mu \tau_i$ for a pseudovector pion. The

Dirac equation satisfied by the Hartree spinors is used to eliminate the $q_\mu \gamma_\mu$ term.

Thus the factors $(M^*(r_1)/M)(M^*(r_2)/M)$ are now required in the matrix element

[110]. The pion term of the particle-hole matrix element is

$$
\begin{aligned}
v_{32;14}^{J}(\pi) = &-\sum_{k}^{\infty}(-1)^{j_2+j_3+J+k}
\begin{Bmatrix}
j_2 & j_4 & k \\
j_1 & j_3 & J
\end{Bmatrix} \\
&\times \langle (l_{1A}\tfrac{1}{2})j_1\|C_k(1)\|(l_{3B}\tfrac{1}{2})j_3\rangle \langle (l_{2A}\tfrac{1}{2})j_2\|C_k(2)\|(l_{4B}\tfrac{1}{2})j_4\rangle \\
&\times \int\int dr_1 dr_2 \left[G_1(r_1)F_3(r_1)+G_1(r_1)F_3(r_1)\right]\frac{M^*(r_1)}{M}f_k{}^{\pi}(r_1,r_2)\frac{M^*(r_2)}{M} \\
&\times \left[G_2(r_2)F_4(r_2)+F_2(r_2)G_4(r_2)\right](3-4T) \\
&-(-1)^{j_2+j_3+2j_4}\frac{1}{2J+1}\sum_{k}^{\infty}\delta_{Jk} \\
&\times \langle (l_{1A}\tfrac{1}{2})j_1\|C_k(1)\|(l_{4B}\tfrac{1}{2})j_4\rangle \langle (l_{2A}\tfrac{1}{2})j_2\|C_k(2)\|(l_{3B}\tfrac{1}{2})j_3\rangle \\
&\times \int\int dr_1 dr_2 \left[G_1(r_1)F_4(r_1)+F_1(r_1)G_4(r_1)\right]\frac{M^*(r_1)}{M}f_k^{\pi}(r_1,r_2)\frac{M^*(r_2)}{M} \\
&\times \left[G_2(r_2)F_3(r_2)+F_2(r_2)G_3(r_2)\right](2T)
\end{aligned}
\tag{I.20}
$$

APPENDIX J

Code

Huertas developed a program for solving the coupled, nonlinear, differential equations derived from the effective field theory approach of FST [16]. The aforementioned program was modified to incorporate a single Λ, as described in chapter 5. In addition, a subroutine was added to calculate the Λ-particle-nucleon-hole splittings as discussed in chapter 6. The resulting program (in C), a working copy of which is available from the author, is given by the following:

```
#include <stdio.h>
#include <math.h>

/*----------------------DEFINE FUNCTIONS----------------------*/
float k(int state,float *energy,double *kappa,float *scalar,\
        float *vector,float *pu3,float x,float gn,float fn,\
int forg,double M);

void half(float *y,float *yh);

void integr_messon(float *gin,float *gout,float *field,\
                   double *mass,double *pg,float *density,int f);
```

162

```c
/*-----------------DEFINE OUTPUT FILES-----------------------*/
FILE *spel;                          /*single particle energy levels,*/
                                     /*total energy, p and n radius*/
FILE *densit;                        /*source densities for the meson*/
                                     /*and E&M equations*/
FILE *out;                           /*output of the final fields*/

FILE *wavef;
FILE *par,*nuc;
char parfile[10],ignore[10],nucfile[10],nucname[6];


/*---------Global variables----------*/
int ngrid=12000;
float step=0.001;
float hbarc=197.33;                  /*conversion factor between MeV*/
                                     /*and fm-1*/
double bmass=939.0;                  /*nucleon mass*/
double lmass=1115.68;                /*lambda mass*/
double lp=1.793,ln=-1.913;           /*anomalous magnetic moments of*/
                                     /*p and n*/
double lam=-.613;                    /*anomalous magnetic moment of*/
                                     /*lambda*/
double gphoton=5.01;

main(int argc, char *argv[]) {
/*Iteration variables*/
  int i,j,n,m,iterat,flag,turn,turnl,rmatch,temp_int,mi;
  float temp_float;

/*Pointers*/
  float *scalar,*vector,*prho,*photon,*energy;
  float *lscalar,*lvector,*lprho;
  double *kappa;
  float *pu3,*lpu3; /*pointer to u3*/
  float *pbvector;  /*pointer to bvec, the combination of all*/
                    /*vector fields*/
  double *pmass,*pg;
  float *pgin,*pgout,*pdensity;

/*Used in Runge-Kutta procedure*/
  float g1,g2,g3,g4,f1,f2,f3,f4;
  float gmatch_in,fmatch_in,gmatch_out,alfa,rmax;
  float glmatch_in,flmatch_in,glmatch_out;
```

```c
    double x0,x1,x2,x3,x4,ee,bmax;
    double scale,xnorm,xnorml,deltae;

/*Misc*/
    float factor;
    float temp1,temp2,test;
    float meansc;

/*--------------------------------------------------------------------*/
/*Define input data*/
    int nstates=40;                     /*=30 number of states by default*/

    float lambda[nstates];              /*whether nucleon, 0, or lambda, 1*/
    double dege[nstates];               /*degeneracy 2j+1*/
    double kapa[nstates];               /*angular momentum kapa*/
    double e_guess[nstates];            /*initial energy guess*/
    double ispin[nstates];              /*isospin of nucleon*/
    char state[12];                     /*spectroscopy notation e.g. 1S1/2*/
    double match_r[nstates];            /*initial matching radius*/

    double eta1,eta2,kapa3,kapa4,xi0,etarho,alpha1,alpha2,fv,frho;
    double betas,betav,gslam,gvlam,gtl,mu1,mu2,mu3;

/*Define output data*/
    float eigen[nstates];
    double e_total=0.0;
    double e_rho=0.0,e_vec=0.0,e_sc=0.0,e_coul=0.0,e_int=0.0;
    float radius_p=0.0,radius_n=0.0,radius_l=0.0;

/*--------------------------------------------------------------------*/
/*The grid*/
    float x[ngrid];

/*# of each baryon and of total baryons*/
    double np=0.0,nn=0.0,nl=0.0,B=0.0;

/*Meson masses*/
    double smass,vmass,rmass=770.0;
    double mass[3],massl[3];

/*Square of coupling constants*/
    double alpha=0.091701,coupling[4];

/*Hartree and Dirac convergence*/
```

```
   float hconvrg=0.05;
   float dconvrg=0.1*hconvrg;

/*Parameters used in the Woods-Saxon model. hdr is the*/
/*half-density radius in fm, tsurf is the surface thickness*/
/*parameter*/
   float hdr=1.07;
   float tsurf=2.4;
   float xr,d;

/*Dirac wavefunctions G and F*/
   float diracg[ngrid],diracf[ngrid];
   float diracgl[ngrid],diracfl[ngrid];

/*Densities*/
   float den_sc[ngrid],den_vec[ngrid],den_rho[ngrid],den_coul[ngrid];
   float den_vec_t[ngrid],den_rho_t[ngrid],den_a_t[ngrid];
   float den_m[ngrid],den_coul_c1[ngrid],den_coul_c2[ngrid];
   float den_coul_d[ngrid],den_coul_ch[ngrid];
   float den_scl[ngrid],den_vecl[ngrid],den_coul_l[ngrid];
   float den_vec_tl[ngrid],den_a_tl[ngrid];
   float den_vec2[ngrid];

/*Divergences of den_vec_t and den_rho_t resp.*/
   float div_den1[ngrid],div_den2[ngrid],div_den3[ngrid];

/*Guesses for meson and coulomb fields at the origin*/
   float sco=490.0,veco=415.0,rhoo=0.0,coulo=0.1;

/*Define the FIELDS:scalar sc, vector vec, rho rho, coulomb coul.*/
/*They are defined using arrays. The fields we use are actually*/
/*already multiplied by the coupling constants: e.g.*/
/*sc = gs*scalar*/
   float sc[ngrid],vec[ngrid],rho[ngrid];
   float coul[ngrid],bvec[ngrid],u3[ngrid];
   sc[0]=sco;
   vec[0]=veco;
   rho[0]=rhoo;
   coul[0]=coulo;

/*Fields incorporating the lambda couplings*/
   float scl[ngrid],vecl[ngrid],u1l[ngrid],u2l[ngrid],u3l[ngrid];

/*Gradients of the scalar and vector fields*/
```

```
   float gradsc[ngrid],gradvec[ngrid];
   float grad_sc[ngrid],grad_vec[ngrid];   /*Used for the*/
                                            /*final fields*/


/*Temporary vectors used in calculating the laplacians*/
   double tem1[ngrid],tem2[ngrid],tem3[ngrid],tem4[ngrid];


/*Laplacians*/
   float lapsc[ngrid],lapvec[ngrid];


/*Greens functions*/
   float gin_sc[ngrid],gout_sc[ngrid];
   float gin_vec[ngrid],gout_vec[ngrid];
   float gin_rho[ngrid],gout_rho[ngrid];
   float gin_coul[ngrid],gout_coul[ngrid];


/*Used in meson equations*/
   float newdensity[ngrid],delta[ngrid];
   double gfsc1[ngrid],gfvec1[ngrid],gfrho1[ngrid],gfcoul1[ngrid];


/*Constants used in the meson equations*/
   double corr1,corr2,corr3,corr4,corr5,corr6,corr7,corr8,corr9;
   double corr10,corr11,corr12,corr13,corr14,corr15,corr16,corr17;
   double corr18,corr19;


/*Constants used to calculate the energy*/
   double const1,const2,const3,const4,const5,const6,const7,const8;


/*Center of mass correction for binding energy and charge radius*/
   double ecm;


/*Define a switch*/
   double swtch;


/*Parameters for calculating the spin - 1/2 splittings*/
   double A1,A2,A3,A4,A5,A6,B1,B2,B3,B4,B5,B6;
   double C1,C2,C3,C4,C5,C6,C7,C8,C9,C10;
   double D1[ngrid],D2[ngrid];
   double Afactor[2],Bfactor,gamma;
   double GN[ngrid],FN[ngrid],GL[ngrid],FL[ngrid];
   double SCALAR,TVECTOR,SVECTOR;


/*--------CALL FOR INPUT FILES TO ASSIGN VALUES TO VARIABLES------*/
/*-----Calling the constants first-----*/
```

```c
printf("Enter name of file with input constats : ");
scanf("%s",parfile);
printf("\n");
printf("Reading constants from file %s\n",parfile);
par=fopen(parfile,"r");

fscanf(par,"%s %lf",ignore,&smass);
fscanf(par,"%s %lf",ignore,&vmass);
mass[0]=smass;
mass[1]=vmass;
mass[2]=rmass;

for (i=0;i<=2;i++) {
   fscanf(par,"%s %lf",ignore,coupling+i);
}
coupling[3]=alpha;

fscanf(par,"%s %lf",ignore,&eta1);
fscanf(par,"%s %lf",ignore,&eta2);
fscanf(par,"%s %lf",ignore,&kapa3);
fscanf(par,"%s %lf",ignore,&kapa4);
fscanf(par,"%s %lf",ignore,&xi0);
fscanf(par,"%s %lf",ignore,&etarho);
fscanf(par,"%s %lf",ignore,&alpha1);
fscanf(par,"%s %lf",ignore,&alpha2);
fscanf(par,"%s %lf",ignore,&fv);
fscanf(par,"%s %lf",ignore,&frho);
fscanf(par,"%s %lf",ignore,&betas);
fscanf(par,"%s %lf",ignore,&betav);
fscanf(par,"%s %lf",ignore,&gslam);
fscanf(par,"%s %lf",ignore,&gvlam);
fscanf(par,"%s %lf",ignore,&gt1);
fscanf(par,"%s %lf",ignore,&mu1);
fscanf(par,"%s %lf",ignore,&mu2);
fscanf(par,"%s %lf",ignore,&mu3);
fscanf(par,"%s %lf",ignore,&swtch);

fclose(par);
printf("The constants to be used are the following\n");
printf("Masses :\n");
printf("scalar = %f \n",mass[0]);
printf("vector = %f \n",mass[1]);
printf("rho = %f \n",mass[2]);
printf("\n");
```

```c
printf("Couplings :\n");
printf("scalar =%f\n",coupling[0]);
printf("vector =%f\n",coupling[1]);
printf("rho =%f\n",coupling[2]);
printf("photon =%f\n",coupling[3]);
printf("\n");

printf("Constants :\n");
printf("eta1 =%.5f\n",eta1);
printf("eta2 =%.5f\n",eta2);
printf("kapa3 =%.5f\n",kapa3);
printf("kapa4 =%.5f\n",kapa4);
printf("xi0 =%.5f\n",xi0);
printf("etarho =%.5f\n",etarho);
printf("alpha1 =%.5f\n",alpha1);
printf("alpha2 =%.5f\n",alpha2);
printf("fv =%.5f\n",fv);
printf("frho =%.5f\n",frho);
printf("betas =%.5f\n",betas);
printf("betav =%.5f\n",betav);
printf("gslam =%.5f\n",gslam);
printf("gvlam =%.5f\n",gvlam);
printf("gtl =%.5f\n",gtl);
printf("mu1 =%.5f\n",mu1);
printf("mu2 =%.5f\n",mu2);
printf("mu3 =%.5f\n",mu3);
printf("swtch =%.5f\n",swtch);
printf("\n");

/*-----Calling nucleus parameters-----*/
  printf("Enter name of file with single particle levels: ");
  scanf("%s",nucfile);
  printf("\n");
  printf("Reading single particle level information from file %s\n",\
          nucfile);
  nuc=fopen(nucfile,"r");
  printf("\n");
  fscanf(nuc,"%d",&nstates);
  printf("Total number of states = %d\n",nstates);
  printf("\n");
  printf("The single particle information :\n");
  for (i=0;i<=(nstates-1);i++) {
    fscanf(nuc,"%f %lf %lf %lf %lf %s %lf",lambda+i,dege+i,kapa+i,\
```

```
            ispin+i,e_guess+i,ignore,match_r+i);
      printf("%.1f %.1f %.1f %.1f %f %s %.2f\n",lambda[i],dege[i],\
            kapa[i],ispin[i],e_guess[i],ignore,match_r[i]);
    }
    printf("\n");
    fclose(nuc);
    printf("Enter name of the nucleus (e.g. Sn132) :");
    scanf("%s",nucname);
    printf("\n");
    printf("Starting calculations for %s using %s parameters\n",\
            nucname,parfile);
    printf("\n");


/*---------------------- END CALLING INPUT FILES --------------*/


/*Get the total number of protons and neutrons*/
    for (n=0;n<=(nstates-1);n++) {
      if (ispin[n]>0.0) np=np+dege[n];
      if (ispin[n]<0.0) nn=nn+dege[n];
      if (ispin[n]==0.0) nl=nl+dege[n];
    }
    B=np+nn+nl;


/*These are the grid points*/
    for (i=0;i<=(ngrid-1);i++) {
      x[i]=step*(float)(1+i);
    }


/*Use a Woods-Saxon model as the initial guess for the fields.*/
/*The Woods-Saxon radius is xr and surface thickness is d in fm.*/
    d=tsurf/(2*log(9.0));
    xr=hdr*pow((double)(np+nn),(double)(1.0/3.0));

    for (i=0;i<=(ngrid-1);i++){
      sc[i]=sco/(1+exp((x[i]-xr)/d));
      vec[i]=veco/(1+exp((x[i]-xr)/d));
      rho[i]=rhoo/(1+exp((x[i]-xr)/d));
      coul[i]=coulo/(1+exp((x[i]-xr)/d));
      u3[i]=0.0;
    }


/*Initailize the eigenvalues*/
    for (n=0;n<=(nstates-1);n++) {
      eigen[n]=0.0;
```

```
    }

/*------------------------MESONS GREENS FUNCTIONS------------------------*/
/*Transform masses into lengths*/
  for (i=0;i<=2;i++){
    massl[i]=mass[i]/hbarc;
  }

  for (i=0;i<=(ngrid-1);i++){
    gin_sc[i]=exp(massl[0]*x[i])/(2.0*x[i]*massl[0]);
    gout_sc[i]=1.0/(exp(massl[0]*x[i])*x[i]);

    gin_vec[i]=exp(massl[1]*x[i])/(2.0*x[i]*massl[1]);
    gout_vec[i]=1.0/(exp(massl[1]*x[i])*x[i]);

    gin_rho[i]=exp(massl[2]*x[i])/(2.0*x[i]*massl[2]);
    gout_rho[i]=1.0/(exp(massl[2]*x[i])*x[i]);

    gin_coul[i]=1.0;
    gout_coul[i]=1.0/x[i];
  }

/*-------------------------- OUTPUT FILES ----------------------------*/

  out=fopen("fields.dat","w");
  densit=fopen("densities.dat","w");
  wavef=fopen("wfunc.dat","w");

/*------------------- MAIN ITERATION LOOP -------------------*/
/*Initailize flag and turn*/
  flag=0;
  turn=0;

/*--------Start iterat loop-------*/
  for (iterat=1;flag<=1;iterat++) {
    printf("ITERATION No %d \n",iterat);
    printf("flag = %d,\n",flag);

/*Let the eigenvalues form the previous loop become e_guess*/
    if (iterat!=1) {
      for (n=0;n<=(nstates-1);n++) {
        e_guess[n]=eigen[n];
      }
    }
```

```
/*Initialize the densities to zero*/
    for (i=0;i<=(ngrid-1);i++){
        den_sc[i]=den_vec[i]=den_rho[i]=den_coul[i]=0.0;
        den_vec_t[i]=den_rho_t[i]=den_a_t[i]=den_m[i]=0.0;
        den_scl[i]=den_vecl[i]=den_coul_l[i]=0.0;
        den_vec_tl[i]=den_a_tl[i]=0.0;
        den_vec2[i]=0.0;
    }


/*------Loop over all nstates-------*/
    for (i=0;i<=(nstates-1);i++) {


/*If a positive eigenvalue is returned then use the i-1 eigenvalue*/
        if (e_guess[i]>0.0) {
            e_guess[i]=eigen[i-1];
        }
        eigen[i]=e_guess[i];


/*First loop through all the nucleon states*/
        if(lambda[i]==0) {


/*Here we start by solving the Dirac-Hartree equations using a 4th*/
/*order Runga-Kutta method. The criterion for convergence is given*/
/*by dconvrg. After 50 tries it declares that there is no*/
/*convergence and tries with the next state.*/


/*---------Start turn loop--------*/
for (turn=1,deltae=10*dconvrg;fabs(deltae)>dconvrg;turn++) {


/*Define the potential u1 for the nucleon Hartree equations*/
  for (j=0;j<=(ngrid-1);j++){
    bvec[j]=vec[j]+ispin[i]*(rho[j]+coul[j])+0.5*(coul[j]);
  }

  if(iterat==1) {
    for (j=0;j<=(ngrid-3);j++){
      bvec[j]=bvec[j]+\
        (betas+2.0*ispin[i]*betav)*\
        (coul[j+2]-2.0*coul[j+1]+coul[j]+\
         (2.0*step/x[j])*(coul[j+1]-coul[j]))/\
        (2.0*(bmass/hbarc)*(bmass/hbarc)*step*step);
    }
    bvec[ngrid-2]=bvec[ngrid-2]+(betas+2.0*ispin[i]*betav)*\
```

```
          (coul[ngrid-1]-2.0*coul[ngrid-2]+coul[ngrid-3])/\
          (2.0*(bmass/hbarc)*(bmass/hbarc)*step*step);

      bvec[ngrid-1]=bvec[ngrid-1]+(betas+2.0*ispin[i]*betav)*\
          (coul[ngrid-1]-2.0*coul[ngrid-2]+coul[ngrid-3])/\
          (2.0*(bmass/hbarc)*(bmass/hbarc)*step*step);
    }else {
      for (j=0;j<=(ngrid-1);j++){
        bvec[j]=bvec[j]-\
          coupling[3]*hbarc*(betas+2.0*ispin[i]*betav)*den_coul_ch[j]/\
          (2.0*(bmass/hbarc)*(bmass/hbarc)*x[j]*x[j]);
      }
    }


/*Define the potential u3 for the nucleon Hartree equations*/
    for (j=0;j<=(ngrid-2);j++){
      u3[j]=(fv*(vec[j+1]-vec[j])+ispin[i]*frho*(rho[j+1]-rho[j])+\
            (0.5*(lp+ln)+ispin[i]*(lp-ln))*(coul[j+1]-coul[j]))/\
          (2.0*(bmass/hbarc)*step);
    }
    u3[ngrid-1]=(fv*vec[ngrid-1]+ispin[i]*frho*rho[ngrid-1]+\
                (0.5*(lp+ln)+ispin[i]*(lp-ln))*coul[ngrid-1]/\
                x[ngrid-1])/((bmass/hbarc)*step);


/*Make aproximations to F and G for small x*/
    if (kapa[i]<0.) {
      diracg[0]=10./pow(step,kapa[i]);
      diracf[0]=(step*diracg[0]*(bvec[0]-sc[0]-eigen[i]))/\
        (hbarc*(1.0-(2.0*kapa[i])));
    }
    else {
      diracg[0]=10.0*pow(step,1.+kapa[i]);
      diracf[0]=(hbarc*diracg[0]*(1.0+2.0*kapa[i]))/\
        (step*(eigen[i]-bvec[0]-sc[0]+2.0*bmass));
    }


/*Determine the matching point*/
    temp_int=(int)(match_r[i]/step);
    temp_float=match_r[i]/step-(float)temp_int;

    if (temp_float<0.5) {
      rmatch=(int)floor(match_r[i]/step);
    }
    else {
```

```
      rmatch=(int)ceil(match_r[i]/step);
   }
   rmatch=rmatch-1;

/*Assign pointers to the fields*/
   scalar=sc;
   vector=vec;
   prho=rho;
   photon=coul;

   pbvector=bvec;
   pu3=u3;
   energy=eigen;
   kappa=kapa;

/*In what follows the pointer vector is changed to pbvector*/
/*Use a 4th order Runga-Kutta method to solve the Hartree*/
/*equations from 0 to rmatch*/
   for (n=1;n<=rmatch;n++) {
      g1=k(i,energy,kappa,scalar,pbvector,pu3,x[n-1],
          diracg[n-1],diracf[n-1],0,bmass);
      f1=k(i,energy,kappa,scalar,pbvector,pu3,x[n-1],
          diracg[n-1],diracf[n-1],1,bmass);

      g2=k(i,energy,kappa,scalar,pbvector,pu3,x[n-1]+0.5*step,\
          diracg[n-1]+0.5*step*g1,diracf[n-1]+0.5*step*f1,0,bmass);
      f2=k(i,energy,kappa,scalar,pbvector,pu3,x[n-1]+0.5*step,\
          diracg[n-1]+0.5*step*g1,diracf[n-1]+0.5*step*f1,1,bmass);

      g3=k(i,energy,kappa,scalar,pbvector,pu3,x[n-1]+0.5*step,\
          diracg[n-1]+0.5*step*g2,diracf[n-1]+0.5*step*f2,0,bmass);
      f3=k(i,energy,kappa,scalar,pbvector,pu3,x[n-1]+0.5*step,\
          diracg[n-1]+0.5*step*g2,diracf[n-1]+0.5*step*f2,1,bmass);

      g4=k(i,energy,kappa,scalar,pbvector,pu3,x[n-1]+step,\
          diracg[n-1]+step*g3,diracf[n-1]+step*f3,0,bmass);
      f4=k(i,energy,kappa,scalar,pbvector,pu3,x[n-1]+step,\
          diracg[n-1]+step*g3,diracf[n-1]+step*f3,1,bmass);

      diracg[n]=diracg[n-1]+(1.0/6.0)*step*(g1+2.0*(g2+g3)+g4);
      diracf[n]=diracf[n-1]+(1.0/6.0)*step*(f1+2.0*(f2+f3)+f4);
   }
   gmatch_in=diracg[rmatch];
   fmatch_in=diracf[rmatch];
```

```
/*End Runge-Kutta outward integration*/

/*Get initial values of F and G for inward integration*/
  alfa=sqrt((-1.)*eigen[i]*(eigen[i]+2.*bmass))/hbarc;

  rmax=step*(float)(ngrid);

  diracg[ngrid-1]=1./exp(alfa*rmax);

  x0=(-1.)*sqrt((-1.)*eigen[i]/(eigen[i]+2.*bmass));

  bmax=12.*bvec[ngrid-1]/hbarc;

  ee=hbarc/(2.*(eigen[i]+2.*bmass));

  x1=ee*(2.*kapa[i]+bmax*(x0+1./x0));
  x2=ee*(2.*bmax+(2.*kapa[i]+1.)*x1/x0)-x1*x1/(2.*x0);
  x3=ee*((2.*kapa[i]+2.)*x2/x0+bmax*(2.*x2+x1*x1/x0))-x1*x2/x0;
  x4=ee*((2.*kapa[i]+3.)*x3/x0+bmax*2.*(x3+x1*x2/x0))-\
    (2.*x1*x3+x2*x2)/(2.*x0);

  diracf[ngrid-1]=diracg[ngrid-1]*(x0+x1/rmax+x2/pow(rmax,2.)*\
                                   x3/pow(rmax,3.)+x4/pow(rmax,4.));

/*Use a 4th order Runga-Kutta method to solve the Hartree*/
/*equations from infinity to rmatch. Previously the left side*/
/*was n-1 and the right n*/
  for (n=ngrid-2;n>=rmatch;n--) {
    g1=k(i,energy,kappa,scalar,pbvector,pu3,x[n],\
        diracg[n+1],diracf[n+1],0,bmass);
    f1=k(i,energy,kappa,scalar,pbvector,pu3,x[n],\
        diracg[n+1],diracf[n+1],1,bmass);

    g2=k(i,energy,kappa,scalar,pbvector,pu3,x[n]-0.5*step,\
        diracg[n+1]-0.5*step*g1,diracf[n+1]-0.5*step*f1,0,bmass);
    f2=k(i,energy,kappa,scalar,pbvector,pu3,x[n]-0.5*step,\
        diracg[n+1]-0.5*step*g1,diracf[n+1]-0.5*step*f1,1,bmass);

    g3=k(i,energy,kappa,scalar,pbvector,pu3,x[n]-0.5*step,\
        diracg[n+1]-0.5*step*g2,diracf[n+1]-0.5*step*f2,0,bmass);
    f3=k(i,energy,kappa,scalar,pbvector,pu3,x[n]-0.5*step,\
        diracg[n+1]-0.5*step*g2,diracf[n+1]-0.5*step*f2,1,bmass);
```

```
g4=k(i,energy,kappa,scalar,pbvector,pu3,x[n]-step,\
      diracg[n+1]-step*g3,diracf[n+1]-step*f3,0,bmass);
f4=k(i,energy,kappa,scalar,pbvector,pu3,x[n]-step,\
      diracg[n+1]-step*g3,diracf[n+1]-step*f3,1,bmass);

diracg[n]=diracg[n+1]-(1.0/6.0)*step*(g1+2.0*(g2+g3)+g4);
diracf[n]=diracf[n+1]-(1.0/6.0)*step*(f1+2.0*(f2+f3)+f4);
}
gmatch_out=diracg[rmatch];

/*End Runge-Kutta inward integration*/
/*Look near rmatch. Scale outward integration such that diracg*/
/*is a continuous function. Then find the correction to the*/
/*eigenvalue*/
scale=gmatch_out/gmatch_in;

for (m=0;m<=(rmatch-1);m++) {
  diracg[m]=scale*diracg[m];
  diracf[m]=scale*diracf[m];
}

xnorm=0.0;
for (m=0;m<=(ngrid-1);m++)
  xnorm=xnorm+diracg[m]*diracg[m]+diracf[m]*diracf[m];

xnorm=xnorm*step;

deltae=(-1.0)*diracg[rmatch]*(diracf[rmatch]-\
                            scale*fmatch_in)*hbarc/xnorm;
if (turn==1) {
  deltae=deltae/2.0;
}
eigen[i]=eigen[i]+deltae;

/*If a negative eigenvalue is returned, then*/
if (eigen[i]>0.0) {
  eigen[i]=-4.0/((double)turn);
}

/*Cutoff if not convergent*/
  if (turn==50) {
    printf("NO CONVERGENCE AFTER %d TRIES FOR STATE %d \n",turn,i);
    fprintf(wavef,"NO CONVERGENCE AFTER %d TRIES FOR STATE %d \n'',\
            turn,i);
```

```
      fprintf(wavef,"ITERAT=%d RMATCH=%d XMATCH=%f\n",iterat,rmatch,\
              match_r[i]);
      for (n=rmatch-3;n<=(rmatch+3);n++) {
        fprintf(wavef,"%d\t%f\t%f\t%f\n",n,x[n],diracg[n],diracf[n]);
      }
    }

    if (turn==50) break;

/*Print results to file*/
    if (flag==1 && (fabs(deltae)<dconvrg)) {
      printf("SAVING RESULTS IN FILE\n");
      fprintf(wavef,"State = %d \n",i);
      fprintf(wavef,"index \t x \t G(x) \t F(x) \n");


      temp1 = sqrt(xnorm);
      for (n=0;n<=(ngrid-1);n=n+ngrid/100) {
        fprintf(wavef,"%d\t%f\t%f\t%f\n",n,x[n],diracg[n]/temp1,\
        diracf[n]/temp1);
      }
    }

/*Get nucleon Fields for the particle-hole splitting*/
    if (i==2) {
      for(j=0;j<=(ngrid-1);j++) {
        GN1[j]=diracg[j];
        FN1[j]=diracf[j];
        }
      xnorma=xnorm;
    }
  }
/*End turn loop*/

/*-----------CALCULATE DENSITIES FOR MESON EQUATIONS-------------*/

factor=dege[i]/(xnorm*4.*3.1415926);
for (n=0;n<=(ngrid-1);n++) {
  den_sc[n]=den_sc[n]+\
    factor*(diracg[n]*diracg[n]-diracf[n]*diracf[n]);

  den_vec[n]=den_vec[n]+\
    factor*(diracg[n]*diracg[n]+diracf[n]*diracf[n]);
```

```
den_rho[n]=den_rho[n]+\
   factor*ispin[i]*(diracg[n]*diracg[n]+diracf[n]*diracf[n]);

den_coul[n]=den_coul[n]+\
   factor*(ispin[i]+0.5)*(diracg[n]*diracg[n]+diracf[n]*diracf[n]);

den_vec_t[n]=den_vec_t[n]+factor*2.*diracg[n]*diracf[n];

den_rho_t[n]=den_rho_t[n]+factor*2.*ispin[i]*diracg[n]*diracf[n];

den_a_t[n]=den_a_t[n]+\
   factor*((lp+ln)+(2.*ispin[i])*(lp-ln))*2.*diracg[n]*diracf[n];
      }
    }

/*Now loop though the lambda states*/
      if(lambda[i]==1) {

/*Redifine the fields for coupling to lambdas*/
for (j=0;j<=(ngrid-1);j++) {
  scl[j]=gslam*sc[j];
  vecl[j]=gvlam*vec[j];
}


/*---------Start turnl loop---------*/
for (turnl=1,deltae=10*dconvrg;fabs(deltae)>dconvrg;turnl++) {

/*Define potential u1 for the Lambda Hartree equations*/
  for (j=0;j<=ngrid-1;j++) {
    u1l[j]=vecl[j]-mu3*sc[j]*vec[j]/(bmass);
  }

/*Define potential u2 for the Lambda Hartree equations*/
  for (j=0;j<=ngrid-1;j++) {
    u2l[j]=scl[j]+(mu1*sc[j]*sc[j]-mu2*vec[j]*vec[j])/\
      (2.0*(bmass));
  }

/*Define the potential u3 for the lambda Hartree equations*/
  for (j=0;j<=(ngrid-2);j++){
    u3l[j]=(gtl*(vec[j+1]-vec[j])+lam*(coul[j+1]-coul[j]))/\
      (2.0*(bmass/hbarc)*step);
  }
  u3l[ngrid-1]=(gtl*vec[ngrid-1]+lam*coul[ngrid-1]/x[ngrid-1])/\
```

```
                ((bmass/hbarc)*step);

/*Make aproximations to F and G for small x*/
  if (kapa[i]<0.) {
    diracgl[0]=10./pow(step,kapa[i]);
    diracfl[0]=(step*diracgl[0]*(vecl[0]-scl[0]-eigen[i]))/\
      (hbarc*(1.0-(2.0*kapa[i])));
  }
  else {
    diracgl[0]=10.0*pow(step,1.+kapa[i]);
    diracfl[0]=(hbarc*diracgl[0]*(1.0+2.0*kapa[i]))\
      /(step*(eigen[i]-vecl[0]-scl[0]+2.0*bmass));
  }

/*Determine the matching point*/
  temp_int=(int)(match_r[i]/step);
  temp_float=match_r[i]/step-(float)temp_int;

  if (temp_float<0.5) {
    rmatch=(int)floor(match_r[i]/step);
  }
  else {
    rmatch=(int)ceil(match_r[i]/step);
  }
  rmatch=rmatch-1;

/*Assign pointers to the fields*/
  lscalar=u21;
  lvector=u11;
  photon=coul;
  lpu3=u31;

  energy=eigen;
  kappa=kapa;

/*Use a 4th order Runga-Kutta method to solve the Hartree*/
/*equations from 0 to rmatch*/
  for (n=1;n<=rmatch;n++) {
    g1=k(i,energy,kappa,lscalar,lvector,lpu3,x[n-1],
        diracgl[n-1],diracfl[n-1],0,lmass);
    f1=k(i,energy,kappa,lscalar,lvector,lpu3,x[n-1],
        diracgl[n-1],diracfl[n-1],1,lmass);

    g2=k(i,energy,kappa,lscalar,lvector,lpu3,x[n-1]+0.5*step,\
```

```
                diracgl[n-1]+0.5*step*g1,diracfl[n-1]+0.5*step*f1,0,lmass);
        f2=k(i,energy,kappa,lscalar,lvector,lpu3,x[n-1]+0.5*step,\
                diracgl[n-1]+0.5*step*g1,diracfl[n-1]+0.5*step*f1,1,lmass);

        g3=k(i,energy,kappa,lscalar,lvector,lpu3,x[n-1]+0.5*step,\
                diracgl[n-1]+0.5*step*g2,diracfl[n-1]+0.5*step*f2,0,lmass);
        f3=k(i,energy,kappa,lscalar,lvector,lpu3,x[n-1]+0.5*step,\
                diracgl[n-1]+0.5*step*g2,diracfl[n-1]+0.5*step*f2,1,lmass);

        g4=k(i,energy,kappa,lscalar,lvector,lpu3,x[n-1]+step,\
                diracgl[n-1]+step*g3,diracfl[n-1]+step*f3,0,lmass);
        f4=k(i,energy,kappa,lscalar,lvector,lpu3,x[n-1]+step,\
                diracgl[n-1]+step*g3,diracfl[n-1]+step*f3,1,lmass);

        diracgl[n]=diracgl[n-1]+(1.0/6.0)*step*(g1+2.0*(g2+g3)+g4);
        diracfl[n]=diracfl[n-1]+(1.0/6.0)*step*(f1+2.0*(f2+f3)+f4);
    }
    glmatch_in=diracgl[rmatch];
    flmatch_in=diracfl[rmatch];

/*End Runge-Kutta outward integration*/

/*Get initial values of F and G for inward integration*/
    alfa=sqrt((-1.)*eigen[i]*(eigen[i]+2.*bmass))/hbarc;

    rmax=step*(float)(ngrid);

    diracgl[ngrid-1]=1./exp(alfa*rmax);

    x0=(-1.)*sqrt((-1.)*eigen[i]/(eigen[i]+2.*bmass));

    bmax=12.*vecl[ngrid-1]/hbarc;

    ee=hbarc/(2.*(eigen[i]+2.*bmass));

    x1=ee*(2.*kapa[i]+bmax*(x0+1./x0));
    x2=ee*(2.*bmax+(2.*kapa[i]+1.)*x1/x0)-x1*x1/(2.*x0);
    x3=ee*((2.*kapa[i]+2.)*x2/x0+bmax*(2.*x2+x1*x1/x0))-x1*x2/x0;
    x4=ee*((2.*kapa[i]+3.)*x3/x0+bmax*2.*(x3+x1*x2/x0))-\
       (2.*x1*x3+x2*x2)/(2.*x0);

    diracfl[ngrid-1]=diracgl[ngrid-1]*(x0+x1/rmax+x2/pow(rmax,2.)*\
                                        x3/pow(rmax,3.)+\
                                        x4/pow(rmax,4.));
```

```
/*Use a 4th order Runga-Kutta method to solve the Hartree*/
/*equations from infinity to rmatch. Previously the left side*/
/*was n-1 and the right n*/
  for (n=ngrid-2;n>=rmatch;n--) {
    g1=k(i,energy,kappa,lscalar,lvector,lpu3,x[n],\
         diracgl[n+1],diracfl[n+1],0,lmass);
    f1=k(i,energy,kappa,lscalar,lvector,lpu3,x[n],\
         diracgl[n+1],diracfl[n+1],1,lmass);

    g2=k(i,energy,kappa,lscalar,lvector,lpu3,x[n]-0.5*step,\
         diracgl[n+1]-0.5*step*g1,diracfl[n+1]-0.5*step*f1,0,lmass);
    f2=k(i,energy,kappa,lscalar,lvector,lpu3,x[n]-0.5*step,\
         diracgl[n+1]-0.5*step*g1,diracfl[n+1]-0.5*step*f1,1,lmass);

    g3=k(i,energy,kappa,lscalar,lvector,lpu3,x[n]-0.5*step,\
         diracgl[n+1]-0.5*step*g2,diracfl[n+1]-0.5*step*f2,0,lmass);
    f3=k(i,energy,kappa,lscalar,lvector,lpu3,x[n]-0.5*step,\
         diracgl[n+1]-0.5*step*g2,diracfl[n+1]-0.5*step*f2,1,lmass);

    g4=k(i,energy,kappa,lscalar,lvector,lpu3,x[n]-step,\
         diracgl[n+1]-step*g3,diracfl[n+1]-step*f3,0,lmass);
    f4=k(i,energy,kappa,lscalar,lvector,lpu3,x[n]-step,\
         diracgl[n+1]-step*g3,diracfl[n+1]-step*f3,1,lmass);

    diracgl[n]=diracgl[n+1]-(1.0/6.0)*step*(g1+2.0*(g2+g3)+g4);
    diracfl[n]=diracfl[n+1]-(1.0/6.0)*step*(f1+2.0*(f2+f3)+f4);
  }
  glmatch_out=diracgl[rmatch];

/*End Runge-Kutta inward integration*/
/*Look near rmatch. Scale outward integration such that diracg*/
/*is a continuous function. Then find the correction to the*/
/*eigenvalue*/
  scale=glmatch_out/glmatch_in;

  for (m=0;m<=(rmatch-1);m++) {
    diracgl[m]=scale*diracgl[m];
    diracfl[m]=scale*diracfl[m];
  }

  xnorml=0.0;
  for (m=0;m<=(ngrid-1);m++)
    xnorml=xnorml+diracgl[m]*diracgl[m]+diracfl[m]*diracfl[m];
```

```
      xnorml=xnorml*step;

      deltae=(-1.0)*diracgl[rmatch]*(diracfl[rmatch]-\
                                    scale*flmatch_in)*hbarc/xnorml;
      if (turnl==1) {
      deltae=deltae/2.0;
      }
      eigen[i]=eigen[i]+deltae;

/*If a negative eigenvalue is returned, then*/
      if (eigen[i]>0.0) {
        eigen[i]=-4.0/(double(turnl));
      }


/*Cutoff if not convergent*/
      if (turnl==50) {
        printf("NO CONVERGENCE AFTER %d TRIES FOR STATE %d \n",turnl,i);
        fprintf(wavef,"NO CONVERGENCE AFTER %d TRIES FOR STATE %d \n",\
                turnl,i);
        fprintf(wavef,"ITERAT=%d RMATCH=%d XMATCH=%f\n",iterat,rmatch,\
                match_r[i]);
        for (n=rmatch-3;n<=(rmatch+3);n++) {
          fprintf(wavef,"%d\t%f\t%f\t%f\n",n,x[n],diracgl[n],\
                  diracfl[n]);
        }
      }


      if (turnl==50) break;

/*Print results to file*/
      if (flag==1 && (fabs(deltae)<dconvrg)) {
        fprintf(wavef,"State = %d \n",i);
        fprintf(wavef,"index \t x \t G(x) \t F(x) \n");

        for (n=0;n<=(ngrid-1);n=n+ngrid/100) {
          fprintf(wavef,"%d\t%f\t%f\t%f\n",n,x[n],diracgl[n],\
                  diracfl[n]);
        }
      }
}
/*End turnl loop*/


/*----------CALCULATE DENSITIES FOR MESON EQUATIONS----------*/
```

```
factor=dege[i]/(xnorml*4.*3.1415926);
for (n=0;n<=(ngrid-1);n++) {
  den_vec2[n]=den_vec[n];
}
for (n=0;n<=(ngrid-1);n++) {
  den_scl[n]=den_scl[n]+\
    factor*(diracgl[n]*diracgl[n]-diracfl[n]*diracfl[n]);

  den_vecl[n]=den_vecl[n]+\
    factor*(diracgl[n]*diracgl[n]+diracfl[n]*diracfl[n]);

  den_sc[n]=den_sc[n]+gslam*den_scl[n]+\
    (mu1*sc[n]*den_scl[n]-mu3*vec[n]*den_vecl[n])/bmass;

  den_vec[n]=den_vec[n]+gvlam*den_vecl[n]-\
    (mu2*vec[n]*den_scl[n]+mu3*sc[n]*den_vecl[n])/bmass;

  den_vec_tl[n]=den_vec_tl[n]+2.0*factor*diracgl[n]*diracfl[n];

  den_a_tl[n]=den_a_tl[n]+2.0*factor*lam*diracgl[n]*diracfl[n];

  den_a_t[n]=den_a_tl[n]+den_a_t[n];
      }
    }
  }


/*----------Get the charge density------------*/
/*The vector meson contribution to the charge density*/
    for (n=0;n<=(ngrid-2);n++) {
      tem1[n]=(rho[n+1]-rho[n])*x[n]*x[n]/step;
      tem2[n]=(vec[n+1]-vec[n])*x[n]*x[n]/step;
    }
    tem1[ngrid-1]=(rho[ngrid-1]-rho[ngrid-2])*\
      x[ngrid-1]*x[ngrid-1]/step;
    tem2[ngrid-1]=(vec[ngrid-1]-vec[ngrid-2])*\
      x[ngrid-1]*x[ngrid-1]/step;

    for (n=0;n<=(ngrid-2);n++) {
      den_m[n]=(1./(hbarc*gphoton*step))*\
        ((tem1[n+1]-tem1[n])/sqrt(coupling[2])+\
         (tem2[n+1]-tem2[n])/(3.*sqrt(coupling[1])));
    }
    den_m[ngrid-1]=den_m[ngrid-2];
```

```
/*Calculate the divergence of the den_a_t*/
    for (n=0;n<=(ngrid-2);n++) {
      den_coul_c1[n]=swtch*(den_a_t[n+1]-den_a_t[n])/\
        (2.0*(bmass/hbarc)*step);
    }
    den_coul_c1[ngrid-1]=den_coul_c1[ngrid-2];

/*Calculate the laplacians of den_vec and den_rho*/
    for (n=0;n<=(ngrid-2);n++) {
      tem1[n]=(den_vec2[n+1]-den_vec2[n])/step-2.0*den_vec2[n]/x[n];
      tem2[n]=(den_rho[n+1]-den_rho[n])/step-2.0*den_rho[n]/x[n];
    }
    tem1[ngrid-1]=(den_vec2[ngrid-1]+den_vec2[ngrid-2])/step-\
      2.*den_vec2[ngrid-1]/x[ngrid-1];
    tem2[ngrid-1]=(den_rho[ngrid-1]+den_rho[ngrid-2])/step-\
      2.*den_rho[ngrid-1]/x[ngrid-1];

    for (n=0;n<=(ngrid-2);n++) {
      den_coul_c2[n]=(1./(2.*step*(bmass/hbarc)*(bmass/hbarc)))*\
        ((tem1[n+1]-tem1[n])*betas+2.*(tem2[n+1]-tem2[n])*betav);
    }
    den_coul_c2[ngrid-1]=den_coul_c2[ngrid-2];

/*The direct nucleon charge density, den_coul_d, and the total*/
/*charge density, den_coul_ch*/
    for (n=0;n<=(ngrid-1);n++) {
      den_coul_d[n]=den_coul[n]+den_coul_c1[n]+den_coul_c2[n];
      den_coul_ch[n]=den_coul_d[n]+den_m[n];
    }

/*Divergences of den_vec_t, den_rho_t, and den_vec_tl*/
    for (n=0;n<=(ngrid-2);n++) {
      div_den1[n]=(den_vec_t[n+1]-den_vec_t[n])/(step);
      div_den2[n]=(den_rho_t[n+1]-den_rho_t[n])/(step);
      div_den3[n]=(den_vec_tl[n+1]-den_vec_tl[n])/(step);
    }
    div_den1[ngrid-1]=div_den1[ngrid-2];
    div_den2[ngrid-1]=div_den2[ngrid-2];
    div_den3[ngrid-1]=div_den3[ngrid-2];

/*----------Save final densities--------------*/
    if (flag==1 && (fabs(deltae)<dconvrg)) {
      fprintf(densit,"Final densities for %s\n",nucname);
```

```
    fprintf(densit,"x scalar vector vector_t rho'',\
            ''proton neutron lambda\n");
    for (n=0;n<=(ngrid-1);n=n+ngrid/100) {
        temp1= x[n]*x[n];
        fprintf(densit,"%.2f %.3e %.3e %.3e %.3e %.3e %.3e %.3e\n",\
                x[n],den_sc[n]/temp1,den_vec[n]/temp1,\
                den_vec_t[n]/temp1,2.*den_rho[n]/temp1,\
                den_coul[n]/temp1,(den_vec2[n]-den_coul[n])/\
                temp1,den_vecl[n]/temp1);
    }
}


    if (flag==1 && (fabs(deltae)<dconvrg)) goto final;

    flag=1;

    for (n=0;n<=(nstates-1);n++) {
        if (fabs(eigen[n]-e_guess[n])>hconvrg) flag=0;

        printf("%3d\t%5.1f\t%7.4f\t%7.4f\t%7.4f\t %5.3f\n",\
                n,ispin[n],eigen[n],e_guess[n],\
                fabs(eigen[n]-e_guess[n]),hconvrg);
    }

    if (flag==1) {
        spel=fopen("e-levels.dat","w");
        fprintf(spel,"Single particle energy levels for %s\n",nucname);
        fprintf(spel,"state\tispin\tEnergy\n");
        for (n=0;n<=(nstates-1);n++) {
fprintf(spel,"%3d\t%5.1f\t%6.3f\n",n,ispin[n],eigen[n]);
        }
    }


/* -------------------- SOLVE MESON EQUATIONS --------------------*/
    printf("SOLVING MESON EQUATIONS\n");

/*Direct integration using Green's functions. The following*/
/*pointers are available for this part: *pmass, *pg,*/
/* *pgin, *pgout*/
    pmass=mass1;
    pg=coupling;

/*Integrate the scalar field*/
    pgin=gin_sc;
```

```
    pgout=gout_sc;
    pdensity=den_sc;

    integr_messon(pgin,pgout,scalar,pmass,pg,pdensity,0);

    for(i=0;i<=(ngrid-1);i++) {
      gfsc1[i]=sc[i];
    }

/*Integrate the vector field*/
    pgin=gin_vec;
    pgout=gout_vec;
    pdensity=den_vec;

    integr_messon(pgin,pgout,vector,pmass,pg,pdensity,1);

    for(i=0;i<=(ngrid-1);i++) {
      gfvec1[i]=vec[i];
    }

/*Integrate the rho field*/
    pgin=gin_rho;
    pgout=gout_rho;
    pdensity=den_rho;

    integr_messon(pgin,pgout,prho,pmass,pg,pdensity,2);

    for(i=0;i<=(ngrid-1);i++) {
      gfrho1[i]=rho[i];
    }

/*Integrate the Coulomb field*/
    pgin=gin_coul;
    pgout=gout_coul;
    pdensity=den_coul_ch;

    integr_messon(pgin,pgout,photon,pmass,pg,pdensity,3);

    for(i=0;i<=(ngrid-1);i++) {
      gfcoul1[i]=coul[i];
    }

/*-------------ITERATION PROCESS FOR MESON EQUATIONS-------------*/
    printf("ITERATION FOR MESON EQUATIONS\n");
```

```
        for(mi=0,test=0;mi>=0;mi++) {

/*Calculate the new charge density. The vector meson contribution*/
/*has changed and must be calculated again with the*/
/*new meson fields*/
        for (n=0;n<=(ngrid-2);n++) {
           tem1[n]=(gfrho1[n+1]-gfrho1[n])*x[n]*x[n]/step;
           tem2[n]=(gfvec1[n+1]-gfvec1[n])*x[n]*x[n]/step;
        }
        tem1[ngrid-1]=(gfrho1[ngrid-1]-gfrho1[ngrid-2])*\
           x[ngrid-1]*x[ngrid-1]/step;
        tem2[ngrid-1]=(gfvec1[ngrid-1]-gfvec1[ngrid-2])*\
           x[ngrid-1]*x[ngrid-1]/step;

        for (n=0;n<=(ngrid-2);n++) {
           den_m[n]=(1.0/(hbarc*gphoton*step))*\
              ((tem1[n+1]-tem1[n])/sqrt(coupling[2])\
               +(tem2[n+1]-tem2[n])/(3.0*sqrt(coupling[1])));
        }
        den_m[ngrid-1]=den_m[ngrid-2];

        for (n=0;n<=(ngrid-1);n++) {
           den_coul_ch[n]=den_coul_d[n]+den_m[n];
        }

/*Constants used to solve the scalar field equation*/
        corr1=kapa3*mass[0]*mass[0]/(2.*bmass*hbarc*hbarc);
        corr2=kapa4*mass[0]*mass[0]/(6.*bmass*bmass*hbarc*hbarc);
        corr3=eta1*coupling[0]*mass[1]*mass[1]/\
           (2.*coupling[1]*bmass*hbarc*hbarc);
        corr4=eta2*coupling[0]*mass[1]*mass[1]/\
           (2.*coupling[1]*bmass*bmass*hbarc*hbarc);
        corr5=etarho*coupling[0]*mass[2]*mass[2]/\
           (2.*coupling[2]*bmass*hbarc*hbarc);
        corr6=alpha1/(2.*bmass);
        corr7=alpha2*coupling[0]/(2.*bmass*coupling[1]);

/*Form the gradients of the scalar and vector fields*/
        for (i=0;i<=(ngrid-2);i++) {
           gradsc[i]=(gfsc1[i+1]-gfsc1[i])/step;
           gradvec[i]=(gfvec1[i+1]-gfvec1[i])/step;
        }
        gradsc[ngrid-1]=gradsc[ngrid-2];
        gradvec[ngrid-1]=gradvec[ngrid-2];
```

```
/*Form the laplacians of the scalar and vector fields*/
        for (n=0;n<=(ngrid-2);n++) {
           tem1[n]=((gfsc1[n+1]-gfsc1[n])/step)*x[n]*x[n];
           tem2[n]=((gfvec1[n+1]-gfvec1[n])/step)*x[n]*x[n];
        }
        tem1[ngrid-1]=(gfsc1[ngrid-1]-gfsc1[ngrid-2])*\
           x[ngrid-1]*x[ngrid-1]/step;
        tem2[ngrid-1]=(gfvec1[ngrid-1]-gfvec1[ngrid-2])*\
           x[ngrid-1]*x[ngrid-1]/step;

        for (n=0;n<=(ngrid-2);n++) {
           lapsc[n]=(tem1[n+1]-tem1[n])/(step*x[n]*x[n]);
           lapvec[n]=(tem2[n+1]-tem2[n])/(step*x[n]*x[n]);
        }
        lapsc[ngrid-1]=(tem1[ngrid-1]-tem1[ngrid-2])/\
           (x[ngrid-1]*x[ngrid-1]*step);
        lapvec[ngrid-1]=(tem2[ngrid-1]-tem2[ngrid-2])/\
           (x[ngrid-1]*x[ngrid-1]*step);

/*Define the new scalar density*/
        for(i=0;i<=(ngrid-1);i++) {
           newdensity[i]=den_sc[i]-\
             x[i]*x[i]*(corr1*gfsc1[i]*gfsc1[i]+\
                        corr2*gfsc1[i]*gfsc1[i]*gfsc1[i]-\
                        corr3*gfvec1[i]*gfvec1[i]-\
                        corr4*gfsc1[i]*gfvec1[i]*gfvec1[i]-\
                        corr5*gfrho1[i]*gfrho1[i]-\
                        corr6*(gradsc[i]*gradsc[i]+2.*\
                        gfsc1[i]*lapsc[i])-corr7*gradvec[i]*\
                        gradvec[i])/(hbarc*coupling[0]);
        }

/*Define the new RHS for the scalar equation*/
        pgin=gin_sc;
        pgout=gout_sc;
        pdensity=newdensity;

/*New iteration on the scalar field*/
        integr_messon(pgin,pgout,scalar,pmass,pg,pdensity,0);

/*Constants used to solve the vector field equation*/
        corr9=fv/(2.*(bmass/hbarc));
        corr10=eta1*mass[1]*mass[1]/(bmass*hbarc*hbarc);
```

```
        corr11=eta2*mass[1]*mass[1]/(2.*bmass*bmass*hbarc*hbarc);
        corr12=xi0/(6.*hbarc*hbarc);
        corr13=alpha2/bmass;
        corr14=swtch*(coupling[3]*hbarc*sqrt((double)(coupling[1])))/\
            (3.*gphoton);
        corr15=gt1/(2.*(bmass/hbarc));

        for(i=0;i<=(ngrid-1);i++) {
          newdensity[i]=den_vec[i]+\
            corr9*div_den1[i]+corr15*div_den3[i]-\
            x[i]*x[i]*(corr10*gfsc1[i]*gfvec1[i]+\
                      corr11*gfsc1[i]*gfsc1[i]*gfvec1[i]+\
                      corr12*gfvec1[i]*gfvec1[i]*gfvec1[i]-\
                      corr13*(gradsc[i]*gradvec[i]+\
                              gfsc1[i]*lapvec[i]))/\
            (hbarc*coupling[1])-\
            corr14*den_coul_ch[i]/(hbarc*coupling[1]);
        }

/*Define the new RHS for the vector equation*/
        pgin=gin_vec;
        pgout=gout_vec;
        pdensity=newdensity;

/*New iteration on the vector field*/
        integr_messon(pgin,pgout,vector,pmass,pg,pdensity,1);

/*Constants used to solve the rho field equation*/
        corr17=frho*hbarc/(2.*bmass);
        corr18=etarho*mass[2]*mass[2]/(bmass*hbarc*hbarc);
        corr19=swtch*coupling[3]*\
          hbarc*sqrt((double)coupling[2])/gphoton;

        for(i=0;i<=(ngrid-1);i++) {
          newdensity[i]=den_rho[i]+corr17*div_den2[i]-\
            x[i]*x[i]*(corr18*gfsc1[i]*gfrho1[i])/\
            (hbarc*coupling[2])-\
            corr19*den_coul_ch[i]/(hbarc*coupling[2]);
        }

/*Define the new RHS for the rho equation*/
        pgin=gin_rho;
        pgout=gout_rho;
        pdensity=newdensity;
```

```
/*New iteration on the rho field*/
        integr_messon(pgin,pgout,prho,pmass,pg,pdensity,2);

/*Define the new RHS for the Coulomb equation*/
        pgin=gin_coul;
        pgout=gout_coul;
        pdensity=den_coul_ch;

/*New iteration on the Coulomb field*/
        integr_messon(pgin,pgout,photon,pmass,pg,pdensity,3);

/*PREPARE THE NEW ITERATION*/
        if(mi==0) meansc=0.5*(gfsc1[10]+sc[10]);

        printf("%d sc=%f delmeansc=%f delsc=%f\n",mi,sc[10],\
                fabs(meansc-0.5*(gfsc1[10]+sc[10])),\
                fabs(gfsc1[10]-sc[10]));

        if(mi>0) {
          if(fabs(meansc-0.5*(gfsc1[10]+sc[10]))>0.1) {
            meansc=0.5*(gfsc1[10]+sc[10]);
          }else{
            test=2;
            printf("mean convergence\n");
          }
        }

        if(fabs(gfsc1[10]-sc[10])<0.0001) test=1;

        if(test==2){
          for(i=0;i<=(ngrid-1);i++){
            sc[i]=0.5*(gfsc1[i]+sc[i]);
            vec[i]=0.5*(gfvec1[i]+vec[i]);
            rho[i]=0.5*(gfrho1[i]+rho[i]);
            coul[i]=0.5*(gfcoul1[i]+coul[i]);
          }
        }

        for(i=0;i<=(ngrid-1);i++){
          gfsc1[i]=sc[i];
          gfvec1[i]=vec[i];
          gfrho1[i]=rho[i];
          gfcoul1[i]=coul[i];
```

```
        }

        if(test==1) break;
      }

/*End of Iteration process for the meson equations*/

/*Output the results of the fields*/
      if (flag==1) {
        fprintf(out,"MF results for %s\n",nucname);
        fprintf(out,"x\tscalar\tvector\trho\tphoton\n");

        for (i=0;i<=(ngrid-1);i=i+ngrid/100) {
          fprintf(out,"%f\t%4.3e\t%4.3e\t%4.3e\t%4.3e\n",\
                  x[i],sc[i],vec[i],rho[i],coul[i]);
        }
      }
      printf("%d\n",iterat);
    }

/*End of iterat loop*/

 final:

/*---------------------SUM OF ALL ENERGY---------------------*/
/*Sum of all the eigenvalues*/
  for (j=0;j<=(nstates-1);j++) {
    e_total=e_total+dege[j]*eigen[j];
  }
  temp1=e_total;

/*Constants needed to calculate the total binding energy.*/
/*Scalar-scalar interaction energy*/
  const1=kapa3*mass[0]*mass[0]/\
    (6.*coupling[0]*bmass*hbarc*hbarc*hbarc);
  const2=kapa4*mass[0]*mass[0]/\
    (12.*coupling[0]*bmass*hbarc*hbarc*hbarc*bmass);
  const3=alpha1/(2.*coupling[0]*bmass*hbarc);

/*Vector-vector interaction energy*/
  const4=xi0/(12.*coupling[1]*hbarc*hbarc*hbarc);

/*Scalar-rho interaction energy*/
  const5=etarho*mass[2]*mass[2]/\
```

```
         (2.*bmass*coupling[2]*hbarc*hbarc*hbarc);

/*Scalar-vector interaction energy*/
    const6=eta1*mass[1]*mass[1]/\
       (2.*bmass*coupling[1]*hbarc*hbarc*hbarc);
    const7=eta2*mass[1]*mass[1]/\
       (2.*bmass*bmass*coupling[1]*hbarc*hbarc*hbarc);
    const8=alpha2/(2.*coupling[1]*bmass*hbarc);

/*Gradients of the final scalar and vector field*/
    for (n=0;n<=(ngrid-2);n++) {
      grad_sc[n]=(sc[n+1]-sc[n])/step;
      grad_vec[n]=(vec[n+1]-vec[n])/step;
    }
    grad_sc[ngrid-1]=grad_sc[ngrid-2];
    grad_vec[ngrid-1]=grad_vec[ngrid-2];

/*Interaction energies and radii*/
    for (j=0;j<=(ngrid-1);j++) {
      e_sc=e_sc+sc[j]*den_sc[j]-\
        x[j]*x[j]*(const1*sc[j]*sc[j]*sc[j]+\
                   const2*sc[j]*sc[j]*sc[j]*sc[j]+\
                   const3*sc[j]*grad_sc[j]*grad_sc[j]-\
                   const5*sc[j]*rho[j]*rho[j]-\
                   const6*sc[j]*vec[j]*vec[j]-\
                   const7*sc[j]*sc[j]*vec[j]*vec[j]-\
                   const8*sc[j]*grad_vec[j]*grad_vec[j]);

      e_vec=e_vec+vec[j]*(den_vec[j]+\
                      fv/(2.*(bmass/hbarc))*div_den1[j]+\
                      gt1/(2.*(bmass/hbarc))*div_den3[j])-\
        x[j]*x[j]*const4*vec[j]*vec[j]*vec[j]*vec[j];

      e_rho=e_rho+rho[j]*(den_rho[j]+\
        frho/(2.*(bmass/hbarc))*div_den2[j]);

      e_coul=e_coul+coul[j]*(den_coul_d[j]);

      radius_p=radius_p+x[j]*x[j]*(den_coul_ch[j]);
      radius_n=radius_n+x[j]*x[j]*(den_vec[j]-\
        den_coul[j]-den_vec1[j]);
      radius_1=radius_1+x[j]*x[j]*(den_vec1[j]);
    }
    factor=2.0*3.1415926*step;
```

```
   e_sc=factor*e_sc;
   e_rho=(-1.0)*factor*e_rho;
   e_vec=(-1.0)*factor*e_vec;
   e_coul=(-1.0)*factor*e_coul;
   e_int=factor*e_int;

/*The center of mass energy*/
   ecm=17.2/pow((double)(B),0.2);

/*The sum of the meson energies*/
   temp2=e_sc+e_vec+e_rho+e_coul;

/*The total binding energy per baryon and the radii*/
   e_total=(e_total+e_sc+e_vec+e_rho+e_coul-ecm)/(B);
   radius_p=sqrt((double)(radius_p/np*2.0*factor)-\
                 (3.0*hbarc*hbarc)/(8.0*bmass*(B)*ecm));
   radius_n=sqrt(radius_n/nn*2.0*factor);
   radius_l=sqrt(radius_l/nl*2.0*factor);

/*Output results*/
   printf("The program is done !!!!!!!!!!!\n");
   for (n=0;n<=(nstates-1);n++) {
      printf("%3d\t%5.1f\t%6.3f\n",n,ispin[n],eigen[n]);
   }

   printf("Energy/Nucleon(MeV/N)=%f \n",e_total);
   printf("RP(fm)=%f  RN(fm)=%f RL(fm)=%f \n",radius_p,radius_n,\
          radius_l);
   printf("Sum eigenvalues=%f\n",temp1);
   printf("Energy from mesons=%f\n",temp2);
   fprintf(spel,"E/B(MeV/N)=\t%f\n",e_total);
   fprintf(spel,"RP(fm)=\t%f\n",radius_p);
   fprintf(spel,"RN(fm)=\t%f\n",radius_n);
   fprintf(spel,"RL(fm)=\t%f\n",radius_l);

   fclose(out);
   fclose(wavef);

/*-----------------------Patricle-hole Splitting--------------*/

   Afactor[0]= - coupling[0]/(4*3.1415927);
   Afactor[1]= coupling[1]/(4*3.1415927);
   Afactor[2]= coupling[2]/(4*3.1415927);
```

```
/*Factor accounting for the 6-j symbols and reduced matrix elements*/
  Bfactor=128/15;

/*Get the nucleon fields for a neutron hole*/
  for(i=0;i<=(ngrid-1);i++) {
    GN[i]=diracg[i];
    FN[i]=diracf[i];
  }

/*Get the nucleon fields for a proton hole*/
  /*for(i=0;i<=(ngrid-1);i++) {
    GN[i]=GN1[i];
    FN[i]=FN1[i];
  }
  xnorm = xnorma;*/

/*Get the lambda fields*/
  for(i=0;i<=(ngrid-1);i++) {
    GL[i]=diracgl[i];
    FL[i]=diracfl[i];
  }

/*The 2-D radial integral*/
  C1 = 0.0;
  factor = gvlam*Afactor[1]*mass[1]/(xnorm*xnorml);
  for(i=0;i<=(ngrid-1);i++) {
    A1=B1=0.0;
    for(j=0;j<=i-1;j++) {
      D1[j] = (cosh(massl[1]*x[j])-sinh(massl[1]*x[j])/\
              (massl[1]*x[j]))/(massl[1]*x[j]);
      D2[i] = (1+1/(massl[1]*x[i]))*exp(-massl[1]*x[i])/\
         (massl[1]*x[i]);
      A1 = A1 + D1[j] * D2[i] * GN[i] * FN[j] * GL[i] * FL[j];
    }
    for(j=i+1;j<(ngrid-1);j++) {
      D1[i] = (cosh(massl[1]*x[i])-sinh(massl[1]*x[i])/\
              (massl[1]*x[i]))/(massl[1]*x[i]);
      D2[j] = (1+1/(massl[1]*x[j]))*exp(-massl[1]*x[j])/\
         (massl[1]*x[j]);
      B1 = B1 + D1[i] * D2[j] * GN[i] * FN[j] * GL[i] * FL[j];
    }
    C1 = C1 + step * step * (A1 + B1);
  }
  SVECTOR = factor * C1;
```

```
      printf("Vector contribution to the splitting = %f\n",SVECTOR);

}

/* ------------------------- END OF PROGRAM -------------------------- */

/*-----------------------------FUNCTIONS----------------------------------*/

float k(int state,float *energy,double *kappa,float *scalar,\
        float *vector,float *pu3,float x,float gn,float fn,\
        int forg,double M) {
  float b,e;
  float temporal[2]={0.0,0.0};
  float temp=0,temp_sc,temp_v,temp2,temp_u3;
  int index;

  b=*(kappa+state)/x;
  e=*(energy+state);

  index=(int)(x/step);
  temp2=x/step-index;
  if (temp2<=0.5) {
    temp_sc=*(scalar+index);
    temp_v=*(vector+index);
    temp_u3=*(pu3+index);
  }
  else {
    temp_sc=0.5*(*(scalar+index)+*(scalar+index+1));
    temp_v=0.5*(*(vector+index)+*(vector+index+1));
    temp_u3=0.5*(*(pu3+index)+*(pu3+index+1));
  }

  temporal[0]=(e+2.*M-temp_sc-temp_v)/hbarc;
  temporal[1]=(temp_v-e-temp_sc)/hbarc;

  switch (forg) {
  case 0: temp=temporal[forg]*fn-b*gn+(temp_u3/hbarc)*gn;
    break;
  case 1: temp=temporal[forg]*gn+b*fn-(temp_u3/hbarc)*fn;
    break;
  }
  return temp;
}
```

```
/*-------------------------------------------------------------------------*/
void half(float *y,float *yh) {
  int i;
  float fac1=-0.0625,fac2=0.5625;

  for (i=2;i<=(ngrid-2);i++) {
    *(yh+i)=fac1*(*(y+i-2)+*(y+i+1))+fac2*(*(y+i)+*(y+i-1));
  }

  *(yh+1)=(3.*(*y)+6*(*(y+1))-(*(y+2)))/8.;
  *(yh+ngrid-1)=(3.*(*(y+ngrid-1))+6.*(*(y+ngrid-1-1))-\
     (*(y+ngrid-3)))/8.;
  *yh=(*y)/4.;
}


/*-------------------------------------------------------------------------*/
void integr_messon(float *gin,float *gout,float *field,\
                   double *mass,double *pg,float *density,int f) {
  int i,j;
  float fin[ngrid],fout[ngrid],fh[ngrid];
  float xi1[ngrid],xi2[ngrid];
  float xi20,xx;
  float *pyh,*py1,*py2;

  pyh=fh;
  py1=fin;
  py2=fout;

  for (i=0;i<=(ngrid-1);i++) {
    fin[i]=(*(gin+i))*(*(density+i));
    fout[i]=(*(gout+i))*(*(density+i));
  }

  half(py1,pyh);

  xi1[0]=(4.*fh[0]+fin[0])/6.;

  for (i=1;i<=(ngrid-1);i++) {
    xi1[i]=xi1[i-1]+(fin[i-1]+4.*fh[i]+fin[i])/6.;
  }

  half(py2,pyh);

  xi2[ngrid-1]=(4.*fh[ngrid-1]+fout[ngrid-1])/6.;
```

```
for (i=ngrid-2;i>=0;i--) {
  xi2[i]=xi2[i+1]+(fout[i+1]+4.*fh[i+1]+fout[i])/6.;
}
xi20=xi2[0]+(4.*fh[0]+fout[0])/6.;

/*divide by the mass of the meson. Check for the photon first.*/

if (f==3)
  xx=0.;
else
  xx=(-1.)/(2.*(*(mass+f)));

xi20=xi20*xx;

for (j=0;j<=(ngrid-1);j++) {

  *(field+j)=(*(gout+j))*(xi1[j]+xi20)+(*(gin+j))*xi2[j];
  *(field+j)=(*(field+j))*step*hbarc*(*(pg+f));
}
}
```

The following is an example of an input file for the constants:

```
mass-scalar 520.3
mass-vector 782.0
gs2         110.16
gv2         162.88
gr2         89.936
eta1        0.64992
eta2        0.10975
kapa3       3.2467
kapa4       0.63152
xi0         2.6416
etarho      0.3901
alpha1      1.7234
alpha2      -1.5798
fv          0.6936
frho        3.8476
betas       -0.09328
betav       -0.45964
gslam       0.87195
gvlam       0.97873
fvl         -0.885
mu1         0.0774
mu2         0.344
mu3         0.0774
swtch       1.0
```

The following is an example of an input file for a selected nucleus (the GS of $^{16}_{\Lambda}$O):

```
7
0.  2.  -1.   0.5   -40.0  1s1/2  2.
0.  4.  -2.   0.5   1.0    1p3/2  3.
0.  2.  1.    0.5   1.0    1p1/2  3.
0.  2.  -1.   -0.5  -40.0  1s1/2  2.
0.  4.  -2.   -0.5  1.0    1p3/2  3.
0.  1.  1.    -0.5  1.0    1p1/2  3.
1.  1.  -1.   0.0   -20.0  1s1/2  3.
```

An example of an output file containing the eigenvalues and total energy per baryon

for a selected nucleus (the GS of $^{16}_{\Lambda}$O) is given by the following:

```
Single particle energy levels for O16L
state ispin Energy
   0    0.5 -33.428
   1    0.5 -15.984
   2    0.5 -9.163
   3   -0.5 -40.074
   4   -0.5 -21.800
   5   -0.5 -14.921
   6    0.0 -12.331
E/B(MeV/N)= -7.795342
RP(fm)= 2.714467
RN(fm)= 2.509983
RL(fm)= 2.707781
```

BIBLIOGRAPHY

[1] R. J. Furnstahl, B. D. Serot, and H.-B. Tang, Nucl. Phys. **A615**, 441 (1997); (E) Nucl. Phys. **A640**, 505 (1998).

[2] B. D. Serot and J. D. Walecka, Int. J. Mod. Phys. **E6**, 515 (1997).

[3] B. D. Serot and J. D. Walecka, in *150 Years of Quantum Many-Body Theory* (World Scientific, Singapore, 2001), p. 203.

[4] *Particle Physics Booklet* (AIP, LBNL and CERN, 2002).

[5] J. D. Walecka, *Theoretical Nuclear and Subnuclear Physics* (Oxford University Press, Oxford, 1995).

[6] F. Gross, *Relativistic Quantum Mechanics and Field Theory* (Wiley, New York, 1993).

[7] B. F. Gibson, Nucl. Phys. **A689**, 57c (2001).

[8] P. H. Pile, *et al.*, Phys. Rev. Lett. **66**, 2585 (1991).

[9] R. Bertini, *et al.*, Phys. Lett. **B83**, 306 (1979).

[10] S. Ajimura, *et al.*, Nucl. Phys. **A585**, 173 (1995).

[11] F. Garibaldi, *et al.*, E-94-107 Proposal: High Resolution 1p shell Hypernuclear Spectroscopy, 1994.

[12] G. M. Urciuoli, *et al.*, Nucl. Phys. **A691**, 43 (2001).

[13] H. Tamura, *et al.*, Mod. Phys. Lett. **A18**, 85 (2003).

[14] F. Halzen and A. D. Martin, *Quarks and Leptons: An Introductory Course in Modern Particle Physics* (Wiley, New York, 1984).

[15] T. Ericson and W. Weise, *Pions and Nuclei* (Oxford University Press, New York, 1988).

[16] M. A. Huertas, Ph.D. thesis, College of William and Mary, 2003.

[17] H. Georgi, Phys. Lett. **B298**, 187 (1993).

[18] A. Manohar and H. Georgi, Nucl. Phys. **B234**, 189 (1984).

[19] A. L. Fetter and J. D. Walecka, *Quantum Theory of Many-particle Systems* (McGraw-Hill, San Francisco, 1971).

[20] B. D. Serot and J. D. Walecka, *Advances in Nuclear Physics* (Plenum Press, New York, 1986), Vol. 16.

[21] M. A. Huertas, Phys. Rev. **C66**, 024318 (2002); (E) Phys. Rev. **C67**, 019901 (2003).

[22] W. Kohn, Rev. Mod. Phys. **71**, 1253 (1999).

[23] J. Schaffner *et al.*, Phys. Rev. Lett. **71**, 1328 (1993).

[24] J. Schaffner-Bielich and A. Gal, Phys. Rev. **C62**, 034311 (2000).

[25] V. G. J. Stoks and T. S. H. Lee, Phys. Rev. **C60**, 024006 (1999).

[26] D. J. Millener, C. B. Dover, and A. Gal, Phys. Rev. **C38**, 2700 (1988).

[27] J. Mares, E. Friedman, A. Gal, and B. K. Jennings, Nucl. Phys. **A594**, 311 (1995).

[28] S. Bart, *et al.*, Phys. Rev. Lett. **83**, 5238 (1999).

[29] J. Dabrowski, Phys. Rev. **C60**, 025205 (1999).

[30] A. Gal, Nucl. Phys. **A691**, 268 (2001).

[31] T. Fukuda, *et al.*, Phys. Rev. **C58**, 1306 (1998).

[32] P. Khaustov, *et al.*, Phys. Rev. **C61**, 054603 (2000).

[33] Y. Yamamoto *et al.*, Prog. Theor. Phys. Suppl. **117**, 361 (1994).

[34] J. McIntire, Phys. Rev. **C66**, 064319 (2002).

[35] C. B. Dover, H. Feshbach, and A. Gal, Phys. Rev. **C51**, 541 (1995).

[36] J. V. Noble, Phys. Lett. **B89**, 325 (1980).

[37] J. Mares and B. K. Jennings, Phys. Rev. **C49**, 2472 (1994); Nucl. Phys. **A585**, 347 (1995).

[38] A. Sakaguchi, *et al.*, Nucl. Phys. **A691**, 205c (2001).

[39] T. Takahashi, *et al.*, Nucl. Phys. **A670**, 265c (2000).

[40] T. Cantwell, *et al.*, Nucl. Phys. **A236**, 445 (1974).

[41] R. J. Furnstahl, Phys. Lett. **152B**, 313 (1985).

[42] Th. A. Rijken, V. G. J. Stoks, and Y. Yamamoto, Phys. Rev. **C59**, 21 (1999).

[43] V. G. J. Stoks and Th. A. Rijken, Phys. Rev. **C59**, 3009 (1999).

[44] P. M. M. Maessen, Th. A. Rijken, and J. J. de Swart, Phys. Rev. **C40**, 2226 (1989).

[45] A. R. Edmonds, *Angular Momentum in Quantum Mechanics* (Princeton University Press, Princeton, 1957).

[46] J. D. Walecka, Ann. of Phys. **63**, 219 (1971).

[47] A. De-Shalit and J. D. Walecka, Nucl. Phys. **22**, 184 (1961).

[48] J. McIntire, nucl-th/0311047.

[49] E. Witten, Phys. Rev. **D30**, 272 (1984).

[50] E. Farhi and R. L. Jaffe, Phys. Rev. **D30**, 2379 (1984).

[51] J. C. Hill, *et al.*, Nucl. Phys. **A675**, 226c (2000).

[52] K. N. Barish, *et al.*, J. Phys. **G23**, 2127 (1997).

[53] T. A. Armstrong, *et al.*, Phys. Rev. **C63**, 054903 (2001).

[54] G. Appelquist, *et al.*, Phys. Rev. Lett. **76**, 3907 (1996).

[55] J. Mares and J. Zofka, Z. Phys. **A345**, 47 (1993).

[56] M. Rufa *et al.*, Phys. Rev. **C42**, 2469 (1990).

[57] M. Barranco, R. J. Lombard, S. Marcos, and S. A. Moszkowski, Phys. Rev. **C44**, 178 (1991).

[58] D. E. Lanskoy and T. Y. Tretyakova, Z. Phys. **A343**, 355 (1992).

[59] H. J. Schulze *et al.*, Phys. Rev. **C57**, 704 (1998).

[60] A. Gal and C. B. Dover, Nucl. Phys. **A585**, 1 (1995).

[61] J. Schaffner *et al.*, Ann. of Phys. **235**, 35 (1994).

[62] C. B. Dover and A. Gal, Nucl. Phys. **A560**, 559 (1993).

[63] S. Balberg, A. Gal, and J. Schaffner, Prog. Theor. Phys. Suppl. **117**, 325 (1994).

[64] D. Halderson, Phys. Rev. **C60**, 064001 (1999).

[65] Th. A. Rijken, Nucl. Phys. **A639**, 29c (1998).

[66] I. Vidana *et al.*, Phys. Rev. **C61**, 025802 (2000).

[67] P. Wang, R. K. Su, H. Q. Song, and L. L. Zhang, Nucl. Phys. **A653**, 166 (1999).

[68] S. Balberg and A. Gal, Nucl. Phys. **A625**, 435 (1997).

[69] S. Banik and D. Bandyopadhyay, J. Phys. **G26**, 1495 (2000).

[70] M. Baldo, G. F. Burgio, and H. J. Schulze, Phys. Rev. **C61**, 055801 (2000).

[71] N. K. Glendenning, *Compact Stars: Nuclear Physics, Particle Physics, and General Relativity* (Springer, New York, 1997).

[72] R. Brockmann and W. Weise, Phys. Lett. **B69**, 167 (1977).

[73] J. Boguta and R. Bohrmann, Phys. Lett. **B102**, 93 (1981).

[74] J. Cohen and J. V. Noble, Phys. Rev. **C46**, 801 (1992).

[75] J. Cohen and H. J. Weber, Phys. Rev. **C44**, 1181 (1991).

[76] B. K. Jennings, Phys. Lett. **B246**, 325 (1990).

[77] R. J. Lombard, S. Marcos, and J. Mares, Phys. Rev. **C51**, 1784 (1995).

[78] N. K. Glendenning et al., Phys. Rev. **C48**, 889 (1993).

[79] H. Shen and H. Toki, Nucl. Phys. **A707**, 469 (2002).

[80] K. Tsushima, K. Saito, and A. W. Thomas, Phys. Lett. **B411**, 9 (1997); (E) Phys. Lett. **B421**, 413 (1998).

[81] C. M. Keil, F. Hofmann, and H. Lenske, Phys. Rev. **C61**, 064309 (2000).

[82] P. Papazoglou et al., Phys. Rev. **C57**, 2576 (1998).

[83] P. Papazoglou et al., Phys. Rev. **C59**, 411 (1999).

[84] Ch. Beckmann et al., Phys. Rev. **C65**, 024301 (2002).

[85] H. Muller and J. Piekarewicz, J. Phys. **G27**, 41 (2001).

[86] Y. Yamamoto, H. Bando, and J. Zofka, Prog. Theor. Phys. **80**, 757 (1988).

[87] E. D. Cooper, B. K. Jennings, and J. Mares, Nucl. Phys. **A580**, 419 (1994); Nucl. Phys. **A585**, 157 (1995).

[88] O. Hashimoto, Hyper. Int. **103**, 245 (1996).

[89] A. Reuber, K. Holinde, and J. Speth, Nucl. Phys. **A570**, 543 (1994).

[90] J. Hao and T. T. S. Kuo, Phys. Rep. **264**, 233 (1996).

[91] I. Vidana, A. Polls, A. Ramos, and M. Hjorth-Jensen, Nucl. Phys. **A644**, 201 (1998).

[92] Y. Yamamoto, S. Nishizaki, and T. Takatsuka, Prog. Theor. Phys. **103**, 981 (2000).

[93] M. Kohno et al., Nucl. Phys. **A670**, 319 (2000); Nucl. Phys. **A674**, 229 (2000).

[94] D. E. Lanskoy and Y. Yamamoto, Phys. Rev. **C55**, 2330 (1997).

[95] S. Fujii, R. Okamoto, and K. Suzuki, Nucl. Phys. **A651**, 411 (1999).

[96] J. Cugnon, A. Lejeune, and H. J. Schulze, Phys. Rev. **C62**, 064308 (2000).

[97] I. Vidana, A. Polls, A. Ramos, and H. J. Schulze, Phys. Rev. **C64**, 044301 (2001).

[98] Q. N. Usmani and A. R. Bodmer, Phys. Rev. **C60**, 055215 (1999).

[99] F. Arias de Saavedra, G. Co, and A. Fabrocini, Phys. Rev. **C63**, 064308 (2001).

[100] M. Oka, Nucl. Phys. **A629**, 379c (1998).

[101] P. Hohenberg and W. Kohn, Phys. Rev. **136**, B864 (1964).

[102] W. Kohn and L. J. Sham, Phys. Rev. **140**, A1133 (1965).

[103] J. F. Dubach, Nucl. Phys. **A450**, 71 (1986).

[104] B. A. Nikolaus, T. Hoch, and D. G. Madland, Phys. Rev. **C46**, 1757 (1992).

[105] H. Matsunobu and H. Takebe, Prog. Theor. Phys. **14**, 589 (1955).

[106] M. Rotenberg, R. Bivins, N. Metropolis, and J. Wooten, *The 3-j and 6-j Symbols* (Technology Press, Cambridge, 1959).

[107] M. Juric, *et al.*, Nucl. Phys. **B52**, 1 (1973).

[108] B. D. Serot, nucl-th/0308047.

[109] J. D. Walecka, Nuovo Cimento **16**, 342 (1960).

[110] R. J. Furnstahl, Ph.D. thesis, Stanford University, 1986.

VITA

Jeffrey William McIntire

Jeffrey William McIntire was born on the seventh of May, 1977 in Philadelphia, Pennsylvania. He graduated from Lisle High School, Lisle, Illinois in May, 1995. He received a Bachelor of Arts in physics with a minor in astronomy from Franklin and Marshall College in Lancaster, Pennsylvania in May, 1999. He received a Master of Science degree in physics from the College of William and Mary in Williamsburg, Virginia in December, 2000. This dissertation was defended on February 25, 2004 at the College of William and Mary in Williamsburg, Virginia.